

**Motion Control of Smart Material Based Actuators:  
Modeling, Controller Design and Experimental  
Evaluation**

Sining Liu

A Thesis  
In the Department  
of  
Mechanical & Industrial Engineering

Presented in Partial Fulfilment of Requirements  
For the Degree of  
Doctor of Philosophy (Mechanical Engineering) at  
Concordia University  
Montreal, Quebec, Canada

November 2013

© Sining Liu, 2013

**CONCORDIA UNIVERSITY**  
**SCHOOL OF GRADUATE STUDIES**

This is to certify that the thesis prepared

By: **Sining Liu**

Entitled: **Motion Control of Smart Material Based Actuators: Modeling,  
Controller Design and Experimental Evaluation**

and submitted in partial fulfillment of the requirements for the degree of

DOCTOR OF PHILOSOPHY (Mechanical Engineering)

complies with the regulations of the University and meets the accepted standards with respect to originality and quality.

Signed by the final examining committee:

\_\_\_\_\_ Chair  
Dr. C. Wang

\_\_\_\_\_ External Examiner  
Dr. X. Chen

\_\_\_\_\_ External to Program  
Dr. W.-P. Zhu

\_\_\_\_\_ Examiner  
Dr. H. Hong

\_\_\_\_\_ Examiner  
Dr. Y. Zhang

\_\_\_\_\_ Thesis Supervisor  
Dr. C.-Y. Su

Approved by \_\_\_\_\_  
Dr. A. Dolatabadi, Graduate Program Director

November 25, 2013

\_\_\_\_\_  
Dr. C. Trueman, Interim Dean  
Faculty of Engineering & Computer Science

# Abstract

## **Motion Control of Smart Material Based Actuators: Modeling, Controller Design and Experimental Evaluation**

**Sining Liu, Ph.D.**

**Concordia University, 2013**

Smart material based actuators, such as piezoelectric, magnetostrictive, and shape memory alloy actuators, are known to exhibit hysteresis effects. When the smart actuators are preceded with plants, such non-smooth nonlinearities usually lead to poor tracking performance, undesired oscillation, or even potential instability in the control systems. The development of control strategies to control the plants preceded with hysteresis actuators has become to an important research topic and imposed a great challenge in the control society. In order to mitigate the hysteresis effects, the most popular approach is to construct the inverse to compensate such effects. In such a case, the mathematical descriptions are generally required. In the literature, several mathematical hysteresis models have been proposed. The most popular hysteresis models perhaps are Preisach model, Prandtl-Ishlinskii model, and Bouc-Wen model. Among the above mentioned models, the Prandtl-Ishlinskii model has a unique property, i.e., the inverse Prandtl-Ishlinskii model can be analytically obtained, which can be used as a feedforward compensator to mitigate the hysteresis effect in the control systems. However, the shortcoming of the Prandtl-Ishlinskii model is also obvious because it can only describe a certain class of hysteresis shapes. Comparing to the Prandtl-Ishlinskii model, a generalized Prandtl-Ishlinskii model has been reported in the literature to describe a more general class of hysteresis shapes in the smart actuators. However, the inverse for the generalized Prandtl-Ishlinskii model has only been given without the strict proof due to the difficulty of the initial loading curve construction though the analytic inverse of the Prandtl-Ishlinskii model is well documented in the literature. There-

fore, as a further development, the generalized Prandtl-Ishlinskii model is re-defined and a modified generalized Prandtl-Ishlinskii model is proposed in this dissertation which can still describe similar general class of hysteresis shapes. The benefit is that the concept of initial loading curve can be utilized and a strict analytical inverse model can be derived for the purpose of compensation. The effectiveness of the obtained inverse modified generalized Prandtl-Ishlinskii model has been validated in the both simulations and in experiments on a piezoelectric micropositioning stage. It is also affirmed that the proposed modified generalized Prandtl-Ishlinskii model fulfills two crucial properties for the operator based hysteresis models, the wiping out property and the congruency property.

Usually the hysteresis nonlinearities in smart actuators are unknown, the direct open-loop feedforward inverse compensation will introduce notably inverse compensation error with an estimated inverse construction. A closed-loop adaptive controller is therefore required. The challenge in fusing the inverse compensation and the robust adaptive control is that the strict stability proof of the closed loop control system is difficult to obtain due to the fact that an error expression of the inverse compensation has not been established when the hysteresis is unknown. In this dissertation research, by developing the error expression of the inverse compensation for modified generalized Prandtl-Ishlinskii model, two types of inverse based robust adaptive controllers are designed for a class of uncertain systems preceded by a smart material based actuator with hysteresis nonlinearities. When the system states are available, an inverse based adaptive variable structure control approach is designed. The strict stability proof is established thereafter. Comparing with other works in the literature, the benefit for such a design is that the proposed inverse based scheme can achieve the tracking without necessarily adapting the uncertain parameters (the number could be large) in the hysteresis model, which leads to the computational efficiency. Furthermore, an inverse based adaptive output-feedback control scheme is developed when the exactly knowledge of most of the states is unavailable and the only accessible state is the output of the system. An observer is therefore constructed to estimate the unavailable states from the measurements of a single output. By taking consideration of the analytical expression of the

inverse compensation error, the global stability of the close-loop control system as well as the required tracking accuracy are achieved. The effectiveness of the proposed output-feedback controller is validated in both simulations and experiments.

*To my parents, and to my beloved husband Ming*

## Acknowledgement

I would like to express sincere gratitude to all the people who helped me with the various aspects of writing my thesis. First and foremost, I would like to especially thank my supervisor, Dr. Chun-Yi Su, for his insightful guidance, support and encouragement throughout the course of this research and during the preparation of this thesis. I would like to thank Dr. Xiongbiao Chen, the External Examiner, Dr. Wei-Ping Zhu, Examiner (External to Program), and the internal examiners, Dr. Youmin Zhang and Dr. Henry Hong for their time and helpful suggestions.

I would also like to thank my husband and my parents. It would not have been possible to accomplish my PhD study without their love, encouragement and support.

Last but not least, I would like to thank my colleagues and friends: Zhi Li, Jun Fu, Ying Feng, and Siavash Taheri, for their kindly help.

# Contents

List of Figures . . . . .	xi
List of Tables . . . . .	xv
Nomenclature and Abbreviations . . . . .	xvi
<b>1 Introduction</b>	<b>1</b>
1.1 Motivation . . . . .	1
1.2 Objective and Contributions . . . . .	5
1.2.1 Objective of the Dissertation . . . . .	5
1.2.2 Contributions of the Dissertation . . . . .	6
1.3 Organization of the Dissertation . . . . .	8
<b>2 Literature Review</b>	<b>10</b>
2.1 Hysteresis Nonlinearity . . . . .	11
2.2 Hysteresis Models . . . . .	13
2.3 Hysteresis Compensation . . . . .	16
2.3.1 Inverse-based Methods . . . . .	16
2.3.2 Direct methods . . . . .	21
<b>3 Modified Generalized Prandtl-Ishlinskii (MGPI) Model</b>	<b>22</b>
3.1 Prandtl-Ishlinskii Model . . . . .	23
3.1.1 The Play Operator . . . . .	23
3.1.2 Prandtl-Ishlinskii Model . . . . .	26
3.2 Generalized Prandtl-Ishlinskii Model . . . . .	28
3.2.1 The Generalized Play Operator . . . . .	28

3.2.2	Generalized Prandtl-Ishlinskii Model . . . . .	29
3.3	Modified Generalized Prandtl-Ishlinskii Model . . . . .	31
3.3.1	The Modified Generalized Play Operator . . . . .	31
3.3.2	Modified Generalized Prandtl-Ishlinskii Model . . . . .	32
3.3.3	Some Examples of Modified Generalized Prandtl-Ishlinskii model . . . . .	34
3.4	Wiping Out Property and Congruency Property of Modified Generalized Prandtl-Ishlinskii . . . . .	35
3.4.1	Memory Curve Structure . . . . .	35
3.4.2	Wiping Out Property . . . . .	38
3.4.3	Congruency Property . . . . .	40
<b>4</b>	<b>Inverse Hysteresis Compensation of Modified Generalized Pradtl-Ishlinskii Model</b>	<b>45</b>
4.1	Concept of Initial Loading Curve . . . . .	46
4.2	Inverse Construction of the Modified Generalized Prandtl-Ishlinskii Model . . . . .	50
4.3	Numerical Implementation of the Inverse MGPI Model . . . . .	52
4.4	Simulation Results of Inverse Compensation . . . . .	53
4.4.1	Linear Envelope Function . . . . .	54
4.4.2	Nonlinear Envelope Function . . . . .	56
<b>5</b>	<b>Analysis of Inverse Compensation Error</b>	<b>58</b>
5.1	The Analytical Inverse Compensation Error . . . . .	61
5.2	Simulation Results of the Inverse Compensation Error . . . . .	64
<b>6</b>	<b>Controller Design I: State-Feedback Control</b>	<b>76</b>
6.1	Problem Statement . . . . .	77
6.2	State-Feedback Controller Design . . . . .	78
6.3	Simulation Studies . . . . .	82
<b>7</b>	<b>Controller Design II: Output-Feedback Control</b>	<b>87</b>

7.1	Problem Statement . . . . .	88
7.2	State Observer . . . . .	89
7.3	Adaptive Output Feedback Controller Design . . . . .	92
7.4	Simulation Studies . . . . .	100
7.4.1	Example 1: . . . . .	100
7.4.2	Example 2: . . . . .	101
<b>8</b>	<b>Experimental Implementation</b>	<b>109</b>
8.1	Experimental Setup . . . . .	109
8.2	Hysteresis Parameters Identification and Model Validation . . . . .	110
8.3	Experimental Verification of Inverse Compensation . . . . .	114
8.4	Experimental Verification of Adaptive Output Feedback Controller . . . . .	115
<b>9</b>	<b>Conclusions and Future Work</b>	<b>122</b>
9.1	Concluding Remarks . . . . .	122
9.2	Recommendations for Future Works . . . . .	124
9.3	Publications . . . . .	125
	<b>References</b>	<b>127</b>

# List of Figures

Figure 1.1	Hysteresis nonlinearity . . . . .	3
Figure 1.2	Closed-loop control system with hysteresis effect . . . . .	5
Figure 2.1	Major and minor loops of hysteresis nonlinearity. . . . .	12
Figure 2.2	Inverse feedforward controller for hysteresis nonlinearity. . . . .	17
Figure 3.1	A piston with plunger of length $2r$ . . . . .	24
Figure 3.2	Input-output relationship of play operator $F_r[v](t)$ . . . . .	25
Figure 3.3	An example of PI model under $v(t) = \frac{5\sin(1.6\pi t) + 4\cos(4.8t)}{1 + 0.4t}$ , $t \in [0, 10]$ . . . . .	27
Figure 3.4	(a) The output of play operator with various thresholds $r$ ; (b) The output of generalized play operator with various thresholds $r$ . . . . .	30
Figure 3.5	Mapping from the play operator to the modified generalized play operator . . . . .	33
Figure 3.6	The output of modified generalized play operator with various thresholds $r$ . . . . .	33
Figure 3.7	Examples of MGPI with different envelope functions . . . . .	36
Figure 3.8	Memory curve structure. . . . .	37
Figure 3.9	(a) The input signal $v(t)$ . (b) The output $w_M(t)$ of the modified generalized play operator. . . . .	39
Figure 3.10	(a) Input signal $v(t)$ for wiping out validation; (b) Output of MGPI model for wiping out verification. . . . .	41
Figure 3.11	Illustration of congruency property. . . . .	42

Figure 3.12	(a) Input signal $v(t)$ for congruency validation. (b) Output of MGPI model congruency verification. . . . .	43
Figure 4.1	Inverse compensation for MGPI mode . . . . .	47
Figure 4.2	The input output relations of (a) The PI model; (b) The corresponding initial loading curve. . . . .	49
Figure 4.3	Input-output relations of (a) MGPI model, (b) the hysteresis loop compensator, (c) and the compensation result, with the linear envelope function. . . . .	55
Figure 4.4	Input-output relations of (a) The MGPI model, (b) The hysteresis loop compensator, (c) The effectiveness of the hysteresis loop compensator, (d) and the compensation result, with the nonlinear envelope function. . . . .	57
Figure 5.1	Inverse compensation without inverse error . . . . .	59
Figure 5.2	Inverse compensation with inverse error . . . . .	60
Figure 5.3	Input-output relation of MGPI mode under $v_c(t) = 7\sin(\pi t)/(1+0.06t)$ . . . . .	65
Figure 5.4	Inverse compensation error without estimation error in density function. . . . .	67
Figure 5.5	Input-output relationship of inverse compensation without estimation error in density function. . . . .	68
Figure 5.6	Compensated output tracks the reference input without estimation error in density function. . . . .	69
Figure 5.7	Inverse compensation error with minor estimation error in density function. . . . .	70
Figure 5.8	Input-output relationship of inverse compensation with minor estimation error in density function. . . . .	71
Figure 5.9	Compensated output tracks the reference input with minor estimation error in density function. . . . .	72
Figure 5.10	Inverse compensation error with major estimation error in density function. . . . .	73

Figure 5.11	Input-output relationship of inverse compensation with major estimation error in density function. . . . .	74
Figure 5.12	Compensated output tracks the reference input with major estimation error in density function. . . . .	75
Figure 6.1	State-feedback control structure . . . . .	78
Figure 6.2	Tracking errors of state-feedback controller (a) with inverse compensation and (b) without inverse compensation. . . . .	84
Figure 6.3	System states $x(t)$ of state-feedback controller (a) with inverse compensation and (b) without inverse compensation. . . . .	85
Figure 6.4	Control signals $v(t)$ of state-feedback controller (a) with inverse compensation and (b) without inverse compensation. . . . .	86
Figure 7.1	Output-feedback control structure . . . . .	89
Figure 7.2	The tracking error of output-feedback controller in example 1. . . . .	102
Figure 7.3	The controller signal $v(t)$ of output-feedback controller in example 1. . . . .	103
Figure 7.4	The desired output $y_d(t)$ and the actual output $y(t)$ of output-feedback controller in example 1. . . . .	104
Figure 7.5	The tracking error of output-feedback controller in example 2. . . . .	106
Figure 7.6	The controller signal $v(t)$ of output-feedback controller in example 2. . . . .	107
Figure 7.7	The desired output $y_d(t)$ and the actual output $y(t)$ of output-feedback controller in example 2. . . . .	108
Figure 8.1	Experiment setup. . . . .	110
Figure 8.2	The identification result of MGPI model for PZT P-753.31C. . . . .	112
Figure 8.3	Displacement error between measured and model responses. . . . .	113
Figure 8.4	(a) The MGPI model of PZT P-753.31C with input signal $v_c(t) = 15.2 + 11.4\sin(2\pi t)$ ; (b) The compensated output with applying the inverse MGPI model. . . . .	116

Figure 8.5	(a) The MGPI model of PZT P-753.31C with input signal $v_c(t) = 19 + 2.28\sin(4.283t) + 3.8\sin(2\pi t)$ ; (b) The compensated output with applying the inverse MGPI model. . . . .	117
Figure 8.6	The tracking error in experiment. . . . .	119
Figure 8.7	The desired output $y_d(t)$ and the actual output $y(t)$ in experiment. . . . .	120
Figure 8.8	The control input voltage $v(t)$ in experiment. . . . .	121

# List of Tables

Table 3.1	Various envelope functions for MGPI model . . . . .	34
Table 4.1	Thresholds and weights selected for the MGPI model with linear envelope function . . . . .	54
Table 4.2	Thresholds and weights obtained for the inverse MGPI model with linear envelope function . . . . .	56
Table 7.1	Output-feedback controller parameters in Example 1 . . . . .	101
Table 7.2	Output-feedback controller parameters in Example 2 . . . . .	105
Table 8.1	Identified parameters of PZT P-753.31C . . . . .	111
Table 8.2	Thresholds and weights obtained for the inverse MGPI model for PZT P-753.31C . . . . .	114

# Nomenclature and Abbreviations

## Nomenclature

$v$	system input
$r$	threshold of play operator
$F_r[v](t)$	play operator
$E_r[v](t)$	stop operator
$C_m[0, t_E]$	space of the piecewise monotone continuous function
$w$	output of play operator
$\omega_{-1}$	initial value of play operator
$\Pi[v](t)$	Prandtl-Ishlinskii model
$p(r)$	density function of Prandtl-Ishlinskii model
$G_r[v](t)$	generalized play operator
$w_g$	output of generalized play operator
$\omega_{g-1}$	initial value of generalized play operator
$\gamma_r, \gamma_l$	envelope functions
$\Pi_g[v](t)$	generalized Prandtl-Ishlinskii model
$p_g(r)$	density function of generalized Prandtl-Ishlinskii model
$G_{mr}[v](t)$	modified generalized play operator
$w_M$	output of modified generalized play operator
$\omega_{m-1}$	initial value of modified generalized play operator
$\Pi_m[v](t)$	modified generalized Prandtl-Ishlinskii model
$\hat{\Pi}_m[v](t)$	estimated modified generalized Prandtl-Ishlinskii model
$p_m(r)$	density function of modified generalized Prandtl-Ishlinskii model
$\hat{p}_m(r)$	estimated density function of estimated MGPI model
$\zeta_1, \zeta_2$	cross-over value of modified generalized play operator
$S(\zeta_2, \zeta_1)$	the MGPI plane
$\Pi_m^{-1}(t)$	inverse MGPI model

$\hat{\Pi}_m^{-1}(t)$	estimated inverse MGPI model
$\Pi_{com}(t)$	hysteresis loop compensator
$\hat{\Pi}_{com}(t)$	estimated hysteresis loop compensator
$\Pi_{sh}(t)$	shifted MGPI model
$\hat{\Pi}_{sh}(t)$	estimated shifted MGPI model
$v_c(t)$	reference input signal of inverse compensation
$\Theta(r)$	initial loading curve of PI model
$\Theta_m(r)$	initial loading curve of MGPI model
$\hat{\Theta}_m(r)$	initial loading curve of estimated MGPI model
$\Theta_{sh}(r)$	initial loading curve of shifted MGPI model
$\hat{\Theta}_{sh}(r)$	initial loading curve of estimated shifted MGPI model
$\Psi(s)$	initial loading curve of hysteresis loop compensator
$\hat{\Psi}(s)$	initial loading curve of estimated hysteresis loop compensator
$e(t)$	inverse compensation error
$D$	boundary of $\int_0^\infty \frac{\eta''(r)}{m_0} F_r[v_c](t) dr$
$u(t)$	inverse compensated output / output of hysteresis actuators
$x(t)$	control system states
$x_d(T)$	desired states trajectory
$y(t)$	control system output
$y_d(t)$	desired output trajectory
$q = [q_1, \dots, q_k]^T$	parameters of state observer
$\hat{x}(t)$	estimated system state
$\epsilon$	estimation error between $x(t)$ and $\hat{x}(t)$
$v_Q(t), v_{Q1}(t)$	control signals of the controller proposed in [1]
$\Pi_\gamma$	the measured displacement of PZT mode P-753.31C

## Abbreviations

SMA	Shape Memory Alloy
KP	Krasnosel'ĭnskii-Pokrovskii
PI	Prandtl-Ishlinskii
GPI	Generalized Prandtl-Ishlinskii
MGPI	Modified Generalized Prandtl-Ishlinskii
J-A	Jiles-Atherton
PZT	Piezoelectric micropositioning stage

# Chapter 1

## Introduction

### 1.1 Motivation

In recent decades, the demands of high precision positioning techniques have increased dramatically in various industrial areas such as biomedical science, optics, semiconductors, microscopy, and so forth. The required performance in such a high level demands a significant improvement of both the actuators and the controllers. The smart material, including the piezoelectric material, the magnetostrictive material and the shape memory alloy (SMA), has become the ideal material to manufacture the improved actuators because of their superior performances, such as high resolution and fast response. However, the smart material based actuators usually exhibit the hysteresis effect [2]. This nonlinear effect will result in the performance limitations of the control systems when it is preceded with the smart material based actuators, including poor tracking accuracy, oscillations, or even potential instabilities in the control systems [3]. On the other hand, due to the multi-valued and non-smooth natures of the hysteresis nonlinearity, as shown in Fig.1.1, it is insufficient to directly adopt the traditional control technologies to mitigate the hysteresis effects [4]. Therefore, the development of effective methods of hysteresis compensation so as to enhance the control systems tracking performance as well as guarantee the system stability has attracted

significant attention in both theoretical and practical fields in recently years.

In order to compensate the hysteresis effects in the control systems, the construction of the hysteresis models definitions is essential. The characterizations of hysteresis nonlinearities in various smart material based actuators are usually different. For example, the hysteresis loops of the piezoelectric actuators are close to symmetric. However, the magnetostrictive and SMA actuators yield highly asymmetric hysteresis nonlinearities. Furthermore, some of the smart material based actuators exhibit the output saturation. In an effort to describe the diverse hysteresis phenomenons, numbers of hysteresis models have been proposed in the literature [5, 6]. The most cited hysteresis models perhaps are the Preisach model [7–9], the Krasnosel'skii-Pokrovskii (KP) model [10, 11], the Prandtl-Ishlinskii (PI) model [12, 13], the Duhem model [14], and so forth. Among these models, the PI model is well known because its unique invertible property. The analytical inverse of PI model has been derived in [15] and applied as the hysteresis compensator to mitigate the hysteresis effect in the control systems. However, the obvious limitation of the PI model is that it can only describe a certain class of hysteresis shapes, i.e., the symmetric and non-saturated hysteresis loops. In recently years, several works [16–18] have been proposed to modify the PI model so as to enlarge its application range. Especially, a generalized Prandtl-Ishlinskii (GPI) model has been defined in [19] to describe a more general family of hysteresis shapes comparing to the PI model. Furthermore, the inverse GPI model has been derived in [20]. However, based on such a definition of GPI model, even though the form of the inverse model has been given and its effectiveness has been testified in the experiment, the strict theoretical proof of the inverse GPI model is difficult of obtain, which prevents it from the compensation error analysis and inverse controller designs. The reason could be the difficulty of defining the initial loading curve that is essential for the inverse construction. Therefore, as a further development, the GPI model will be modified and a modified generalized Prandtl-Ishlinskii (MGPI) model will be defined in this dissertation. The benefit of this modification is that the MGPI model not only can describe the similar generalize class of hysteresis shapes comparing to the PI model, but also make it possible to obtain an inverse model with the strict theoretical proof

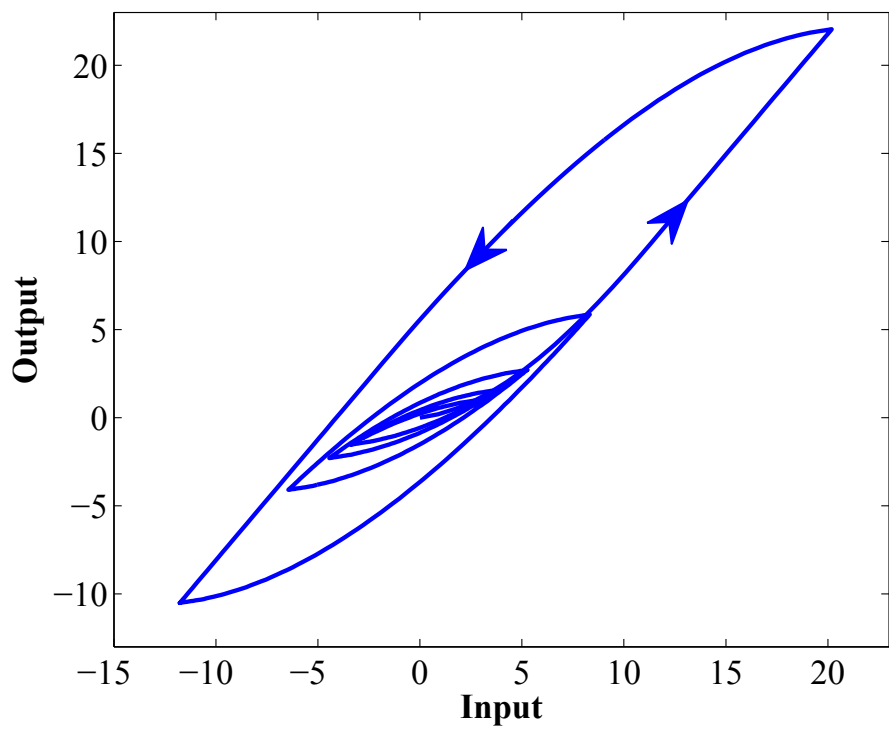


Figure 1.1: Hysteresis nonlinearity

since the concept of initial loading curve can be utilized.

Based on the available hysteresis models, the corresponding compensation methods have been reported in the literature, which can be classified into two groups. The first one is using the inverse hysteresis model as a feedforward compensator, which is pioneered by Tao and Kokotovic [3], and the second group is without using the inverse construction but directly applying the feedback controllers. For the first group, the strict stability proof is still a challenge task except [3] and [21] due to the fact that an error expression of the inverse compensation has not been established yet when the hysteresis is unknown. This explains the reason why the second group of controllers were developed, which usually satisfies the Lyapunov condition. In this dissertation research, it will be shown that a strict stability proof can be established for the inverse compensation scheme taking consideration of error expression of the inverse compensation in the controller design, where the MGPI model is used to describe the hysteresis nonlinearities. Comparing with a typical approach [13] in the second category, the benefit for such a design is that the proposed inverse based scheme can achieve the tracking without necessarily adapting the uncertain parameters (the number could be large) in the hysteresis model, which is made possible by the introduction of the stop operator in the error formulation. Though the proposed approach incurs extra cost in implementing hysteresis inversion, it achieves gain in computational efficiency by not having to adapt the hysteresis parameters. Furthermore, for the case when not all the states are measurable in the control systems, an observer based adaptive output-feedback controller together with the inverse construction will be designed for a class of unknown nonlinear systems preceded by the unknown hysteresis described by the MGPI model. It has been validated that, by using the proposed inverse based output-feedback controller, both the global stability and the tracking accuracy are achieved.

## 1.2 Objective and Contributions

### 1.2.1 Objective of the Dissertation

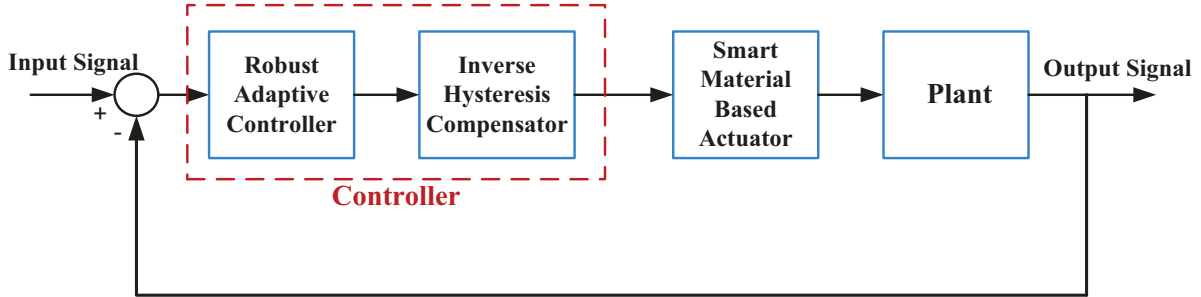


Figure 1.2: Closed-loop control system with hysteresis effect

Figure 1.2 shows a closed-loop control system of a plant preceded by a smart material based actuator. The smart material based actuators usually exhibit the hysteresis nonlinearity, which will highly restrict the performance of the closed-loop control system. In the literature, many important works of hysteresis compensation have been reported for such a system. However, there are still some challenges left, some of which are listed as follows,

≤ The PI model is widely used in describing the hysteresis effects in the smart material based actuators because of its unique invertibility, but it can only describe a restrict type of hysteresis loops. Moreover, the definition of PI model has been extended to a general form in the literature so as to describe a more general class of hysteresis shapes. However, the analytical expression of the inverse general PI models is difficult to obtain with a strict theoretical proof.

≤ In the literature, one of the most common ways to compensate the hysteresis effect is to construct an inverse. Since the hysteresis nonlinearity is usually unknown in the control systems, the inverse compensation error due to the hysteresis modeling uncertainties is unavoidable. Nevertheless, the strict stability proofs of the control systems can not be established due to the difficulty of deriving the analytical expression of the inverse compensation error.

≤ Other than the inverse based approaches, the direct methods are also adopted in the literature for the hysteresis compensation without constructing the hysteresis inverse. However, there are few works reporting the performance comparisons between these two control strategies. Furthermore, the direct compensation methods usually need to adapt many hysteresis parameters, which significantly increases the computation burden.

≤ Most of the developed control methods in the literature are valid only for all the system states are measured except a few works [22,23]. However, for a given particular dynamical system, in most of the case, the exact knowledge of all the states is unavailable and the only accessible state is the output of the system. Therefore, it is necessary to develop control methods with observers to estimate the unavailable states from the measurements of a single output. How to fuse the hysteresis model, especially the PI-type model, with the available output-feedback control technologies to mitigate the hysteresis effect is still a challenge task.

Therefore, to address the above mentioned challenges, the objective of this dissertation is to propose an improved hysteresis model and design the inverse based control strategies so as to mitigate the hysteresis effect described by the proposed hysteresis model as well as ensure the global stability of the control systems, while tracking a desired trajectory with a certain precision. The performance of the inverse based controller will be compared with the direct method. In addition, this dissertation research also aims to design an output-feedback controller for the nonlinear systems preceded by the hysteresis nonlinearities.

## 1.2.2 Contributions of the Dissertation

This dissertation deals with the inverse based adaptive controller design for unknown nonlinear systems preceded by unknown hysteresis nonlinearities. The main contributions of the dissertation are highlighted as follows.

≤ For the purpose of enlarging the application of the PI model as well as facilitate the inverse model derivation with a strict theoretical proof, a modified generalized Prandtl-Ishlinskii (MGPI) model has been proposed in the dissertation research. Comparing to the PI model, the proposed MGPI model is able to describe a more general class of hysteresis shapes. Comparing to the GPI model, the concept of initial loading curve can be utilized, which makes it possible to obtain an analytical expression of the inverse MGPI model with the strict theoretical proof.

≤ Two essential properties, the wiping out property and the congruency property, for the modified generalized Prandtl-Ishlinskii model have been inspected. It has been shown that the modified generalized Prandtl-Ishlinskii model fulfills these properties. This result provides the necessary and sufficient conditions for the hysteresis nonlinearity to be represented by the proposed modified generalized Prandtl-Ishlinskii model.

≤ The analytical inverse of the MGPI model with both linear and nonlinear envelope functions has been derived based on a strict theoretical proof. The numerical implementation of the inverse model has been subsequently provided. The effectiveness of the inverse model has been verified in both the simulations and experiments.

≤ When the hysteresis is unknown, the analytical form of the inverse compensation error has been derived. The nonlinear part of the obtained inverse compensation error expression is proved bounded. Based on such an expression, the adaptive controllers can then be designed and the closed-loop stability analysis can be established based on the Lyapunov method.

≤ In this dissertation, the error expression of the inverse compensation has been fused with the adaptive variable structure controller design. The global stability of the system and tracking a desired trajectory to a certain precision are achieved without adapting the uncertain hysteresis parameters (except one parameter that corresponds to the bound of the inverse compensation error). Though the proposed approach incurs extra cost in implementing hysteresis inversion, it achieves gain in computational

efficiency. From the simulation results, it can be shown that, by taking consideration of error expression of the inverse compensation in the controller design, the inverse based scheme for the hysteresis compensation generates a superior transient performance over the direct approach without inverse constructions.

≤ When not all the system states are available, an inverse based adaptive output-feedback controller has been designed for nonlinear systems preceded by unknown hysteresis effect described by the MGPI model. A state observer has also been designed for the system states estimations. The global stability of the system has been guaranteed and the tracking accuracy has been ensured. The performance of the developed controller has been validated in both simulations and experiments.

### 1.3 Organization of the Dissertation

This dissertation is systematically organized in nine chapters. The topic of each chapter is briefly introduced as follows.

In Chapter 2, an exhaustive literature review of the mathematical models of the hysteresis nonlinearity and control methods of systems with the hysteresis effect will be provided.

In Chapter 3, an extensive review of the PI model and the GPI model will be presented. Then, a MGPI model will be proposed. Two essential properties, the wiping out property and the congruency property, of the proposed MGPI model will be investigated thereafter.

The analytical expression of the inverse MGPI model will be derived in Chapter 4 based on a strict theoretical proof. The numerical implementation of the inverse compensation will then be provided. The simulation results will also be included for the purpose of validation.

In Chapter 5, the analytical expression of the inverse compensation error of the MGPI model will be derived.

In Chapter 6, an adaptive variable structure controller with consideration of the expression of the inverse compensation error will be designed for the unknown nonlinear systems pre-

ceded with the unknown hysteresis described by the MGPI model. The stability analysis of the closed-loop control system will be given. The performance of the inverse based hysteresis compensation scheme will be compared with the direct method in simulation studies.

When the system states of the uncertain nonlinear systems which is preceded by unknown hysteresis nonlinearities cannot be fully measured from the output, an inverse based adaptive output-feedback controller together with an state observer will be designed in Chapter 7. The stability analysis of the closed-loop system will be provided. The effectiveness of the proposed controller will be verified in simulations.

In Chapter 8, all the theoretical results obtained in previous chapters will be verified through the experiment studies.

The conclusion and the major contributions will be summarized in Chapter 9 together with the recommendations of the future work.

# Chapter 2

## Literature Review

The hysteresis nonlinearity exists in various fields, ranging from mechanical to economics, from physics to electronics, and from bioscience to terrestrial hydrology. In some areas, the hysteresis effects can bring the benefits. For instance, the hysteresis effect provides a mechanism that enhances the robustness of cell functions against random perturbations in cell-biology [24]. In marketing, the hysteresis effect may create a long-run investment benefit from marketing actions for the firms [25]. However, in most areas, the hysteresis effects are usually considered as the undesired influences. For example, the smart material based actuators, such as piezoelectric actuators [26,27], magnetostrictive actuators [28], and SMA actuators [10,29], in industrial control systems usually exhibit the hysteresis effects. Such non-smooth nonlinearities will considerably degrade the performance of these actuators, or even result in the control systems instability. Hysteresis is a multi-valued mapping. It is non-smooth, non-differentiable, and usually unknown. Therefore, it is difficult to mitigate its harmful effects by using the existing traditional control approaches. In recent decades, control of systems exhibiting the hysteresis effects becomes to an interesting topic and great challenge. In this dissertation, the research will focus on analyzing and modeling the hysteresis characterization in the smart based actuators and designing the controllers for the nonlinear plants preceded by smart material based actuators.

## 2.1 Hysteresis Nonlinearity

The word “hysteresis” comes from a Greek work “hysterein” which means “to lag behind”. However, with the development of the hysteresis studies, the definitions of hysteresis have been interpreted by a number of researchers and varies from area to area and from paper to paper. Usually, one may refer to a relation between two scalar time-dependent quantities that cannot be expressed in terms of a single-valued function, but take the form of loops [12]. As pointed out by I. D. Mayergoyz [7], this description may be misleading and can create the impression that the looping is the essence of hysteresis. In this work, the definition of hysteresis which was introduced by a Scottish physicist, Alfred Ewing, is adopted in order to avoid the confusion and ambiguity [30].

### **Definition of Hysteresis**

*When there are two quantities  $M$  and  $N$ , such that cyclic variations of  $N$  cause cyclic variations of  $M$ , then if the changes of  $M$  lag behind those of  $N$ , we may say that there is hysteresis in the relation of  $M$  and  $N$ .*

The hysteresis nonlinearity has some essential characteristics, such as memory, wiping-out, congruency, minor and major loops, and so forth.

First of all, the principal characteristic of hysteresis is the memory. It can be described that the output of the hysteresis nonlinearity not only depends on the current input value, but also influenced by the previous history of the inputs.

Another significant property of the hysteresis is wiping-out which is closely related to the memory. Any local maximum of the input value wipes out the memory impressed by previous smaller local maxima. Similarly, any local minimum of the input function wipes out the memory impressed by previous larger local minima.

The congruency property means that, regardless of the input history, the minor loops caused by the same input range are congruent. The congruency property and the wiping-out property are two essential properties of the hysteresis nonlinearity.

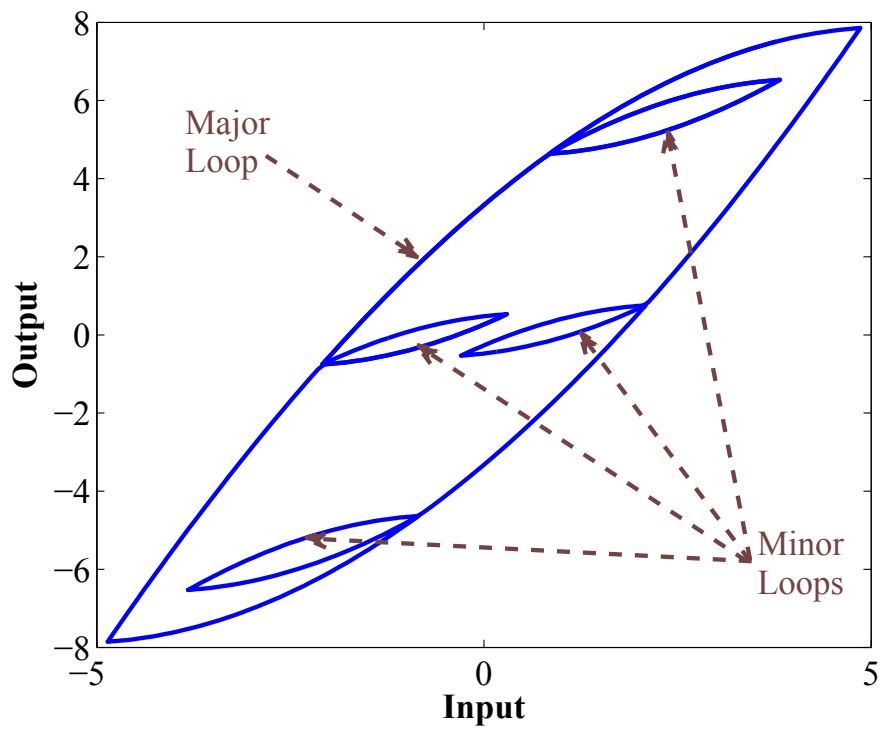


Figure 2.1: Major and minor loops of hysteresis nonlinearity.

The major hysteresis loop is the contour of the hysteresis region and the minor loops exist inside the major loop, as shown in Fig.2.1. It should be noticed that although the major and minor loops are widely occur in the hysteresis nonlinearities in smart material based actuators, not all the hysteresis model can produce the minor loops.

The hysteresis effect can also be characterized by either rate-independent or rate-dependent models. The hysteresis is rate-dependent if the output of the hysteresis effect is not only dependent on the past input extremum, but also determined by the rate of change of the input variation between the extreme points. On the other hand, the rate-independent hysteresis means that the output of the hysteresis only influenced by the history of input extremum.

Besides the above mentioned properties, the hysteresis loops can be described as symmetric loops and asymmetric loops. The hysteresis nonlinearities in some of the smart material based actuators, such as piezoelectric actuators, possess close symmetric shapes. In some other smart material based actuators, i.e., magnetostrictive actuators, the asymmetric hysteresis loops are observed. Furthermore, some smart material based actuators, such as the two-wire SMA actuators, possesses the output saturation.

## 2.2 Hysteresis Models

Hysteresis nonlinearities in the smart material based actuators usually lead to the poor performances of control systems. Therefore, control of the systems preceded with the hysteresis effects becomes to an important topic and attractive challenge in the control system area. In order to describe the hysteresis nonlinearities so as to facilitate the hysteresis compensation, several hysteresis models have been proposed in the literature since the end of 19th century. Generally, the hysteresis models can be classified into two categories, physic-based models [31, 32] and phenomenological models [3, 8, 9, 11, 33–36].

The physic-based hysteresis models are built on first principles of physics. They are derived based on the comprehensive knowledge of the physical phenomenon, for instance

displacement, energy, or stress-strain relationship. In [31], Jiles and Atherton proposed a physic-based hysteresis model, the Jiles-Atherton (J-A) model, on the basis of observed physical properties of ferromagnetic materials. The J-A model is widely used in modelling ferromagnetic hysteresis [37,38] since it is capable of exhibiting all of the main features of hysteresis in ferromagnetic hysteresis such as the initial magnetization curve, saturation of magnetization, coercivity, and hysteresis loss. Another physic-based hysteresis model has been proposed by Basso and Bertotti in [32] to simulate the magnetic component part in a power electronic converter. Furthermore, an electromechanical piezo model, based on physical principles, is presented in [39] to describe the hysteresis exhibits in the piezoelectric actuator. Since the physic-based hysteresis models are usually very complicated and limited to specific physics or structures, this kind of models is very difficult for applying to various materials and actuators in the industry.

The phenomenon hysteresis models, on the other hand, do not require the knowledge of the physical phenomenon. They are used to produce the similar behaviour to those physical systems that possess hysteresis. Most of the phenomenon hysteresis models were initially proposed to describe the hysteresis effects in specific material or physical systems and then extended to a general expression for the application in other systems. These models can predict the hysteresis accurately as well as facilitate the design of controller for compensating the hysteresis effect. The most popular phenomenon hysteresis model is the Preisach model. The Preisach model, which can be considered as a superposition of elementary hysteretic “relay” operators, was initially developed to describe hysteresis in the ferromagnetic material [8,40]. However, in the recently decades, the Preisach model has undergone many enhancements to enlarge its application range. It has been shown by many experimental setups that the Preisach model can be used to characterize the hysteresis nonlinearities in various smart material based actuators, such as magnetostrictive [28], piezoceramic [41–43], and SMA actuators [44,45]. As a further development of the Preisach model, the Krasnoselą̀skii-Pokrovskii (KP) model was proposed in 1970s. Instead of the “relay operator”, the KP model is defined based on the Lipschitz continuous KP operators. The KP model has been used

to model the hysteresis effects in different smart material based actuators [46, 47]. Similar to the Preisach model and the KP model, the Prandtl-Ishlinskii (PI) model, early proposed in [48, 49], is constructed based on the continuous play or stop hysteresis operators. The detailed discussion of the PI model can be found in [12, 50]. The PI model is usually used to describe a certain class of hysteresis effects, such as symmetric, rate-independent, and non-saturated hysteresis. The utilization of Preisach model and the PI model to describe the hysteresis nonlinearity in piezoelectric actuators can be found in [51]. In recent years, several significant improvements have been proposed so as to expand the applicants of the PI model. Al Janaideh *et al.* have proposed a rate-dependent PI model based on the integration of the rate-dependent play operators with the dynamic thresholds in [52]. To express the asymmetric hysteresis, a modified PI model has been reported in [16]. The improved model is defined based on a combination of two asymmetric operators which can independently simulate the ascending branch and descending branch of hysteresis. Kuhene and Janocha [53] modified the play operator by combining the one-sided dead-zone operator so as to describe the asymmetric hysteresis nonlinearity. In [19], a generalized PI (GPI) model has been proposed by introducing the envelope functions. The GPI model can be used to describe both the asymmetric and saturated hysteresis nonlinearity.

Besides the above mentioned operator based phenomenon hysteresis model, some hysteresis models are defined in the form of differential equations. The most accepted differential equation models are the Duhem model and the Bouc-Wen model. The development of the Duhem model dates from 1897 [54] and focusses on the fact that the output can only change its character when the input changes direction. It has been shown that the Duhem model is useful in applied electromagnetics [55, 56]. The Bouc-Wen model proposed by Bouc in [57] and extended by Wen in [36] is an nonlinear differential equation-based model. This model is widely used to describe the hysteresis effect between the applied displacement and the output force in wide range of mechanical systems [6]. In particular, the Bouc-Wen model has been applied to express the hysteresis in piezoelectric elements [58, 59], magnetoheological dampers [60], and wood joints [61].

## 2.3 Hysteresis Compensation

In recent decades, more and more smart material based actuators have been used in control systems. Such devices can offer high resolution of displacement and can be used in microposition applications. However, the hysteresis effect exhibited in smart materials may cause the undesirable inaccuracy or oscillation, or even instability in the control systems [3]. In this case, the demand of compensating the hysteresis effect has received considerable attentions. Since the hysteresis effect is an non-smooth and non-differentiable nonlinearity, the traditional control methods for nonlinear system are insufficient to solve such a problem. Therefore, the new nonlinear control approaches are required. The control approaches for hysteresis compensations can be generally classified into two categories, the inverse-based methods and the direct methods. The representative works of both categories will be reviewed in this section.

### 2.3.1 Inverse-based Methods

In the literature, the most common method to compensate the hysteresis nonlinearity is to construct the inverse model of the hysteresis model, which is pioneered by Tao and Kokotovic [3] in 1995. As shown in Fig. 2.2, for a given reference input signal, an inverse model is cascaded to the hysteresis model as a feedforward hysteresis compensator so that, theoretically, the compensated output of the open-loop system can track the reference input signal. In Tao and Kokotovic's work, an adaptive control algorithm was developed to mitigate the hysteresis nonlinearity of a system consisting of a linear plant and a hysteresis characteristic as its input. An adaptive hysteresis inverse was constructed when hysteresis nonlinearity is described in a regular shapes and cascaded with the plant to cancel the hysteresis effect and stabilize the linear plant. Motivated by this work, numbers of inverse model-based approaches have been addressed in literature. Among these works, the main challenge is how to construct the inverse hysteresis model for a general hysteresis models. The inverse compensation methods of the Preisach model, the KP model and the PI model will be reviewed

as follows.



Figure 2.2: Inverse feedforward controller for hysteresis nonlinearity.

As introduced in the previous section, the Preisach model is one of the most popular and widely used hysteresis models. Compensation of hysteresis represented by Preisach model has been studied by many researchers. In [62], Ge and Jouaneh have derived a feedforward computer-based tracking control approach to mitigate the hysteresis effect described by the Preisach model in a piezoceramic actuator. They also designed a PID feedback control to adjust the control error. By fusing the PID feedback control and the tracking approach in the feedforward loop, the results showed that the system can track the desired sinusoidal trajectory successfully. The system had better time and frequency tracking characteristics and smaller tracking error than using a regular PID controller alone. If the reference signal frequency is low enough, the control accuracy is mainly limited by the control system hardware. However, the controller addressed in this work is only valid for tracking sinusoidal reference signals and requires resetting for different inputs. An integrated inversion-based approach to compensate creep, hysteresis and vibrations of piezoactuators in Scanning Probe Microscopy (SPM) applications has been proposed in [63]. Rather than modeling the Preisach model and then constructing its inverse model, the authors directly implement the inverse hysteresis model using the Preisach approach. N. Takahashi *et al.* [64] have proposed an approach to employ the Preisach model itself as the inverse model to compensate another Preisach model. Nevertheless, such an operator, strictly speaking, cannot be considered as the inverse of the original operator because of the congruency property [65]. Tan and Baras [28] have proposed a new dynamic hysteresis model for magnetostrictive actuator by coupling a Preisach model and an ordinary differential equation. This dynamic model described the hysteresis effect in the

magnetostrictive actuator as well as the eddy current loss and the magnetoelastic dynamics of the magnetostrictive rod. The inverse Preisach model with an adaptive controller is then developed to compensate the hysteresis nonlinearity. In a more recent paper [66], a unified approach is presented to obtain fast inversion of a broad class of Preisach-type model by exploiting the massive parallelism offered by field-programmable gate arrays. In [67], the authors compare the performance of inverse-based compensation of both the physics-based Jiles-Atherton model and phenomenon-based Preisach model in terms of the identification complexity, the runtime, and the space efficiency of the control-oriented implementation. It turns out that the Preisach model works smoothly in the control framework and performance robust while the Jiles-Atherton model shows significant advantage in the space and runtime complexity. Xiao and Li [68] have proposed a novel modified inverse Preisach model featured with weight sum of  $\mu$ -density functions based on the linearity property. The proper  $\mu$ -density functions and weights are determined by the fast Fourier transform. The effectiveness of the developed inverse model has been verified on a piezoceramic actuator. It has been shown that the proposed open-loop hysteresis adjust method dramatically improves the tracking accuracy of the piezoceramic actuator for the multifrequency composed signals. The Preisach model was also used to model the rate-dependent hysteresis nonlinearity of a Giant Magnetostrictive Actuator (GMA) in [69]. A PID feedback controller combined with an inverse compensation in the feedforward loop was proposed for the tracking control in this work.

In addition to the investigation of inverse Preisach model, the inverse-based compensation methods of Krasnosel'skii-Pokrovskii (KP) model have also been studied. Webb *et al.* [10] have proved that an exact inverse under a condition of the value of the rise constant of kernel functions for the parameterized KP model exists. This inverse model has been combined with adaptive laws for implementing the parameters on-line identification and for eliminating the hysteresis effect. In another work [70], Galinaitis and Rogers proposed an approximate KP model to describe the hysteresis in a piezoelectric stack actuator. The inverse model was also developed and verified through the computer simulation. In [71], an inverse KP

model has been constructed for an off-line KP approximate model of the unknown hysteresis. Furthermore, an adaptive control algorithm was designed to update the model parameters so as to ensure that the tracking error asymptotically converges to zero.

It is worth to be mentioned that the inverse models of Preisach model and the KP model are usually derived using numerical methods. Although the compensation performance by using numerical inverse models is satisfied under some particular conditions, the limitations still can not be overlooked. First of all, the numerical inverse is only an approximate inverse so that the compensated system usually exist uncertain inversion errors. In this case, the stability of the closed-loop control system comprising the controlled plant preceded by the numerical inverse compensation cannot be established. Second, in order to obtain the numerical inverse model, the outputs of the actuators are usually required to be known. However, in most of the practical control systems in the industries, the actuators are embedded in the plants and the output of the actuators are impossible to be measured directly. Third, the numerical inverse of a hysteresis model cannot be considered to be unique and one inverse model can only be applied to the specified input and initial conditions. In addition, because of the complexity of the hysteresis models, the derivations of numerical inverse models are computationally intensive.

Comparing to Preisach model and KP model, the Prandtl-Ishlinskii (PI) model is well known because of its unique analytically invertible property. In [15], a feedforward controller designed based on the inverse of PI model has been addressed to remove the hysteresis effect in piezoelectric actuators. In their work, the analytical expression of the inverse PI model has been derived for the first time. The knowledge of the exact description of inverse PI model and thus the compensation error would facilitate the design of robust controllers and stability analysis. In [72], the inverse of PI model was applied with a smooth robust adaptive controller with the hyperbolic tangent function for the compensation of hysteresis effect described by the PI model. An adaptive inverse strategy was proposed in [73] to compensate the discrete PI model without any prior knowledge of the PI model. The unknown hysteresis parameters were identified online by the least mean square method or the gradient method.

In [74], an inverse rate-dependent Prandtl-Ishlinskii model has been utilized for feedforward compensation of the rate-dependent hysteresis nonlinearities in a piezomicropositioning stage over different excitation frequencies. The proposed inversion holds under the condition that the distances between the threshold do not decrease in time. Moreover, a modified PI model has been introduced in [53, 75] to describe a more complex hysteretic actuator nonlinearities. This modified PI model was the combination of the backlash operators and the one-side deadzone operators. The inverse model was also derived to compensate the hysteresis effect. The above result has been applied in [18] on a piezoelectric-actuator system. To reduce the inverse compensation error and the system uncertainty and disturbances, a sliding model controller was designed. The experimental results on a nano-stage verified the effectiveness of this method. In [19], a generalized PI model has been proposed to describe a more general class of hysteresis shapes. The corresponding inverse compensator to this generalized PI model has been reported in [20]. The effectiveness of the inverse GPI model has been verified in the experiment though the strict theoretical proof of the inverse model derivation was missing.

Other than the above mentioned inverse approaches, neural networks and fuzzy-based models are also proposed to compensate the hysteresis effect by constructing the corresponding inverse models through the neural networks and fuzzy logics, respectively [76–78]. For the case when not all the system states are available, the inverse compensation has been combined with the observer-based adaptive output-feedback controller. In [23, 79], the authors proposed an inverse-based adaptive output-feedback controller for the dead-zone and the backlash nonlinearity, respectively. Besides the phenomenological models, the inverse models are constructed as well for the physic-based models. In [80], the inverse of the Ferromagnetic material hysteresis model was constructed to mitigate the hysteresis nonlinearity in the Piezoelectric actuators. A more exhaustive review of inverse model-based methods for hysteresis compensation can be found in [65].

### 2.3.2 Direct methods

Due to the complexity of hysteresis properties, especially the multi-branches property and the non-smoothness, the compensation methods based on inverse models are usually complicated, computationally costly and strongly sensitive to unknown modeling errors and measurement errors. These issues will directly cause the difficulty of system stability analysis excepted for certain special cases [3]. To overcome the disadvantage of inverse compensation approaches, a number of control methods, such as robust adaptive control [1, 13, 81–83], energy-based control [44], and sliding mode control [84–86], have been proposed without constructing the inverse models. Su *et al.* have dealt with the hysteresis represented by PI models in [1, 81]. In their works, the PI model was fused with the robust adaptive control approach without deriving the inverse model. The proposed controllers lead to the desired output and the global stability. The developed controller has been further substantiated in the experiment in [87]. In [88], the above proposed controller has been extend to be applied on a SMA micro-actuators based flap positioning system. Moreover, in [89], an adaptive robust control strategy has been proposed for the GPI model without constructing the inversion. Passivity-based stability and control of hysteresis were attempted by Gorbet and Pare [44, 90]. Pare [90] proposed a transformation which convert the hysteresis in to a passivity operator, and then, developed a simple stability theorem. In [44], Gorbet derived a passivity property of the Preisach model and designed an energy-based approach to mitigate the hysteresis effect. The direct compensation methods avoid the mathematical complex in constructing the inverse model. However, this kind of approaches may lead to computational burden of adapting the hysteresis parameters and inferior transient performance of the control systems.

Besides the control methods discussed before, the compensation of differential hysteresis models were also studied. In [91], Su *et al.* have developed an adaptive control of a class of nonlinear dynamics systems preceded by unknown backlash-like hysteresis nonlinearities, which was represented by Duhem model, without constructing the inverse. The adaptive laws ensured the global stability and high precision of tracking. The compensation methods for hysteresis described by Bouc-Wen model have been investigated in [26, 92].

# Chapter 3

## Modified Generalized Prandtl-Ishlinskii (MGPI) Model

The hysteresis nonlinearities exhibit widely in the smart material based actuators, which may lead to the inaccuracy, oscillation or even instability of the control systems. In order to describe the hysteresis nonlinearities in the smart actuators so as to facilitate the compensation, a number of hysteresis models have been proposed in the literature. The Prandtl-Ishlinskii (PI) model is one of the most popular hysteresis models and is well known because of its unique invertibility. The inverse model can be considered as a feedforward compensator to mitigate the hysteresis effects in the control systems. The PI model has been applied in the control systems to describe the hysteresis effects in various smart material based actuators, especially the piezoelectric actuators [27,93]. However, the limitations of the PI model are obvious. First, the PI model will yield considerable errors when describe the asymmetric hysteresis loops which are observed in the output-input properties of the SMA [94] and magnetostrictive actuators [95]. In addition, the PI model usually fail to describe the output saturation of the hysteresis loops in the smart material based actuators. In [19], a generalized Prandtl-Ishlinskii (GPI) model has been proposed to overcome the limitations of the PI model by introducing envelope functions. The GPI model can describe

both the asymmetric and saturated hysteresis loops. However, based on the definition of the GPI model, the inverse model cannot be obtained with the strict theoretical proof due to the difficulty of the initial loading curve construction. In this chapter, the GPI model is re-defined and a modified generalized Prandtl-Ishlinskii (MGPI) model will be proposed which can still describe similar general class of hysteresis shapes. The benefit is that the concept of initial loading curve can be utilized, based on which a strict analytical inverse model can be derived for the purpose of compensation. Two essential properties, the wiping out property and the congruency property, will be validated for the proposed MGPI model.

Before introducing the MGPI model, the definitions of the PI model and the GPI model will be reviewed.

## 3.1 Prandtl-Ishlinskii Model

The PI model can be considered as the weighted superposition of the elementary hysteresis operators, i.e., the play operators. The definition and the properties of the play operators will be addressed as follows.

### 3.1.1 The Play Operator

The one dimensional play operator can be considered as a free-to-move cylinder of length  $2r$  and a moving piston as shown in Fig. 3.1. The output  $w(t)$  is the position of the center of the cylinder and the input  $v(t)$  represents the piston position.

According to the definition in [12], the description of the play operator  $F_r[v](t)$  from the mathematical point of view can be given as follows.

Let  $C_m[0, t_E]$  denotes the space of the piecewise monotone continuous function.  $0 = t_0 < t_1 < t_2 < \dots < t_N = t_E$  are intervals in  $[0, t_E]$ . For any piecewise monotone input function  $v(t) \in C_m[0, t_E]$  such that  $v(t)$  is monotone on each of the subintervals  $[t_i, t_{i+1}]$  where  $i = 0, 1, 2, \dots, N-1$ , the play operator  $w(t) = F_r[v](t)$  with threshold  $r \in [0, \infty)$  and

initial value  $\omega_{-1}$  is defined by

$$\begin{aligned} w(0) &= F_r[v](0) = f_r(v(0), \omega_{-1}), \\ w(t) &= F_r[v](t) = f_r(v(t), w(t_i)) \end{aligned} \quad (3.1)$$

where

$$f_r(v, w) = \max\{v - r, \min\{v + r, w\}\} \quad (3.2)$$

for  $t_i < t \leq t_{i+1}$ ,  $0 \leq i < N$ .

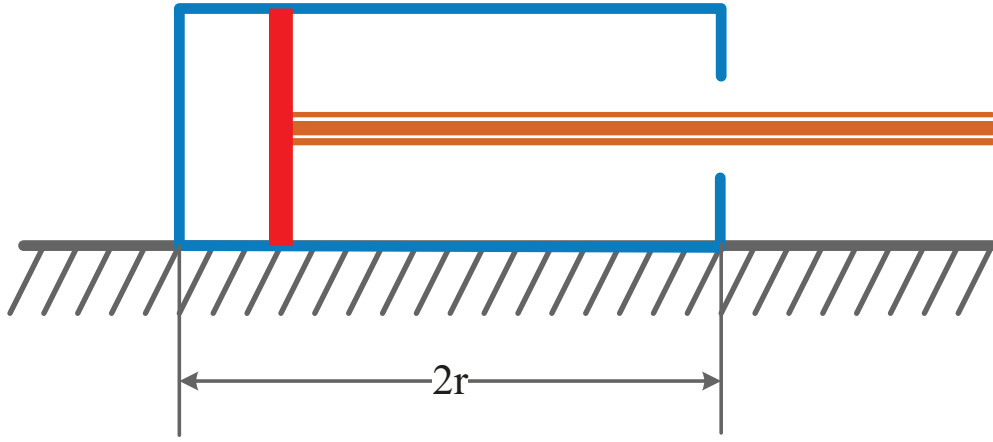


Figure 3.1: A piston with plunger of length  $2r$ .

The argument of the operator is written in square brackets to indicate the functional dependence, since it maps a function to a function.

The play operator has the rate-independent memory. It means that the output of this operator is only determined by the current input value and the past extrema of input function  $v(t)$ . The velocity of input variation between each extreme will not affect the shape of input-output relationship. The input-output relationship of play operator  $F_r[v](t)$  can be expressed in Fig. 3.2.

Some of the significant properties of the play operator are briefly reviewed as follows.

$\leq$  **Lipschitz-continuity**

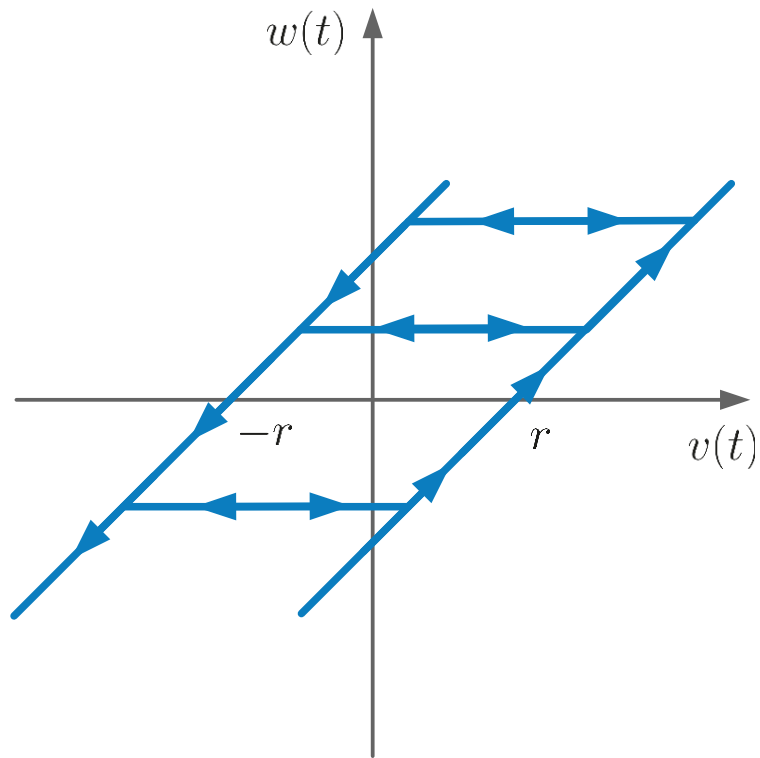


Figure 3.2: Input-output relationship of play operator  $F_r[v](t)$ .

For a given  $v(t)$  and  $r \geq 0$ , the output of the play operator is Lipschitz-continuous [12, 35], which is important for the inverse construction of the PI model.

### ≤ **Rate-independence**

The branches of the play operator are only determined by the past input extrema. The velocity of input variation between each extremum will not affect the shape of the branches, i.e.,

$$F_r[v \bullet \alpha] = F_r[v] \bullet \alpha \quad (3.3)$$

where  $\alpha$  is a continuous increasing function,  $\alpha : [0, T]$ , satisfying  $\alpha(0) = 0$  and  $\alpha(T) = T$ .

### ≤ **Counter-clockwise**

The play operator creates the counter-clockwise input-output trajectories.

## 3.1.2 Prandtl-Ishlinskii Model

The Prandtl-Ishlinskii model, a operator-based phenomenological hysteresis model, is defined as a weighted superposition of a number of play operators. The analytical formula of the PI model  $\Pi[v]t$  utilizing the play operator  $F_r[v](t)$  is defined by

$$\Pi[v](t) = p_0 v(t) + \int_0^\infty p(r) F_r[v](t) dr \quad (3.4)$$

where  $p_0$  is a positive constant and  $p(r)$  is an integrable density function. This density function satisfies  $p(r) \geq 0$  with  $\int_0^\infty r p(r) dr < \infty$ . It represents the distribution of the weighting for the play operators with distinct thresholds  $r$  and vanishes when  $r$  is sufficient large. With the defined density function, the PI model maps  $C[t_0, \infty)$  to  $C[t_0, \infty)$ , i.e., the Lipschitz continuous input will lead to the Lipschitz continuous output [11]. Since the density function  $p(r)$  vanishes when  $r$  is sufficient large, the choice of  $R = \infty$  as the upper limit of the integration is widely accepted and used in the literature for the sake of convenience [12].

As an illustration, Fig. 3.3 shows the input-output relationship of the PI model given in (3.4), with  $p_0 = 5$  and  $p(r) = 5e^{-0.0014r}$ , for  $r \in [0, 90]$ , under the input signal  $v(t) =$

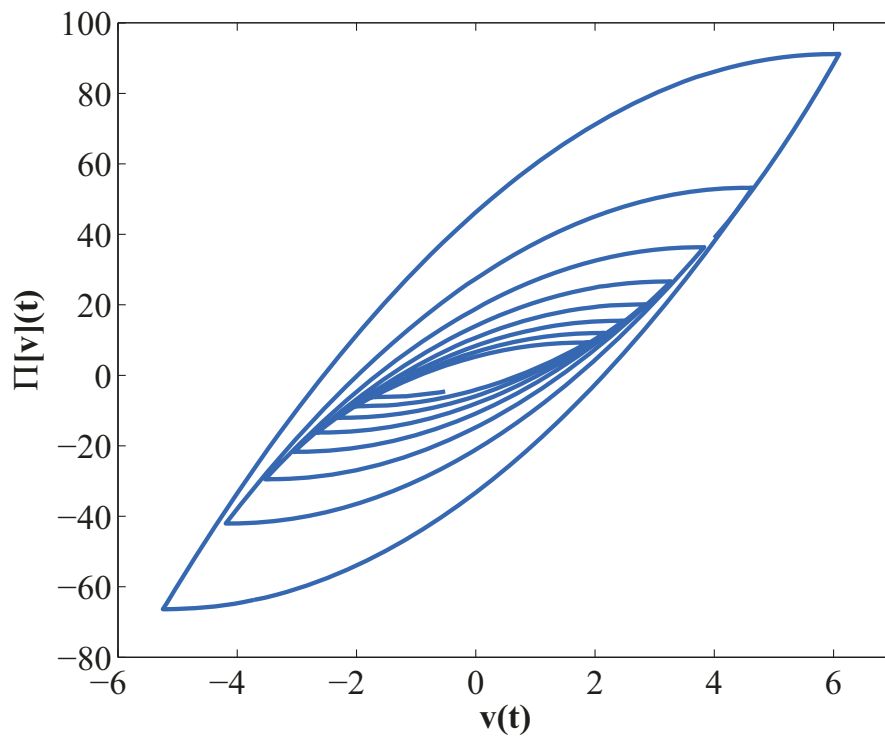


Figure 3.3: An example of PI model under  $v(t) = \frac{5\sin(1.6\pi t)+4\cos(4.8t)}{1+0.4t}$ ,  $t \in [0, 10]$ .

$\frac{5\sin(1.6\pi t)+4\cos(4.8t)}{1+0.4t}$ , for  $t \in [0, 10]$  with initial value  $\omega_{-1} = 0$ . It can be shown that the PI model generates the hysteresis curves. The hysteresis described by the PI model is symmetric and non-saturated.

## 3.2 Generalized Prandtl-Ishlinskii Model

Although the PI model has been widely applied to represent hysteresis nonlinearity for different smart materials, its limitations are still obvious. It can only describe a certain class of hysteresis shapes. For the asymmetric or saturated hysteresis loops which are usually observed in various smart actuators and ferromagnetic materials, the PI model is insufficient to describe. To overcome the limitations of the PI model, a generalized Prandtl-Ishlinskii (GPI) model has been proposed in [19]. Comparing to the PI model, the proposed GPI model has enhanced the prediction ability of the PI model, particularly in the content of the above named nonlinearities, by defining an alternate play operator, the generalized play operator.

### 3.2.1 The Generalized Play Operator

For any piecewise monotone input function  $v(t) \in C_m[0, t_E]$  such that  $v(t)$  is monotone on each of the subintervals  $[t_i, t_{i+1}]$  where  $i = 0, 1, 2, \dots, N-1$ , the generalized play operator  $w_g(t) = G_r[v](t)$  with threshold  $r \in \mathbb{R}$  and initial value  $\omega_{g-1}$  is defined by

$$\begin{aligned} w_g(0) &= G_r[v](0) = g_r(v(0), \omega_{g-1}), \\ w_g(t) &= G_r[v](t) = g_r(v(t), w_g(t_i)) \end{aligned} \quad (3.5)$$

where

$$g_r(v, w) = \max\{\gamma_r(v) - r, \min\{\gamma_l(v) + r, w\}\} \quad (3.6)$$

for  $t_i < t \leq t_{i+1}$ ,  $0 \leq i < N$ . Comparing to the play operator defined in (3.1) and (3.2), the envelope functions  $\gamma_r(v)$  and  $\gamma_l(v)$  are introduced, which are strictly increasing and fulfill

that  $\gamma_l(v) \subset \gamma_r(v)$ . It is these envelope functions that make it possible to describe a more general class of hysteresis shapes.

### 3.2.2 Generalized Prandtl-Ishlinskii Model

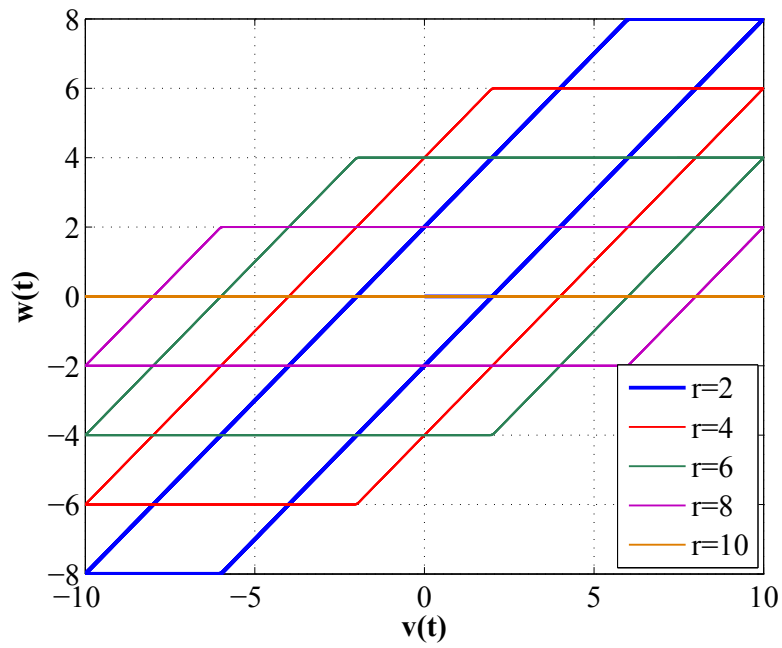
The generalized PI model  $\Pi_g[v](t)$  utilizing the generalized play operator  $G_r[v](t)$  is defined in [19] as follow.

$$\Pi_g[v](t) = \int_0^R p_g(r)G_r[v](t)dr \quad (3.7)$$

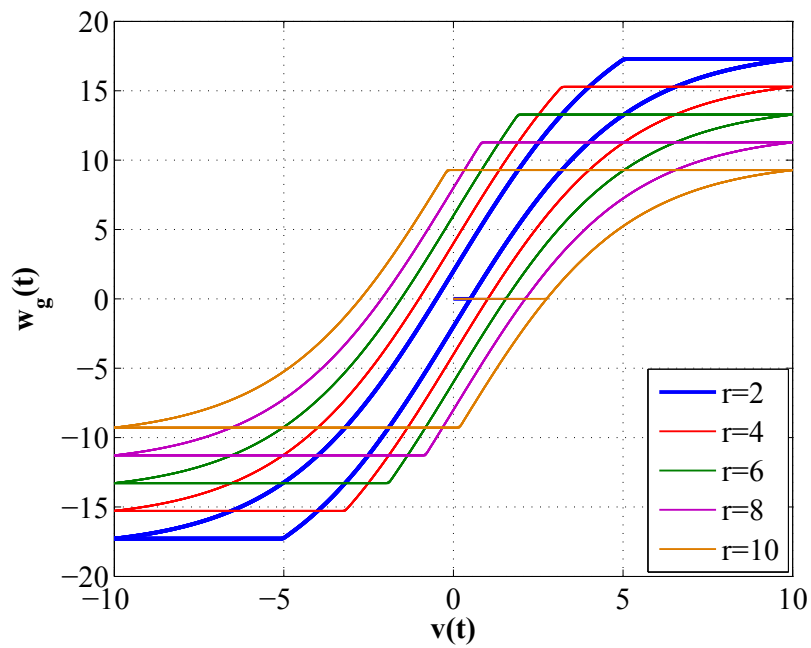
where  $p_g(r)$  is an integrable density function satisfying  $p_g(r) \geq 0$  with  $\int_0^\infty rp_g(r)dr < \infty$ . Since the generalized play operator  $G_r[v](t)$  is Lipschitz continuous and density function  $p_g(r)$  is integrable, the generalized PI model  $\Pi_g[v](t)$  is Lipschitz continuous for a given input  $v(t) \in C_m[0, t_E]$ .

With these envelope functions, it is possible for the generalized PI model to describe a more general class of hysteresis shapes. However, the introduction of the envelope functions in the generalized play operator (3.5) has changed the meaning of the threshold  $r$ . Fig. 3.4 shows the outputs of both the play operators and the generalized play operators with various choices of threshold  $r$ . In the classic play operator (3.1) and (3.2), the  $r$  is the threshold for the input signal itself. However, in the definition of the generalized play operator (3.6), it is obvious that  $r$  becomes the threshold for the functions  $\gamma_r(v)$  and  $\gamma_l(v)$ , rather than the input signal itself. In this case, the value  $r$  no longer directly related to the input signal itself, causing difficulty for construction of an initial loading curve.

To remedy this difficulty, the definition of the generalized PI model is required to be modified. As the further development, the modified generalized Prandtl-Ishlinskii model (MGPI) is proposed as follows.



(a)



(b)

Figure 3.4: (a) The output of play operator with various thresholds  $r$ ; (b) The output of generalized play operator with various thresholds  $r$ .

### 3.3 Modified Generalized Prandtl-Ishlinskii Model

The modified generalized PI model is defined based on the modified generalized play operator which can be expressed as follows.

#### 3.3.1 The Modified Generalized Play Operator

For any piecewise monotone input function  $v(t) \in C_m[0, t_E]$  such that  $v(t)$  is monotone on each of the subintervals  $[t_i, t_{i+1}]$  where  $i = 0, 1, 2, \dots, N-1$ , the modified generalized play operator  $w_M(t) = G_{mr}[v](t)$  with threshold  $r \in \mathbb{R}$  and initial value  $w_{m-1}$  is defined by

$$\begin{aligned} w_M(0) &= G_{mr}[v](0) = g_{mr}(v(0), w_{m-1}), \\ w_M(t) &= G_{mr}[v](t) = g_{mr}(v(t), w_M(t_i)) \end{aligned} \quad (3.8)$$

where

$$g_{mr}(v, w) = \max\{\gamma_r(v - r), \min\{\gamma_l(v + r), w\}\} \quad (3.9)$$

for  $t_i < t \leq t_{i+1}$ ,  $0 \leq i < N$ . The envelope functions  $\gamma_r(v)$  and  $\gamma_l(v)$  are strictly increasing and fulfill that  $\gamma_l(v) \geq \gamma_r(v)$ . In the modified generalized play operator, the trajectories  $(v - r)$  and  $(v + r)$  of the classical play operator, not the input signal  $v(t)$  itself, are mapped directly into the envelope functions  $\gamma_r(v - r)$  and  $\gamma_l(v + r)$ , as shown in Fig. 3.5. The new cross-over values  $\zeta_1$  and  $\zeta_2$  are linearly related to  $r$ , i.e.,

$$\begin{aligned} \zeta_1 &= \gamma_r^{-1}(0) + r \\ \zeta_2 &= \gamma_l^{-1}(0) - r. \end{aligned} \quad (3.10)$$

With the increase of  $v(t)$ , the output of the modified generalized play operator increase along the trajectory  $\gamma_r(v - r)$ . When the input function  $v(t)$  decreases, the output of the modified generalized play operator decreases along another curve  $\gamma_l(v + r)$ . Therefore, the threshold  $r$  still works as the threshold of the input signal itself rather than the envelope

functions, which can also be observed by comparing Fig. 3.4(a) and Fig. 3.6 with various choices of threshold  $r$ .

The properties for the play operator in the PI model are still valid for the modified generalized play operator, which are listed as follows.

**$\leq$  Lipschitz-continuity**

If the envelope functions are Lipschitz-continuous, then the proposed modified generalized play operator is Lipschitz-continuous.

**$\leq$  Rate-independence**

The branches of the modified generalized play operator are only determined by the past input extrema. The velocity of input variation between each extremum will not affect the shape of the branches, i.e.,

$$G_{mr}[v \bullet \alpha] = G_{mr}[v] \bullet \alpha \quad (3.11)$$

where  $\alpha$  is a continuous increasing function,  $\alpha : [0, T]$ , satisfying  $\alpha(0) = 0$  and  $\alpha(T) = T$ .

**$\leq$  Counter-clockwise**

The modified generalized play operator creates the counter-clockwise input-output trajectories.

### 3.3.2 Modified Generalized Prandtl-Ishlinskii Model

The MGPI model is defined as a weighted superposition of the modified generalized play operators  $G_{mr}[v](t)$ . The analytical formula is given by

$$\Pi_m[v](t) = \int_0^R p_m(r) G_{mr}[v](t) dr \quad (3.12)$$

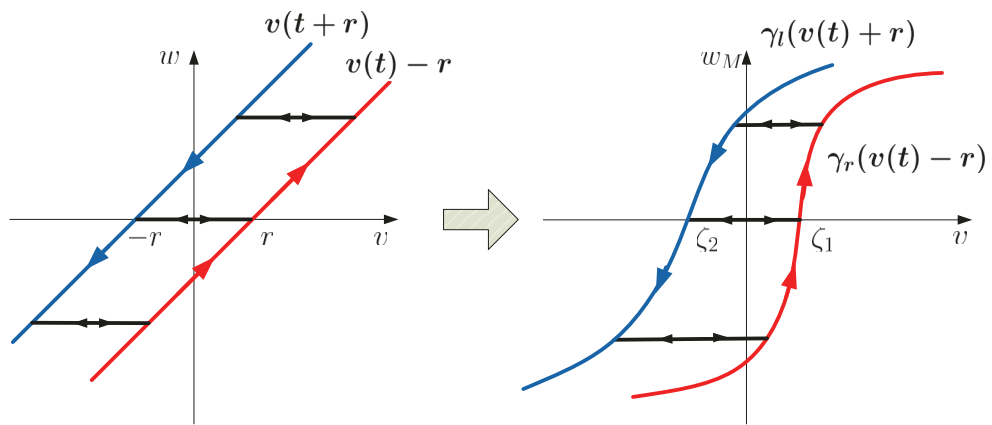


Figure 3.5: Mapping from the play operator to the modified generalized play operator

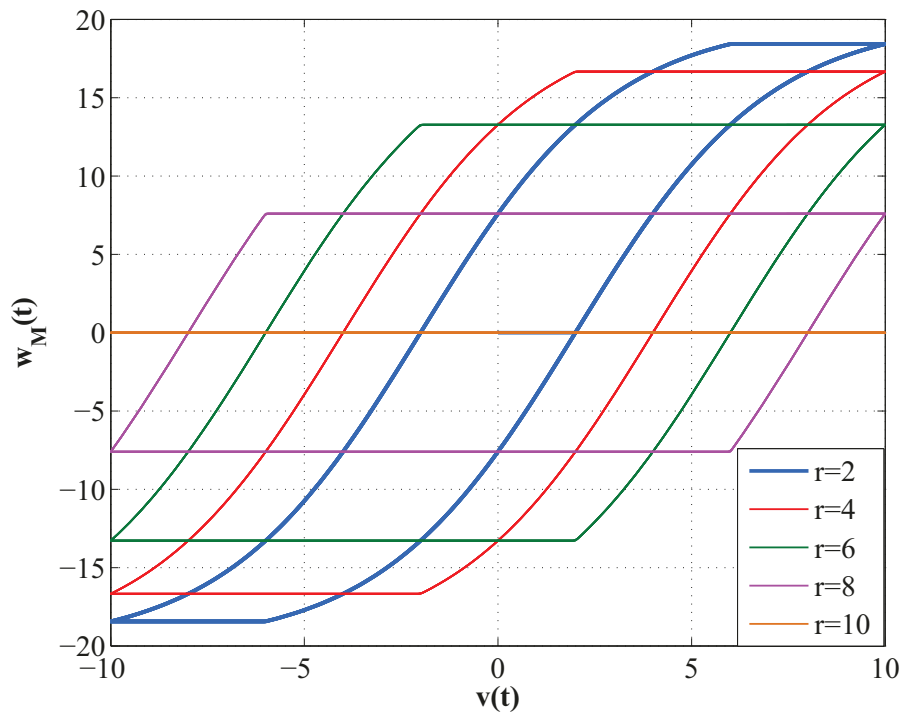


Figure 3.6: The output of modified generalized play operator with various thresholds  $r$ .

where  $p_m(r)$  is an integrable density function satisfying  $p_m(r) \geq 0$  with  $\int_0^\infty r p_m(r) dr < \infty$ . It represents the distribution of the weighting for the modified generalized play operators with distinct thresholds  $r$  and vanishes when  $r$  is sufficient large. The MGPI model is a Lipschitz-continuous, rate-independent, counter-clockwise hysteresis model.

**Remark:** If the envelope function are selected as  $\gamma_r(v) = v$  and  $\gamma_l(v) = v$ , the MGPI model will be the same as the classical PI model. Therefore, the PI model can be considered as a special case of MGPI model.

### 3.3.3 Some Examples of Modified Generalized Prandtl-Ishlinskii model

In this subsection, some examples of the MGPI model with various choices of envelope functions will be shown under a complex input function  $v(t) = 5\sin(1.6\pi t) + 4\cos(4.8t)$ ,  $t \in [0, 20]$ . The envelope functions selected for each example can be found in Table 3.1. The density functions of the proposed MGPI models are chosen as follows.

$$p_m(r) = 1.7e^{-0.36r}. \quad (3.13)$$

Table 3.1: Various envelope functions for MGPI model

Example 1	$\gamma_l(v) = v$ $\gamma_r(v) = v$
Example 2	$\gamma_l(v) = 2.4v$ $\gamma_r(v) = 2.4v$
Example 3	$\gamma_l(v) = \tanh(0.45v)$ $\gamma_r(v) = \tanh(0.45v)$
Example 4	$\gamma_l(v) = 20\tanh(0.15v + 0.1) - 0.5$ $\gamma_r(v) = 20\tanh(0.1v + 0.3)$

In Fig. 3.7(a), the MGPI model describes the same shape as the PI model does, which shows that the PI model is a special case of the proposed MGPI model. In Fig.3.7(b)

and 3.7(c), the envelope functions are chosen as linear and nonlinear functions respectively. Particularly, the MGPI model with nonlinear envelope function can describe the saturated hysteresis shapes. Furthermore, the MGPI model can also characterize the asymmetric hysteresis nonlinearity as shown in Fig. 3.7(d),

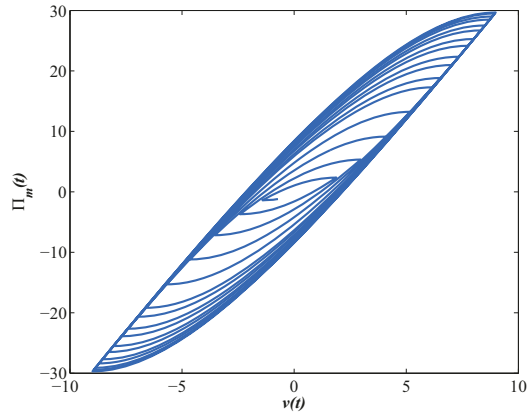
## 3.4 Wiping Out Property and Congruency Property of Modified Generalized Prandtl-Ishlinskii

As shown in the previous section, the proposed MGPI model can yield asymmetric as well as saturated minor and major input-output hysteresis loops. In this section, two essential properties, the wiping out property and the congruency property, will be validated for the developed MGPI model by following the similar procedure in [96]. These two properties are the necessary and sufficient conditions for the hysteresis nonlinearity to be represented by the proposed MGPI model on the set of piece-wise monotonic inputs [7].

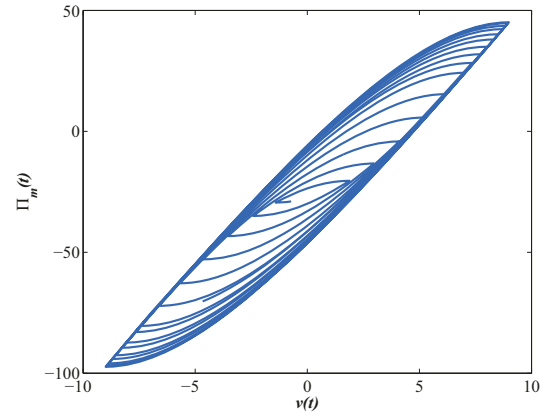
### 3.4.1 Memory Curve Structure

The memory curve of a hysteresis model is a curve that can reveal the state of this hysteresis model at each instant. Inspired by the Preisach plane [97], we construct a *MGPI plane* denoted by  $S = \{(\zeta_2, \zeta_1) : \zeta_1 \subset \zeta_2, \gamma_r(\zeta_1) = -\gamma_l(\zeta_2)\}$  for the given envelope functions to define the memory curve for the MGPI model. For the given envelope functions, there exists a unique modified generalized play operator  $w_M(t) = G_{mr}[v](t)$  for every point  $(\zeta_2, \zeta_1)$ . Let  $P \rightarrow S$  be a compact set and assume that the density function  $p_m(r)$  vanishes outside  $P$ . Define the domain  $P_+$  and  $P_-$  as  $P_+(t) = \{(\zeta_2, \zeta_1) / P : w_M(t) > 0\}$  and  $P_-(t) = \{(\zeta_2, \zeta_1) / P : w_M(t) < 0\}$ .

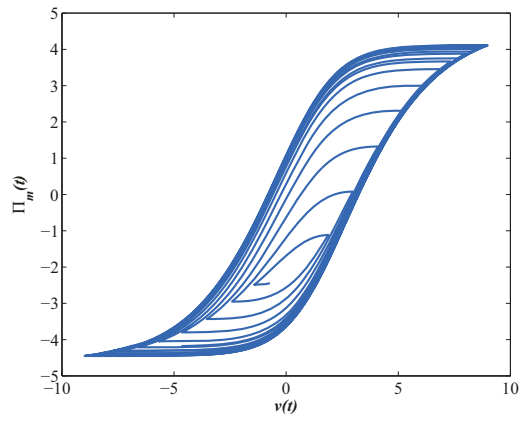
Suppose that all the outputs of modified generalized play operators are negative initially. First, the input signal increases monotonically to value  $v_1$  at time  $t_1$ . At this moment, all the modified generalized play operators with  $\zeta_1 < v_1$  have the positive outputs while the



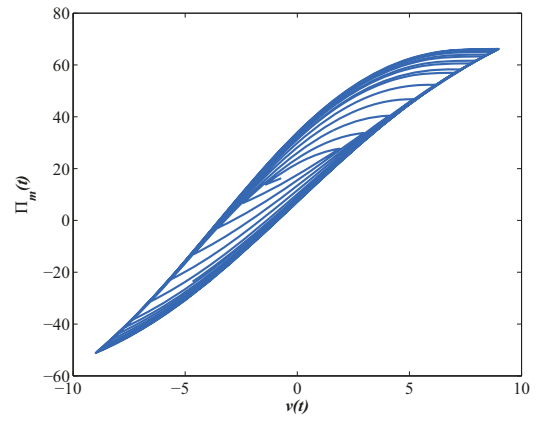
(a) Example 1



(b) Example 2



(c) Example 3



(d) Example 4

Figure 3.7: Examples of MGPI with different envelope functions

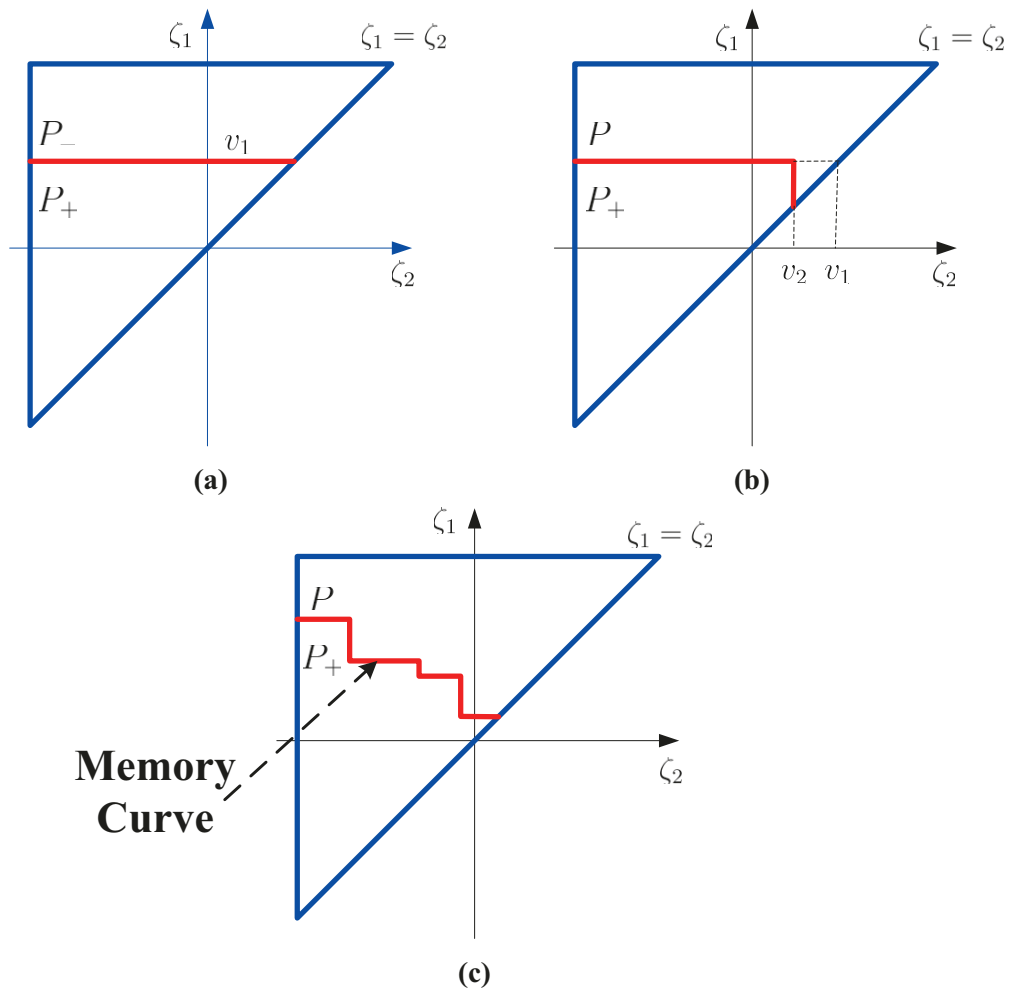


Figure 3.8: Memory curve structure.

others remain the negative outputs, as shown in Fig. 3.8(a). The boundary between  $P_+$  and  $P_-$  is called the memory curve. Next, the input signal decreases monotonically to value  $v_2$  at time  $t_2$ . Then, all the modified generalized play operators with  $\}(\zeta_2, \zeta_1) : \zeta_1 < v_1, \zeta_2 > v_2|$  and  $\zeta_1 > v_1$  have the negative outputs while the others have the positive outputs, as shown in Fig. 3.8(b). In this manner, an arbitrary, piecewise-monotone input can lead a memory curve that has the staircase structure, as shown in Fig.3.8(c). The corners of this memory curve represent all the extrema in the input history and the intersection of the memory curve with the line  $\zeta_1 = \zeta_2$  indicates the current input value.

### 3.4.2 Wiping Out Property

The wiping out property refers to the behavior that any local maximum of the input value wipes out the memory impressed by previous smaller local maxima. On the other hand, any local minimum of the input function wipes out the memory impressed by previous larger local minima. It can be attested that MGPI model fulfills the wiping out property.

First, it will be shown that the modified generalized play operator possesses the wiping out property. Fig. 3.9 shows an input signal  $v(t)$  (Fig. 3.9(a)) and the output of the modified generalized play operator defined in (3.8) (Fig. 3.9(b)).

In the beginning, the input  $v(t)$  increases from the initial value 0 to the first maximum value  $v_{1M}$ . The output trajectory of the modified generalized play operator increases through the curve  $(0, 0), (\zeta_1, 0)$  and arrives at  $(v_{1M}, w_{M_{1M}})$  as shown in Fig. 3.9(b). After that, the input function decreases from the value  $v_{1M}$  to its first minimum  $v_{1m}$ . The process takes the trajectory from point  $(v_{1M}, w_{M_{1M}})$  to  $(v_{1M'}, w_{M_{1M}})$ , and then to point  $(v_{1m}, w_{M_{1m}})$ . Then, the input function  $v(t)$  increases again to the second maximum value  $v_{2M}$ . Correspondingly, the output trajectory moves from point  $(v_{1m}, w_{M_{1m}})$  to point  $(v_{1m'}, w_{M_{1m}})$ , and after that, arrives at point  $(v_{2M}, w_{M_{2M}})$ . With the decrease of input  $v(t)$  to the second minimum value  $v_{2m}$ , the output of modified generalized play operator decreases again through the trajectory  $(v_{2M}, w_{M_{2M}}), (v_{2M'}, w_{M_{2M}})$  and  $(v_{2m}, w_{M_{2m}})$ . After reaching  $v_{2m}$ , the input rises again to

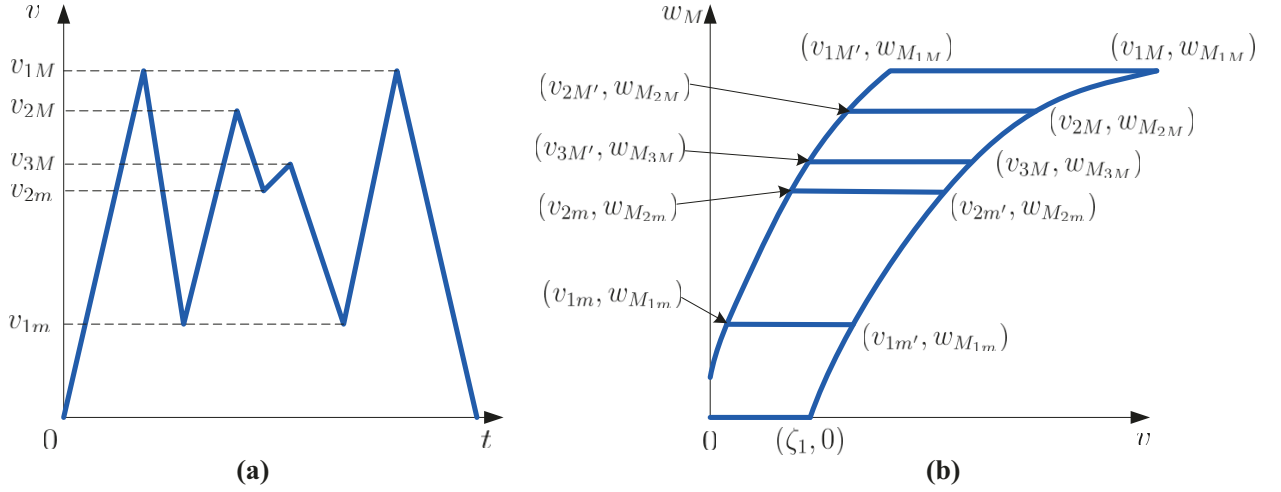


Figure 3.9: (a) The input signal  $v(t)$ . (b) The output  $w_M(t)$  of the modified generalized play operator.

the third maximum value  $v_{3M}$ , which leads the trajectory to travel from point  $(v_{2m}, w_{M_{2m}})$  to point  $(v_{2m'}, w_{M_{2m}'})$ , and then, to the point  $(v_{3M}, w_{M_{3M}})$ . Now, there are three maxima and three minima in the input history. Since all the maxima (minima) are smaller (larger) than the previous ones, no memory has been wiped out so far. However, when the input reduces to the fourth minimum which coincides with the first minimum  $v_{1m}$ , the trajectory travels from point  $(v_{3M}, w_{M_{3M}})$  to point  $(v_{1m}, w_{M_{1m}})$  via point  $(v_{3M'}, w_{M_{3M}'})$  and wipes out the memory of  $v_{1m}$  and  $v_{2m}$  successfully. After reaching the last maximum value  $v_{1M}$ , the input function goes back to zero. The corresponding trajectory of the modified generalized play operator output first moves from  $(v_{1m}, w_{M_{1m}})$  to  $(v_{1m'}, w_{M_{1m}'})$  and increases to  $(v_{1M}, w_{M_{1M}})$ . So far, the memory of the maxima  $v_{1M}$ ,  $v_{2M}$  and  $v_{3M}$  has been wiped out. In this end, the trajectory moves to  $(v_{1M'}, w_{M_{1M}'})$ , and finally decreases back to the origin. This process will not be affected by any past extrema for the further input because all the memories about the past input extrema have been completely wiped out. It can be concluded that the modified generalized play operator possesses the wiping out property.

Since the wiping out property follows the linear superposition, it also holds for the MGPI model. In Fig. 3.10, an input function is specifically chosen in the simulation so as to verify

the wiping out property of the MGPI model proved above. The alternating extrema of input function  $v(t)$  is  $\{0 \infty 10 \infty 2 \infty 8 \infty 4 \infty 6 \infty 2 \infty 10 \infty 0\}$  . The other parameters are chosen as follows.

$$\begin{aligned}\gamma_r(v) &= 5.5\tanh(0.25v) + 0.3, \\ \gamma_l(v) &= 7\tanh(0.15v), \\ p_m(r) &= 2.4e^{-0.49r}.\end{aligned}\tag{3.14}$$

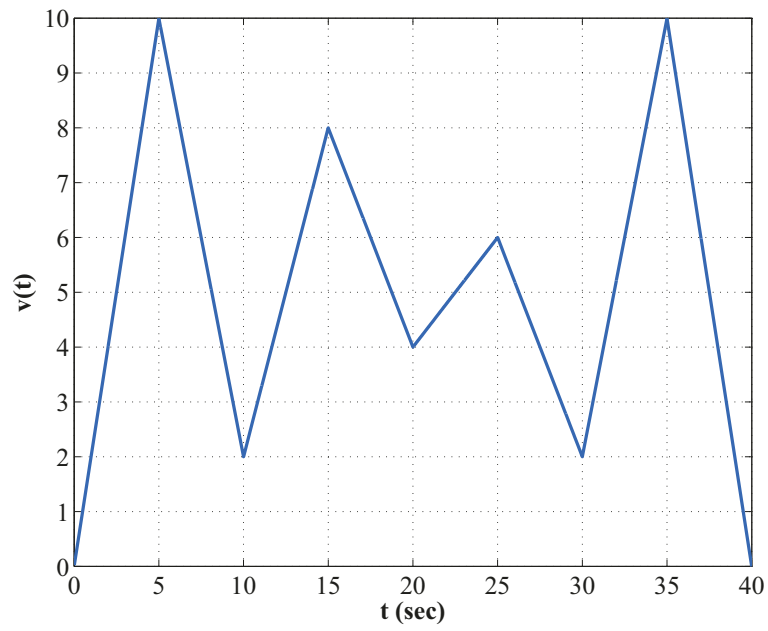
The result shows that no memory of the input extrema has been wiped out until  $t = 25s$ . The output trajectory depends on the current input and all the input extrema in the history. At the time  $t = 30s$ , the memory of the input minimum recorded at  $t = 20s$  has been wiped out and the output trajectory after  $t = 30s$  is not affected by the memory of this minimum. Similarly, all the input extrema have been wiped out after the input reduces back to zero at  $t = 40s$ .

### 3.4.3 Congruency Property

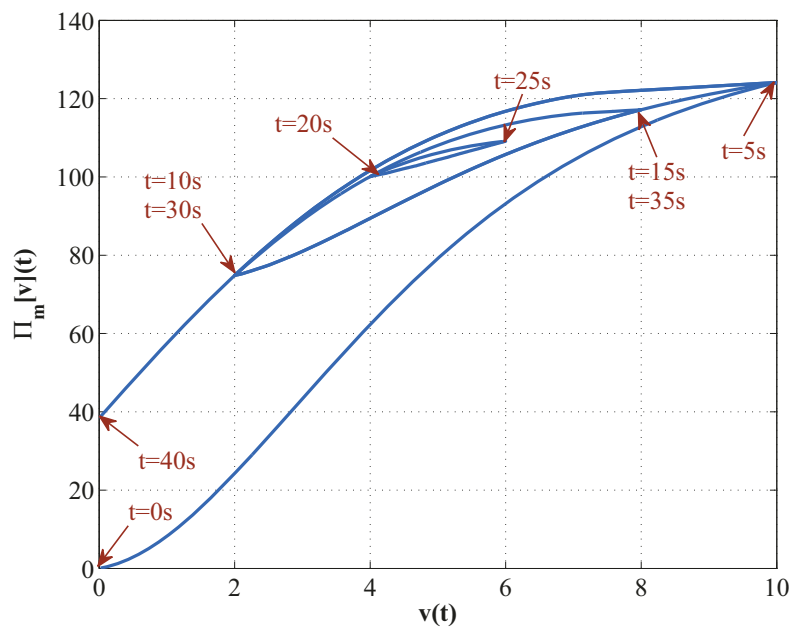
Congruency property means that, regardless of the input history, the minor loops caused by the same input range are congruent. By using the memory curve, it can be shown that the MGPI model possesses the congruency property as well.

As shown in Fig.3.11(a),  $\beta_1$  and  $\beta_2$  are two memory curves for the same MGPI model with different input histories. Assume that they have the same current input value  $v_1$  at time  $t_1$ . The input function increases monotonically to  $v_2$  at time  $t_2$ , and then goes back to  $v_1$  at time  $t_3$ . As shown in Fig. 3.11(b) and (c), this variance affects the memory curve  $\beta_1$  by the triangle  $A_1$  and affects the memory curve  $\beta_2$  by the triangle  $A_2$ . It is obvious that the triangles  $A_1$  and  $A_2$  are coincident. Therefore, one can conclude that the MGPI model fulfills the congruency property [12].

The above outcome can also be supported in the simulation by adopting a special input function as shown in Fig. 3.12(a). In Fig. 3.12(b), the lower minor loop is caused by the



(a)



(b)

Figure 3.10: (a) Input signal  $v(t)$  for wiping out validation; (b) Output of MGPI model for wiping out verification.

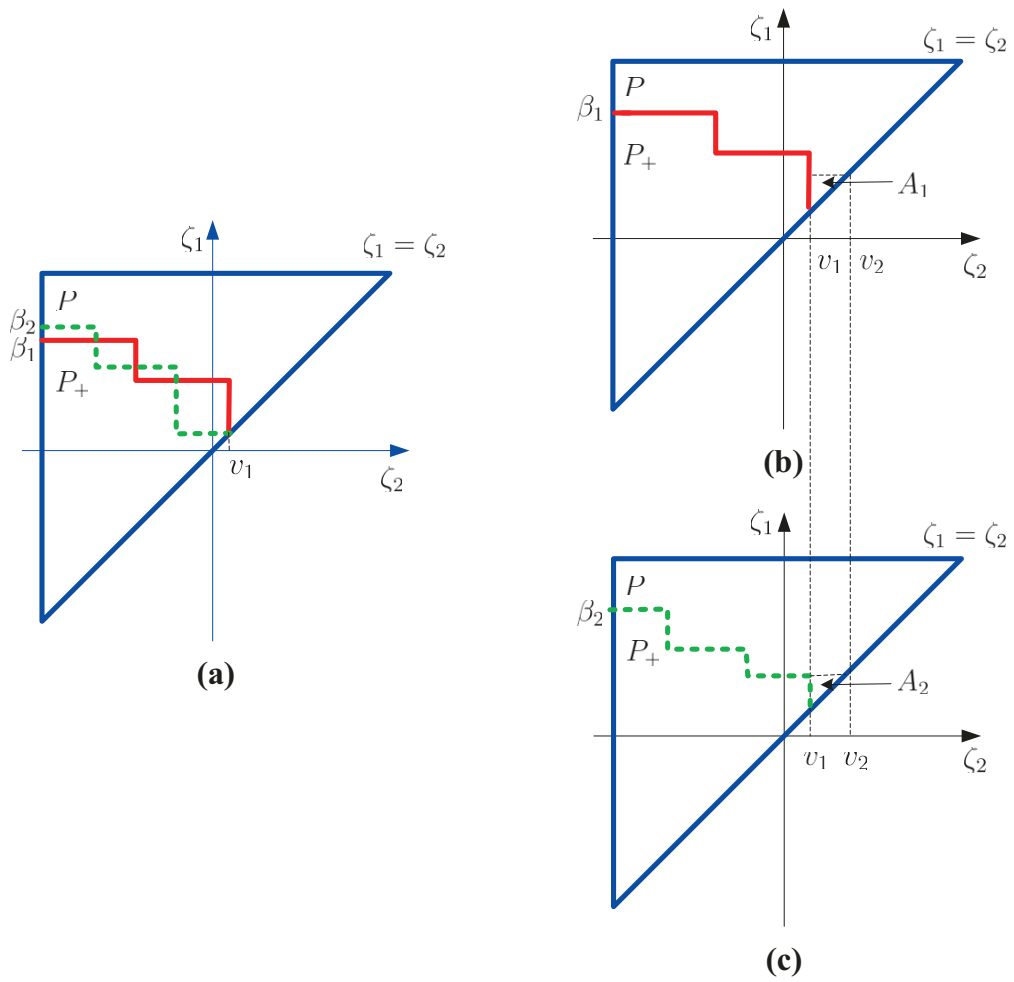
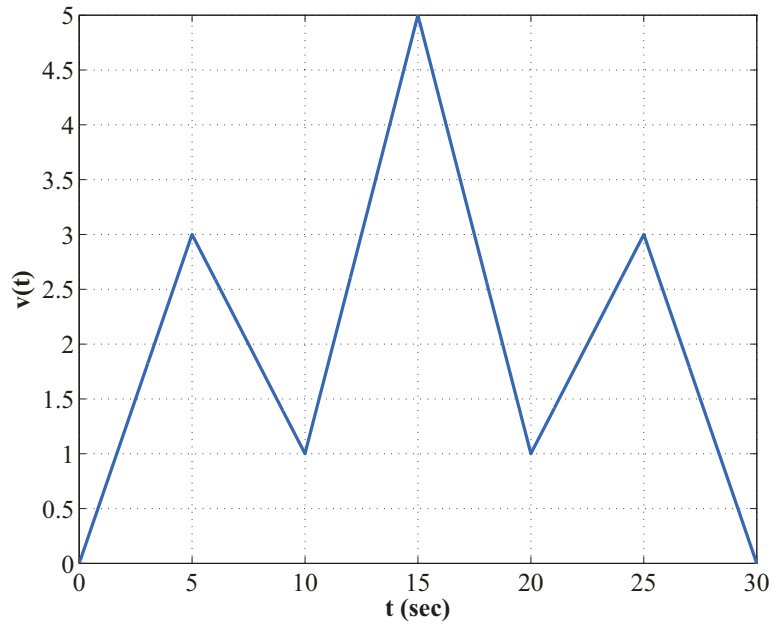
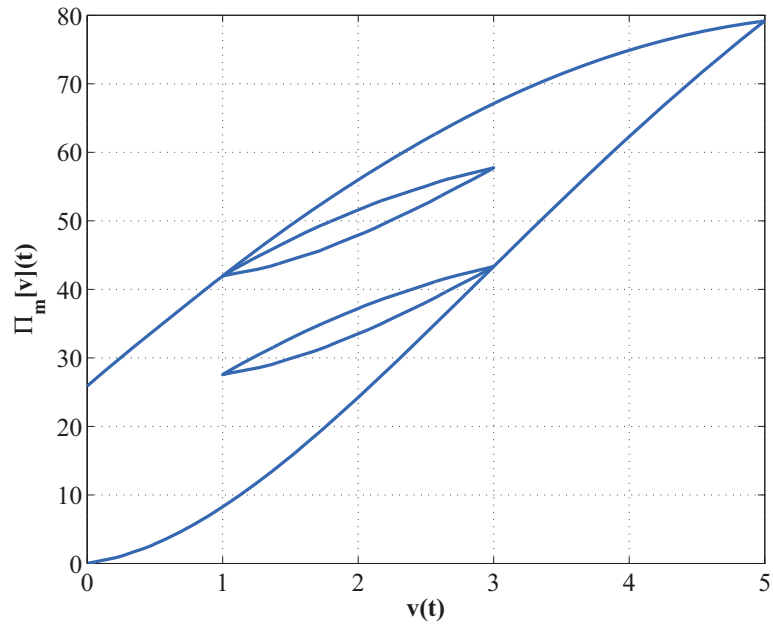


Figure 3.11: Illustration of congruency property.



(a)



(b)

Figure 3.12: (a) Input signal  $v(t)$  for congruency validation. (b) Output of MGPI model congruency verification.

input wavering between the value 1 and 3 in the ascending process. The upper minor loop is led by the input wavering in the same range in the descending process. These two minor loops are congruent.

Based on the above discussion, it can be concluded that the proposed modified generalized Pradntl-Inshlinskii model fulfills both the wiping out property and the congruency property.

## Chapter 4

# Inverse Hysteresis Compensation of Modified Generalized Pradtl-Ishlinskii Model

The hysteresis nonlinearities are known to deteriorate the control systems performances. One of the most common way to compensate the hysteresis effects is to construct the inverse model and apply it as a feedforward compensator. The precise inverse of the Preisach model and the Krasnosel'ĭskii-Pokrovskii model are not available. Only the numerical methods can be used to determine the approximate inversions of those models [24, 28, 70, 71]. Different from the Preisach model and the KP model, the Prandtl-Ishlinskii model is analytical invertible and its inversion can be applied as a feedforward compensator in the control systems to mitigate the hysteresis effects. Furthermore, based on the analytical inversion, the inverse compensation error can be therefore obtained, which make it possible to design robust controllers with stability analysis. The analytical expression of the inverse PI model has been reported in [15] as a real-time feedforward controller for piezo-electric actuators. It has been demonstrated that, by using the inverse compensator, the tracking errors caused by the hysteresis effect were reduced significantly. However, as explained in the previous chapters, the applications

of the PI model is restricted because of the limited hysteresis shapes it can describe.

As proposed in Chapter 3, the modified generalized Prandtl-Ishlinskii model can be considered as an extension of the PI model. The purpose of the work in this chapter is to compensate the hysteresis described by the proposed MGPI model through constructing an inverse MGPI model and applying this inverse model as the feedforward hysteresis compensator. To follow the similar procedures which determine the inverse model for the classical PI model using the initial loading curve [15], it requires that the increasing trajectory  $\gamma_r(v-r)$  and the decreasing trajectory  $\gamma_l(v+r)$  of the modified generalized play operator are parallel. Therefore, the inverse construction is limited to the case that the envelope functions of the MGPI model are equal, i.e.  $\gamma_r(v) = \gamma_l(v) = \gamma(v)$ . For  $\gamma_r(v) \neq \gamma_l(v)$ , it is still under investigation. It should be noted that the case that  $\gamma_r(v) = \gamma_l(v) = \gamma(v)$  is still more general than the classical PI model.

As shown in Fig. 4.1, the inverse model of the MGPI model  $\Pi_m^{-1}$  is composed by two parts. The first part  $\Pi_{com}$  is the hysteresis loop compensator. It is used to mitigate the hysteresis loop. The compensated input-output relationship after applying the hysteresis loop compensation becomes from multi-values mapping to the single-valued mapping. This part is the main challenge of constructing the inverse MGPI model. The second part of the inverse model is  $\gamma^{-1}(\cdot)$ . It is introduced here in order to compensate the effect of the envelope function. After applying the inverse model  $\Pi_m^{-1}$  as the feedforward compensator, the compensated output of MGPI model  $\Pi_m$  is able to track the reference input, i.e.  $\Pi_m \bullet \Pi_m^{-1}(t) = v_c(t)$ .

## 4.1 Concept of Initial Loading Curve

Equation (3.4) provides the widely accepted expression of the PI model for hysteresis description. However, such a definition is difficult to obtain an analytical inverse PI model. As

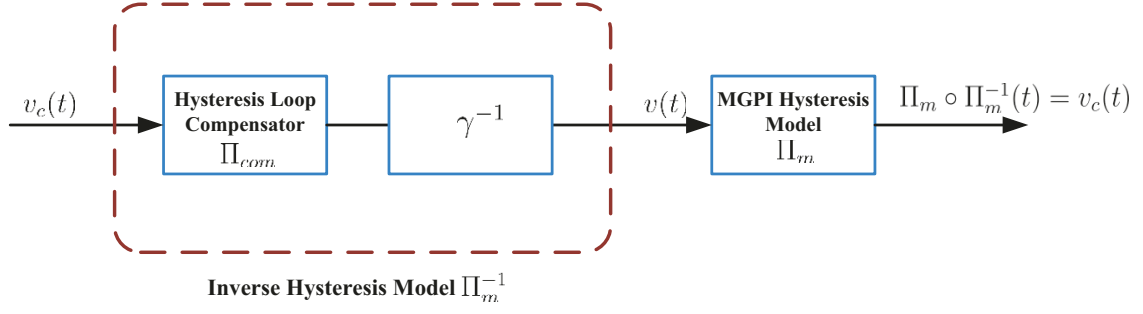


Figure 4.1: Inverse compensation for MGPI mode

an alternative description, the concept of initial loading curve is required to be introduced. The curve can be explained, physically, as a stress-strain curve, and is formed when the input signal increases from zero to a final value. The initial loading curve of the PI model is defined by [12]

$$\Theta(r) = p_0 r + \int_0^r p(\vartheta) \max\{0, r - \vartheta\} d\vartheta \quad (4.1)$$

where  $p_0$  and  $p(r)$  have the same definition as given in (3.4). The derivative of initial loading curve (4.1) with respect to  $r$  can be obtained by

$$\Theta'(r) = p_0 + \int_0^r p(\vartheta) d\vartheta. \quad (4.2)$$

It can be observed that the density function of PI model can be expressed by the double derivative of (4.1) with respect to the threshold  $r$ , that is

$$p(r) = \Theta''(r). \quad (4.3)$$

In addition, the constant  $p_0$  can be obtained by substituting  $r = 0$  into (4.2) as

$$p_0 = \Theta'(0). \quad (4.4)$$

Therefore, based on (4.3) and (4.4), the PI model can be alternatively expressed in terms of the initial loading curve as

$$\Pi[v](t) = \Theta'(0)v(t) + \int_0^\infty \Theta''(r) F_r[v](t) dr. \quad (4.5)$$

**Remark:** For the initial loading curve  $\Theta(r) = r$ , the PI model is reduced to  $\Pi[v](t) = v(t)$ , which means that no hysteresis effect exists.

Fig. 4.2 shows an example of the PI model with density function  $p(r) = 0.53e^{-0.1r}$  and  $p_0 = 0.53$  under a harmonic input  $v(t) = 8\sin(2\pi t)/(1 + 0.3t)$  for  $t \in [0, 10]$  and its corresponding initial loading curve. The output of the PI model in this example, as shown in Fig. 4.2(a) is expressed by

$$\Pi[v](t) = 0.53v(t) + \int_0^\infty 0.53e^{-0.1r} F_r[v](t) dr. \quad (4.6)$$

According to the definition in (4.1), the corresponding initial loading curve of the PI model (4.6) shown in Fig. 4.2(b) is defined in the following form

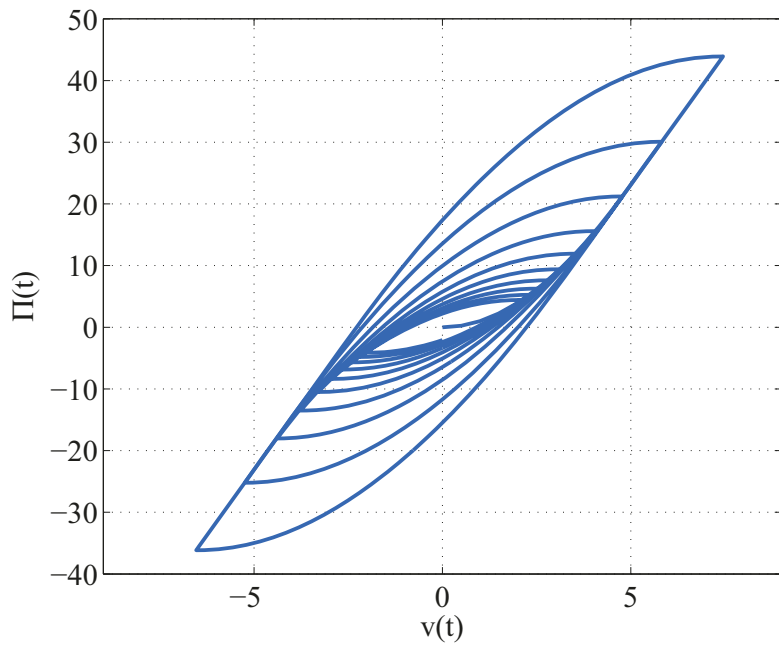
$$\Theta(r) = 0.53r + \int_0^r 0.53e^{-0.1\vartheta} \max\{0, r - \vartheta\} d\vartheta. \quad (4.7)$$

It should be noted that, in the PI model, the increasing branches of play operator for various threshold  $r$  are parallel horizontally with each other. The initial loading curve of PI model is defined based on the integration of these branches. However, in the GPI model, the increasing branches of generalized play operator for different threshold  $r$  are parallel vertically with each other. Therefore, it is difficult to construct the initial loading curve for the GPI model. On the other hand, in the proposed MGPI model, the increasing branches of modified generalized play operator for various threshold  $r$  are parallel horizontally with each other, which is the same as in the PI model. The initial loading curve of MGPI model can then be similarly defined by the integration of these branches, which gives a main reason for proposing the MGPI model.

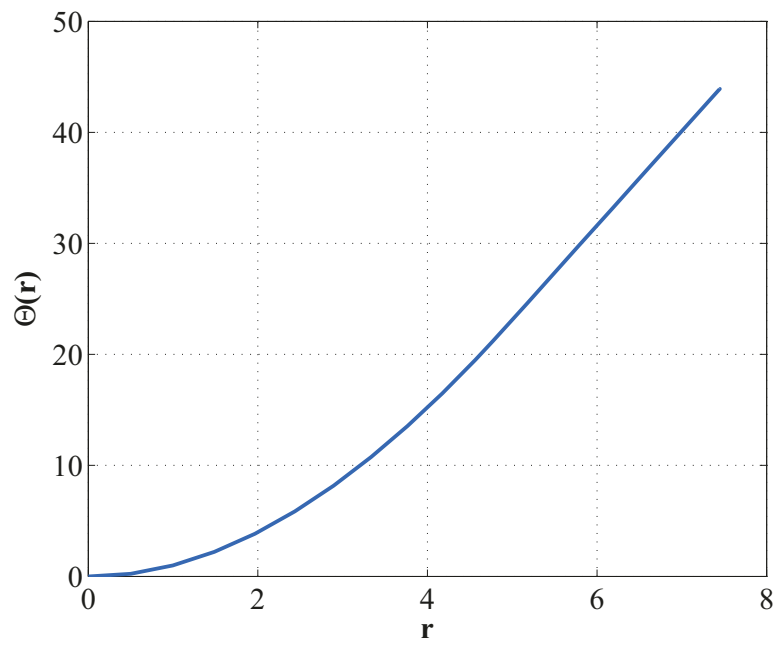
Similar to the (4.1), the initial loading curve for the proposed MGPI model is defined as,

$$\Theta_m(r) = \int_0^r p_m(\xi) \max\{\gamma(0), \gamma(r - \xi)\} d\xi. \quad (4.8)$$

In the next subsection, the initial loading curves of both the classical PI model and MGPI model will be adopted in order to derive the analytical hysteresis loop compensator for the MGPI model.



(a)



(b)

Figure 4.2: The input output relations of (a) The PI model; (b) The corresponding initial loading curve.

## 4.2 Inverse Construction of the Modified Generalized Prandtl-Ishlinskii Model

It has already been proved in [12] that the inverse of the classical PI model can work as the compensator to mitigate the hysteresis loops. In [15], the analytical formulas of the threshold and the density function of the inverse model have been derived. In this section, the similar procedures as outlined in [15] is employed to construct the inverse model of the proposed MGPI model. Comparing to the previous work, the analytical expressions of the threshold and density function of the compensator will be discussed for the first time based on the MGPI model.

As shown in Fig. 4.1, the inverse MGPI model constructed in this work is defined in the form of

$$\Pi_m^{-1}[v_c](t) = \gamma^{-1} \bullet \Pi_{com}[v_c](t). \quad (4.9)$$

The hysteresis loop compensator there is defined as follows,

$$\Pi_{com}(t) = \int_0^S q_m(s) F_s[v](t) ds \quad (4.10)$$

where  $F_s[v](t)$  is the classical play operator with the threshold  $s$ . The thresholds  $s$  and the density function  $q_m(s)$  are required to be determined so that the hysteresis loop of MGPI model (3.12) can be compensated by (4.10).

The hysteresis loop compensator developed based on the classical PI model is symmetric with respect to the origin and the proposed MGPI model is asymmetric with the bias to the origin due to the existence of the envelop function. In order to compensate the asymmetric MGPI model with the symmetric compensator, the MGPI model (3.12) is shifted first, which is just the coordinate translation and does not affect the final compensation result, resulting in

$$\Pi_{sh}(t) = \int_0^R p_m(r) (G_{mr}[v](t) - \gamma(0)) dr. \quad (4.11)$$

In the next step, the initial loading curves of both hysteresis loop compensator  $\Pi_{com}(t)$

(4.8) and the shifted MGPI model  $\Pi_{sh}(t)$  (4.11) are used to determine the analytical expression of the compensator's thresholds  $s$  and density function  $q_m(s)$ .

The initial loading curve of the hysteresis loop compensator (4.10) is expressed by

$$\Psi(s) = \int_0^s q_m(\vartheta) \max\{0, s - \vartheta\} d\vartheta \quad (4.12)$$

where  $q_m(\vartheta)$  is the density function and  $s$  is the threshold.

Following the definition of initial loading curve of MGPI model in (4.8), the corresponding shifted initial loading curve for  $\Pi_{sh}$  is expressed by,

$$\Theta_{sh}(r) = \int_0^r p_m(\xi) \max\{0, \gamma(r) - \xi\} d\xi \quad (4.13)$$

where  $p_m(\xi)$  is the density function and  $r$  is the threshold.

To compensate the multi-branches hysteresis loops of the MGPI model, the composition of the initial loading curves (4.12) and (4.13) is required to have the following relation.

$$\Psi \bullet \Theta_{sh}(r) = \gamma(r) - \gamma(0) \quad (4.14)$$

where  $\bullet$  denotes the composition operator.

Comparing (4.14) with (4.12), the threshold of the hysteresis loop compensator  $s$  in (4.10) can be calculated from

$$s = \Theta_{sh}(r). \quad (4.15)$$

Based on the above selection of threshold  $s$ , the analytical form of the corresponding density function  $q_m(s)$  of the hysteresis loop compensator will be determined from (4.12) and (4.14).

Taking the derivative of both sides of (4.14) with respect to  $\gamma(r)$ , one has

$$\frac{d\Psi(\Theta_{sh}(r))}{d\Theta_{sh}(r)} \times \frac{d\Theta_{sh}(r)}{d\gamma(r)} = 1. \quad (4.16)$$

With the threshold  $s$  determined in (4.15), the left-hand side of (4.16) can be continuously deducted as

$$\frac{d\Psi(\Theta_{sh}(r))}{d\Theta_{sh}(r)} = \frac{d\Psi(s)}{ds} = \int_0^s q_m(\vartheta) d\vartheta \quad (4.17)$$

$$\frac{d\Theta_{sh}(r)}{d\gamma(r)} = \frac{\Theta'_{sh}(r)}{\gamma'(r)} = \frac{\int_0^r p_m(\xi)\gamma'(r-\xi)d\xi}{\gamma'(r)}. \quad (4.18)$$

Substituting (4.17) and (4.18) into (4.16), the density function of the hysteresis loop compensator can be obtained from the following formula

$$\int_0^s q_m(\vartheta)d\vartheta = \frac{\gamma'(r)}{\int_0^r p_m(\xi)\gamma'(r-\xi)d\xi}. \quad (4.19)$$

Finally, the analytical form of hysteresis loop compensator (4.10) has been obtained. The threshold  $s$  and density function  $q_m(s)$  are determined by (4.15) and (4.19). This compensator can remove the hysteresis loop while preserving the shape of the envelop function.

### 4.3 Numerical Implementation of the Inverse MGPI Model

In practice, because of the continuity property of the modified generalized play operator, the complex continuous hysteresis nonlinearities described by the MGPI model can be modeled in a sufficiently precise way with a small number of elementary operators [98]. Therefore, the definition of MGPI model given in (3.12) can be approximated by

$$\Pi_M(t) = \sum_{i=0}^N p_{ri}G_{mr_i}[v](t). \quad (4.20)$$

where  $N$  denotes the number of the modified generalized play operators considered,  $0 = r_0 < r_1 < \dots < r_N = R$ .

The corresponding hysteresis loop compensator can also be written in terms of the superposition as

$$\Pi_{com}(t) = \sum_{i=0}^N q_{si}F_{s_i}[v](t). \quad (4.21)$$

In (4.20) and (4.21),  $p_{ri}$  and  $q_{si}$  are the weights of the density functions of the MGPI model and the hysteresis loop compensator respectively, defined by

$$\begin{aligned} p_{ri} &= p_m(r_i) \\ q_{si} &= q_m(s_i). \end{aligned} \quad (4.22)$$

From (4.15), we can obtain the discrete thresholds of the hysteresis loop compensator as follows,

$$\begin{aligned} s_j &= \Theta_{sh}(r_j) \\ &= p_{r0}(\gamma(r_j) - \gamma(0)) + \sum_{i=1}^j p_{ri}(\gamma(r_j - r_i) - \gamma(0)) \end{aligned} \quad (4.23)$$

for  $j = 1, 2, \dots, N$ .

We still need to compute the discrete density weights of the hysteresis loop compensator. From (4.19), it can be observed that, in each interval  $[s_j, s_{j+1}]$  for  $j = 1, 2, \dots, N$ , we have

$$q_{s0} + \sum_{i=1}^j q_{si} = \frac{\gamma'(r_j)}{p_{r0}\gamma'(r_j) + \sum_{i=1}^j p_{ri}\gamma'(r_j - r_i)}. \quad (4.24)$$

Hence, in particular,

$$q_{s0} = \frac{1}{p_{r0}} \quad (4.25)$$

and

$$q_{sj} = \frac{\gamma'(r_j)}{p_{r0}\gamma'(r_j) + \sum_{i=1}^j p_{ri}\gamma'(r_j - r_i)} - \sum_{i=0}^{j-1} q_{si} \quad (4.26)$$

for  $j = 1, 2, \dots, N$ .

**Remark 2:** If we choose the envelop function  $\gamma(v)$  as  $\gamma(v) = v$ , equations (4.23), (4.25) and (4.26) will be coincident with the corresponding formulas in [15]. Therefore, the results concluded in [15] can be considered as a special case of our work.

## 4.4 Simulation Results of Inverse Compensation

In this section, the hysteresis loop compensator developed above will be verified in the simulation studies. Both the linear and nonlinear envelope functions will be selected.

### 4.4.1 Linear Envelope Function

In this section, the envelope function  $\gamma$  is chosen in the linear form.

$$\gamma(v_c) = m_0 v_c + m_1, (m_0 > 0) \quad (4.27)$$

where  $m_0$  and  $m_1$  are chosen as 1.2 and 1.9 respectively as an example.

There are 10 modified generalized play operators considered in this simulation as an example. The thresholds  $r_i$  and weights  $p_{r_i}$  for  $i = 0, 1, \dots, N$  of the MGPI model are selected as shown in Table 4.1.

Table 4.1: Thresholds and weights selected for the MGPI model with linear envelope function

$r_0$	$r_1$	$r_2$	$r_3$	$r_4$	$r_5$	$r_6$	$r_7$	$r_8$	$r_9$	$r_{10}$
0	0.54	1.08	1.62	2.16	2.70	3.24	3.78	4.32	4.86	5.40
$p_{r0}$	$p_{r1}$	$p_{r2}$	$p_{r3}$	$p_{r4}$	$p_{r5}$	$p_{r6}$	$p_{r7}$	$p_{r8}$	$p_{r9}$	$p_{r10}$
0.18	0.0358	0.0339	0.0321	0.0305	0.0289	0.0273	0.0259	0.0245	0.0233	0.0220

The corresponding thresholds  $s_i$  and the weights  $q_{s_i}$  for  $i = 0, 1, \dots, N$  of the inverse MGPI model can be calculated through (4.23), (4.25), and (4.26), respectively. The calculation results are summarized in Table 4.2.

The effectiveness of the inverse compensation can be illustrated from the input-output relationship as shown in Fig. 4.3. Fig. 4.3(a) shows the input-output relation of the MGPI model, which is the non-smooth multi-value hysteresis nonlinearity. The hysteresis loop compensator, in the form of (4.10) with the thresholds and weights summarized in Table 4.2, is shown in Fig. 4.3(b). Based on the compensated result shown in Fig. 4.3(c), it can be demonstrated that the proposed inverse MGPI model can effectively compensated the hysteresis effect and achieve the accurate tracking.

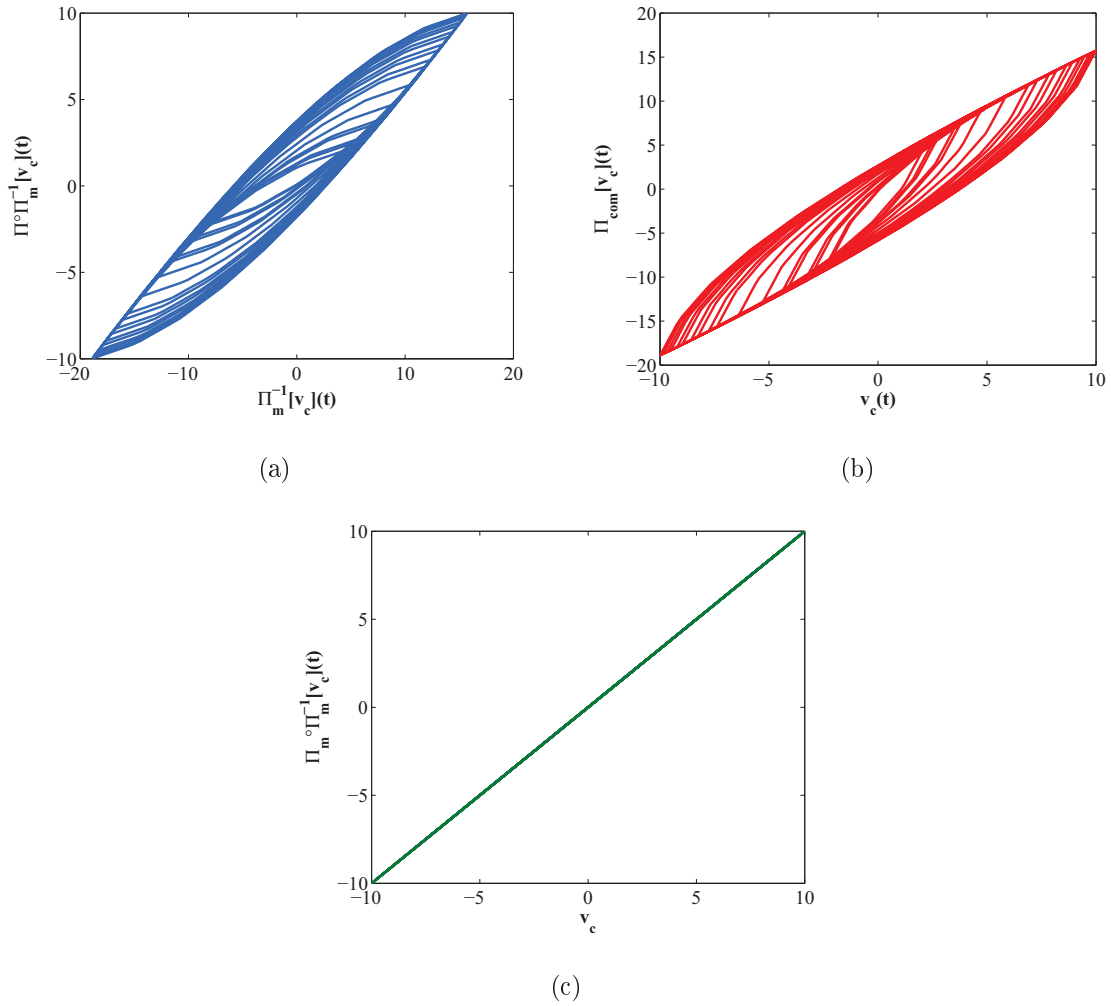


Figure 4.3: Input-output relations of (a) MGPI model, (b) the hysteresis loop compensator, (c) and the compensation result, with the linear envelope function.

Table 4.2: Thresholds and weights obtained for the inverse MGPI model with linear envelope function

$s_0$	$s_1$	$s_2$	$s_3$	$s_4$	$s_5$
0	0.1166	0.2565	0.4183	0.6010	0.8034
$s_6$	$s_7$	$s_8$	$s_9$	$s_{10}$	
1.0245	1.2633	1.5189	1.7904	2.0770	
$q_{s0}$	$q_{s1}$	$q_{s2}$	$q_{s3}$	$q_{s4}$	$q_{s5}$
5.5556	0.9219	0.6295	0.4566	0.3459	0.2708
$q_{s6}$	$q_{s7}$	$q_{s8}$	$q_{s9}$	$q_{s10}$	
0.2174	0.1782	0.1485	0.1255	0.1073	

#### 4.4.2 Nonlinear Envelope Function

Besides the linear function adopted in the previous subsection, the envelope functions can also be chosen as the nonlinear functions. The application range of the proposed MGPI model can be therefore extended.

In the simulation, the envelope function  $\gamma(v)$  is chosen in the following nonlinear form,

$$\gamma(v) = m_0 \tanh(m_1 v + m_2) + m_3, (m_0 > 0) \quad (4.28)$$

where  $m_0$ ,  $m_1$ ,  $m_2$  and  $m_3$  are chosen as 2.0258, 0.0179, 0.0371 and 0.1202 respectively as an example.

There are 300 modified generalized play operators selected in this simulation, i.e.  $N = 300$ . The thresholds  $r_i$  and density weights are selected as  $r_i = 0.22i$  for  $i = 1, 2, \dots, N$  and  $p_m = 0.5e^{-0.0014r^2}$ . The thresholds  $s_0, s_1, \dots, s_N$  and weights  $q_{s0}, q_{s1}, \dots, q_{sN}$  of hysteresis loop compensator can be calculated using (4.23), (4.25) and (4.26) respectively.

Fig. 4.4(a) shows the output of the MGPI model under a complex input function  $v_c(t) = 40\sin(2\pi t) + 60\cos(6t)$ ,  $t \in [0, 20]$ . The hysteresis loop compensator  $\Pi_{com}$  determined in (4.10) is shown in Fig. 4.4(b). The compensation result of the hysteresis loop

compensator can be seen in Fig. 4.4(c). The hysteresis loop has been perfectly canceled and the shape of the nonlinear envelope function has been preserved. The Fig. 4.4(d) shows final compensation result. The nonsmooth multi-branches hysteresis loops and the influence of the nonlinear envelope function have been compensated successfully.

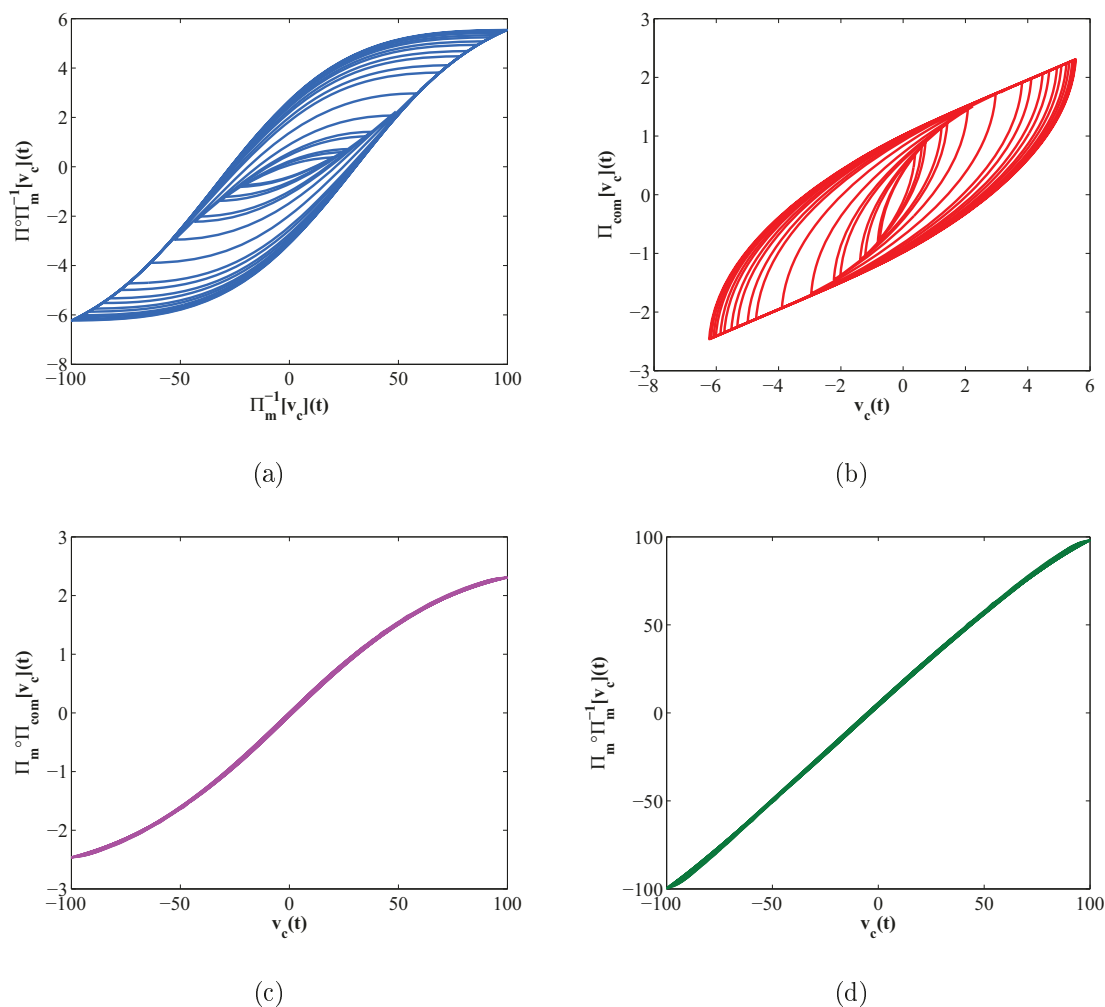


Figure 4.4: Input-output relations of (a) The MGPI model, (b) The hysteresis loop compensator, (c) The effectiveness of the hysteresis loop compensator, (d) and the compensation result, with the nonlinear envelope function.

# Chapter 5

## Analysis of Inverse Compensation Error

As addressed in previous chapters, the hysteresis nonlinearities can be remarkably remedied by applying the inverse model as a feedforward compensator. Theoretically, as shown in Fig. 5.1, when the hysteresis nonlinearity is entirely depicted by the hysteresis model, the hysteresis effect can be completely compensated through the inverse method, which has also been demonstrated by the simulation studies in Chapter 4. The compensated output is  $u(t) = \Pi_m^{-1} \bullet \Pi_m[v_c](t) = v_c(t)$ . However, in practice, the hysteresis is unknown so that the hysteresis effects can not be fully described by the hysteresis models. Usually, the unknown hysteresis implies the unknown density functions in the hysteresis models, which means that, in our case, the density function of the modified generalized Prandtl-Inshlinskii model  $p_m(r)$  can only be estimated as  $\hat{p}_m(r)$  in experiments for the hysteresis description and inverse construction. Therefore, the corresponding inverse MGPI model can only be derived based on the estimated MGPI model, which, as shown in Fig. 5.2, will be expected to yield some degree of inverse hysteresis compensation error  $e(t)$ , i.e.,  $u(t) = \hat{\Pi}_m^{-1} \bullet \Pi_m[v_c](t) = \gamma^{-1}(\hat{\Pi}_{com} \bullet \Pi_m[v_c](t)) = v_c(t) + e(t)$ , where  $\hat{\Pi}_m^{-1}[v_c](t)$  is the inverse MGPI model derived from the estimated MGPI model  $\hat{\Pi}_m[v_c](t)$  with the estimated density function  $\hat{p}_m(r)$ . Therein,  $\hat{\Pi}_{com}[v_c](t)$ , compared with the  $\Pi_{com}[v_c](t)$  defined in (4.10), stands for the estimated hysteresis loop compensator derived from the estimated MGPI model  $\hat{\Pi}_m[v_c](t)$  with the estimated density function  $\hat{p}_m(r)$ .

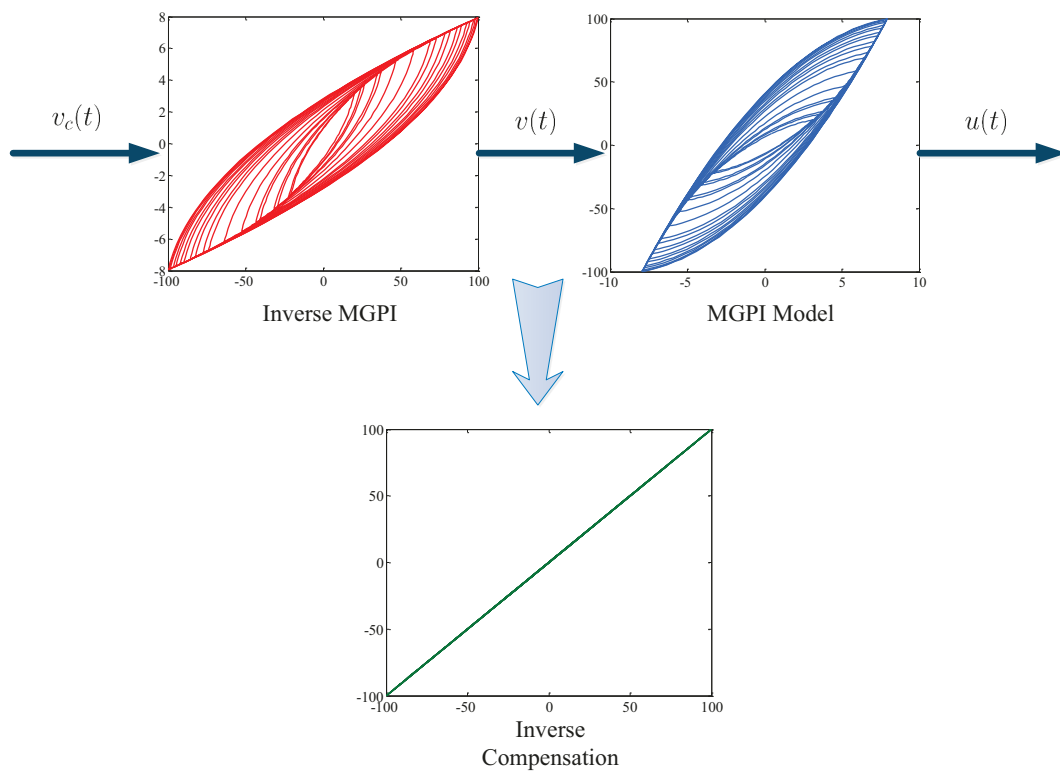


Figure 5.1: Inverse compensation without inverse error

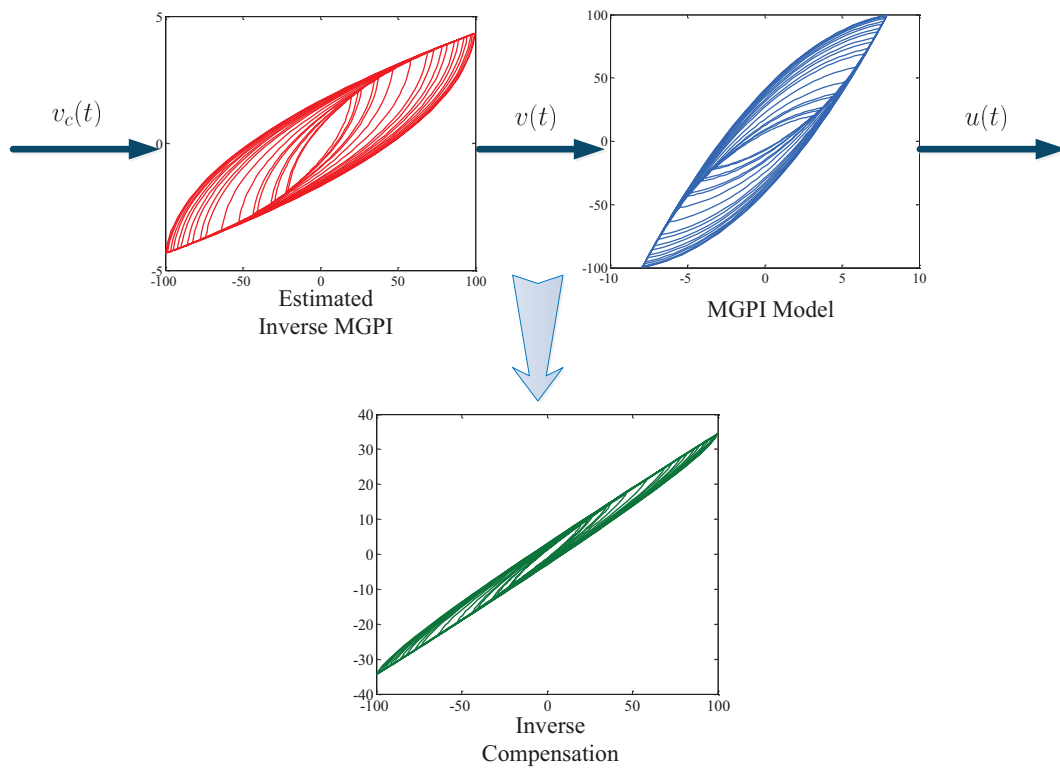


Figure 5.2: Inverse compensation with inverse error

In this chapter, the linear envelope function  $\gamma(v) = m_0v + m_1$ , where  $m_0 > 0$ , has been chosen as a special case and the analytic expression of the inverse compensation error will be derived. The development of the error expression of the inverse compensation is extremely essential since that, by taking consideration of the error expression, the adaptive controllers can be further designed and, more important, the strict stability proofs can therefore be established based on the Lyapunov methods. In [99], the inverse compensation error of the PI model has been developed. In the following development, the analysis expression of the inverse compensation error of the MGPI model will be investigated.

## 5.1 The Analytical Inverse Compensation Error

Since the hysteresis is usually unknown in practice, only an estimated MGPI hysteresis model  $\hat{\Pi}_m(t)$  with the estimated density function  $\hat{p}_m(r)$  can be used to approximately describe the unknown hysteresis. Comparing to (4.11), the estimated shifted MGPI model  $\hat{\Pi}_{sh}[v_c](t)$  is expressed by

$$\begin{aligned}\hat{\Pi}_{sh}[v_c](t) &= \int_0^R \hat{p}_m(r)(G_{mr}[v_c](t) - \gamma(0))dr \\ &= \int_0^R \hat{p}_m(r)m_0F_r[v_c](t)dr\end{aligned}\tag{5.1}$$

where  $\hat{p}_m(r)$  is the estimations of  $p_m(r)$  and  $F_r[v_c](t)$  is the classic play operator defined in (3.1). For the linear envelope functions,  $\hat{\Pi}_{sh}[v_c](t)$  can be considered as a classic PI model with the density function  $m_0\hat{p}_m(r)$ .

The initial loading curve of (5.1) is now defined as

$$\hat{\Theta}_{sh}(r) = \int_0^r m_0\hat{p}_m(\xi)\max\{0, r - \xi\}d\xi\tag{5.2}$$

The inverse model

$$\hat{\Pi}_m^{-1}(t) = \gamma^{-1} \bullet \hat{\Pi}_{com}(t)\tag{5.3}$$

constructed based on the estimated MGPI model  $\hat{\Pi}_m(t)$  would be expected to yield some degree of inverse hysteresis compensation error  $e(t)$ . Comparing to (4.10),  $\hat{\Pi}_{com}[v_c](t)$  is

expressed by

$$\hat{\Pi}_{com}[v_c](t) = \int_0^S \hat{q}_m(\hat{s}) F_{\hat{s}}[v_c](t) d\hat{s} \quad (5.4)$$

where  $\hat{s}$  and  $\hat{q}_m$  are the threshold and density function of the estimated hysteresis loop compensator, respectively. The corresponding initial loading curve of  $\hat{\Pi}_{com}[v_c](t)$  is

$$\hat{\Psi}(\hat{s}) = \int_0^{\hat{s}} \hat{q}_m(\vartheta) \max\{0, \hat{s} - \vartheta\} d\vartheta \quad (5.5)$$

According to the composition corollary in [50], the composition of the  $\hat{\Pi}_{com}$  and  $\Pi_{sh}$  can be rewritten as

$$\hat{\Pi}_{com} \bullet \Pi_{sh}(t) = \Pi_{\eta}(t) \quad (5.6)$$

where  $\eta = \hat{\Psi} \bullet \Theta_{sh}(r)$  and  $\Pi_{\eta}$  is a classic PI model with the initial loading curve  $\eta(r)$ .

Based on above results, the analytical expression of the inverse compensation error  $e(t)$  can be derived as

$$\begin{aligned} e(t) &= v_c(t) - u(t) \\ &= v_c(t) - \gamma^{-1}(\hat{\Pi}_{com} \bullet \Pi_{sh}(t) + \gamma(0)) \\ &= v_c(t) - \gamma^{-1}(\Pi_{\eta}(t) + m_1) \\ &= v_c(t) - \frac{\eta'(0)v_c(t) + \int_0^{\infty} \eta''(r) F_r[v_c](t) dr}{m_0} \\ &= \left(1 - \frac{\eta'(0)}{m_0}\right) v_c(t) - \int_0^{\infty} \frac{\eta''(r)}{m_0} F_r[v_c](t) dr \end{aligned} \quad (5.7)$$

**Remark:** If the parameters of the MGPI model and its inverse are exact, the composition of the initial loading curves  $\eta(r)$  can be simplified as

$$\eta(r) = \Psi \bullet \Theta_{sh}(r) = m_0 r, \quad (5.8)$$

and

$$\eta'(r) = m_0, \quad (5.9)$$

$$\eta''(r) = 0. \quad (5.10)$$

Then, the inverse compensation error (5.7) is

$$e(t) = 0 \quad (5.11)$$

and the compensated output

$$u(t) = v_c(t), \quad (5.12)$$

which implies that there is no inverse compensation error and the hysteresis effects have been completely compensated.

The analytic expression of inverse compensation error of MGPI model has been obtained in (5.7). However, Since the term  $\int_0^\infty \frac{\eta''(r)}{m_0} F_r[v_c](t)$  in (5.7) is unbounded, it is difficult to directly apply the control approaches to remedy it. Therefore, an alternative form will be provided in the following development.

Note that the play operator  $F_r[v_c](t)$  in (5.7) can be rewritten as [12]

$$F_r[v_c](t) = v_c - E_r[v_c](t) \quad (5.13)$$

where  $E_r[v_c](t)$  denotes the stop operator as

$$\begin{aligned} E_r(0) &= e_r(v_c(0) - \omega_{-1}), \\ E_r(t) &= e_r(v_c(t) - v_c(t_i) + E_r[v_c](t_i)) \end{aligned} \quad (5.14)$$

for  $t_i < t \leq t_{i+1}$ ,  $0 \leq i < N - 1$ , with

$$e_r(v_c) = \min(r, \max(-r, v_c)) \quad (5.15)$$

and  $\omega_{-1}$  as the initial value.

Therefore, the inverse compensation error can be further written as

$$\begin{aligned} e &= \left[ 1 - \frac{\eta'(0)}{m_0} \int_0^\infty \frac{\eta''(r)}{m_0} dr \right] v_c(t) + \int_0^\infty \frac{\eta''(r)}{m_0} E_r[v_c](t) dr \\ &\triangleq (1 - \chi_0) v_c(t) + d[v_c](t) \end{aligned} \quad (5.16)$$

where  $\chi_0 \triangleq \frac{\eta'(0)}{m_0} + \int_0^\infty \frac{\eta''(r)}{m_0} dr$  and  $d[v_c](t) \triangleq \int_0^\infty \frac{\eta''(r)}{m_0} E_r[v_c](t) dr$ . The boundness of  $d[v_c](t)$  can be guaranteed as proved in [81], i.e.,  $d[v_c](t) \geq D$  where  $D$  is a bounded constant. Hence,  $d[v_c](t)$  can be treated as a bounded disturbance in the controller design. Based on this result, an adaptive controller  $v(t)$  can then be designed to remove the inverse compensation error and achieve the precise tracking. As will be clear later, it is this expression that makes it possible to achieve the tracking without necessarily adapting the uncertain hysteresis parameters.

**Remark:** It is important to note that it is this analytical expression of the inverse compensation error that makes it possible to conduct the stability analysis in the controller design, which generally constitutes a challenge in the literature with the inverse approaches except [3].

## 5.2 Simulation Results of the Inverse Compensation Error

The analytic expression of the inverse compensation error obtained in (5.16) will be verified in the simulation studies. The actual density function of the MGPI model for the simulation is selected as  $p_m(r) = 0.17 + 0.1r$ . The input-output relation of the MGPI model with envelope function  $\gamma(v) = 1.7v$  is shown in Fig. 5.3 under a harmonic input signal  $v_c(t) = 7\sin(\pi t)/(1 + 0.06t)$ . In the following simulation studies, the inverse compensation will be conducted in the cases that the estimated density function  $\hat{p}_m(r)$  has no estimation error, minor estimation error, or major estimation error, respectively. The accuracy of the analytical expression of inverse compensation error (5.16) will be shown by comparing the analytical error calculated from (5.16) and the simulation error obtained from the direct deduction of input signal  $v_c(t)$  and compensated output  $u(t)$ .

**Case 1:** The density function of MGPI model in this case is exactly known, based on which the inverse MGPI model is constructed. Therefore, there is no inverse compensation

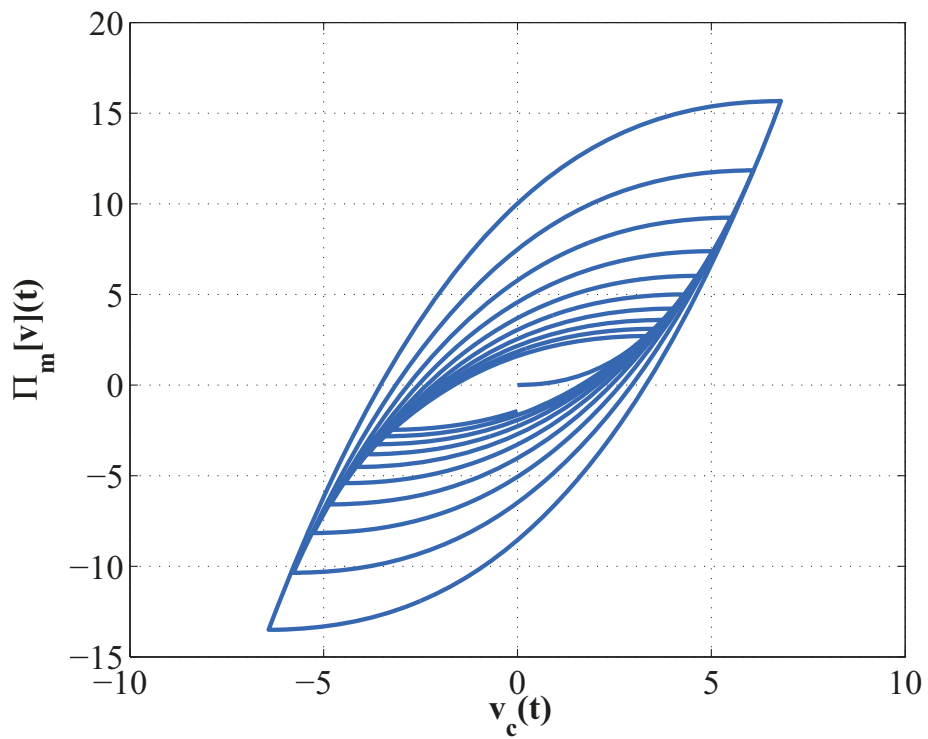


Figure 5.3: Input-output relation of MGPI mode under  $v_c(t) = 7\sin(\pi t)/(1 + 0.06t)$ .

error, which can be seen from Fig. 5.4. The simulation error and the analytical error are coincident and both equal to zero. The perfect inverse compensation can also be told from Fig. 5.5 where the relationship of the reference input signal and the compensated output is shown. It can be seen that the multi-branch non-smooth hysteresis nonlinearity has been completely remedied. As shown in Fig. 5.6, the system compensated output can successfully track the reference input signal.

**Case 2:** The estimated density function  $\hat{p}_m(r)$  has minor estimation error in this case, i.e.,  $\hat{p}_m(r) = 0.18 + 0.15r$ . As shown in Fig. 5.7, the analytical error calculated from (5.16) is still the same as the simulation error. It shows that the minor estimation error in the density function leads to the inverse compensation error. From Fig. 5.8, it can be seen that the input-output relation of the input signal and the compensated output is no longer a straight line but very narrow hysteresis loops. The comparison between the reference input signal and the compensated output as shown in Fig. 5.9 implies that with the minor estimation error in the density function, the inverse model cannot fully mitigate the hysteresis nonlinearity.

**Case 3:** In this case, the estimated density function  $\hat{p}_m(r)$  has a major estimation error, i.e.,  $\hat{p}_m(r) = 0.2 + 0.2r$ . The major estimation error leads to a larger inverse compensation error compared with Case 2, which is confirmed by both the analytical error and the simulation error shown in Fig. 5.10. The input-output relation of the input signal and the compensated output, shown in Fig. 5.11, becomes to the wider hysteresis loops in this case compared to Fig. 5.8. The compensation output shown in Fig. 5.12 also supports the above outcomes.

Based on the simulation results, it can be concluded that the obtained analytical expression in (5.16) can accurately describe the inverse compensation error brought by the unknown density function in the MGPI model. Such an expression is essential for the controller designs and the stability analysis of the closed-loop control system.

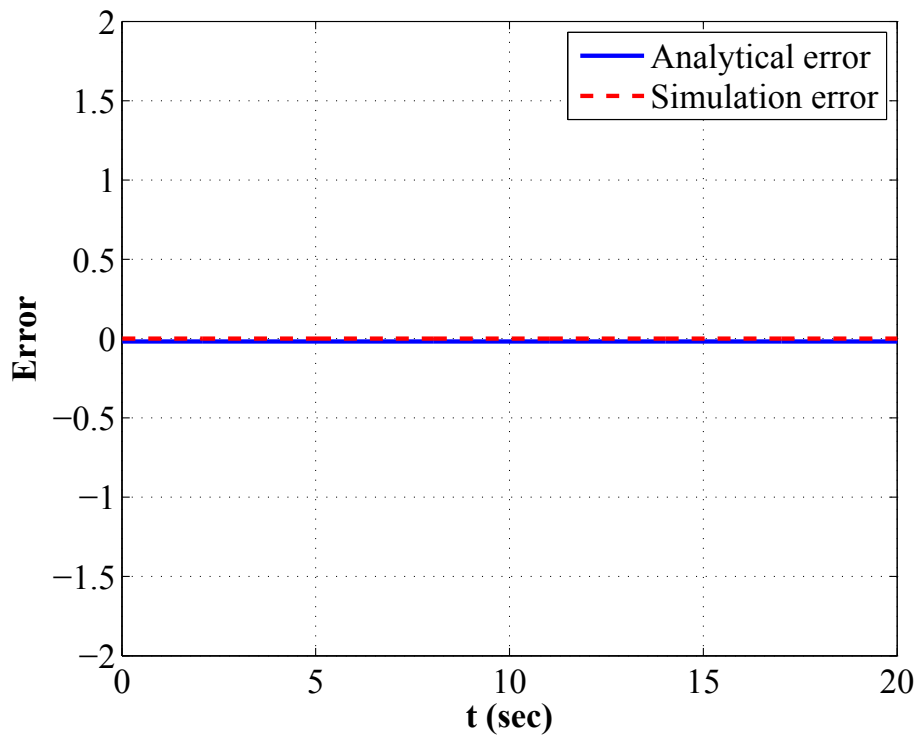


Figure 5.4: Inverse compensation error without estimation error in density function.

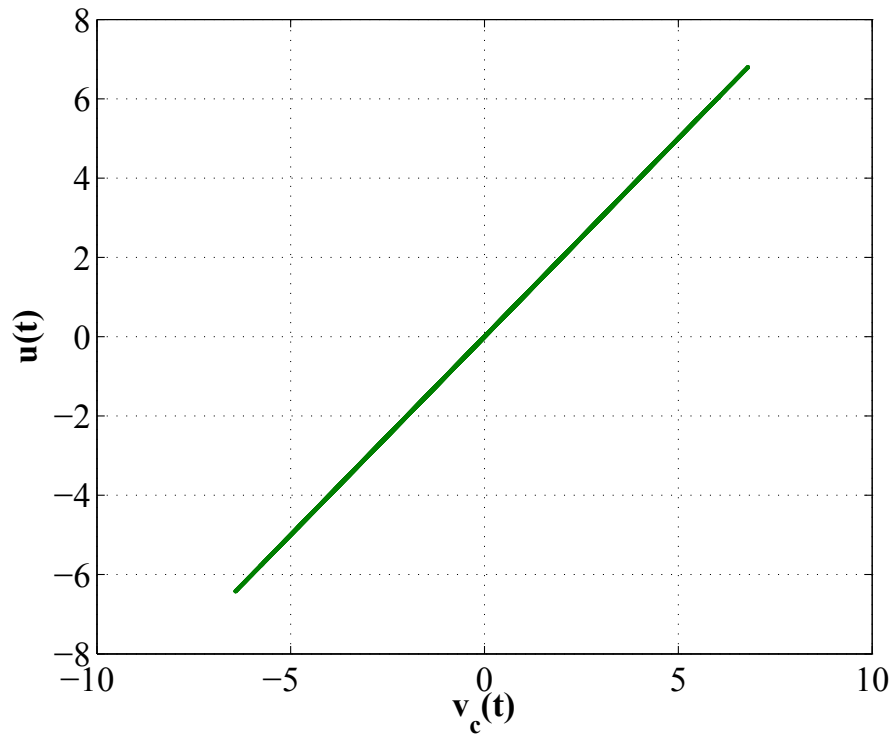


Figure 5.5: Input-output relationship of inverse compensation without estimation error in density function.

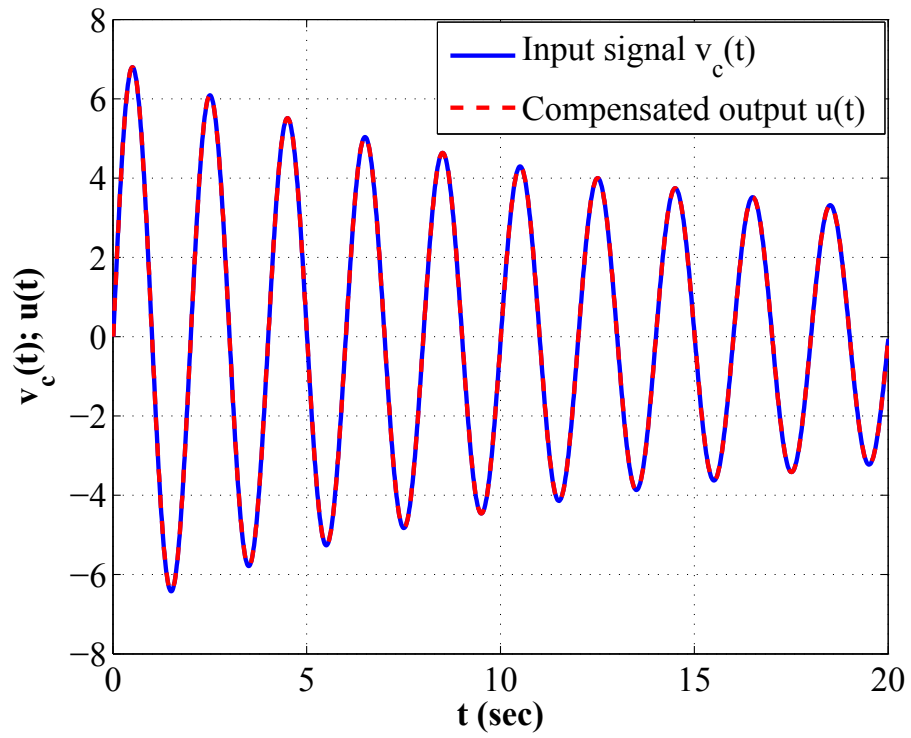


Figure 5.6: Compensated output tracks the reference input without estimation error in density function.

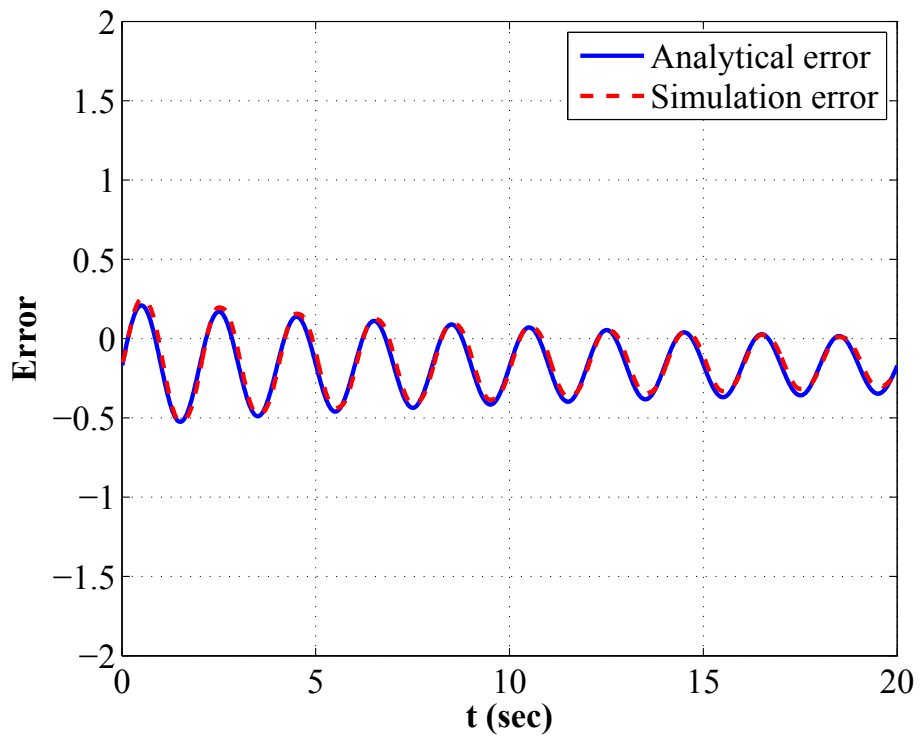


Figure 5.7: Inverse compensation error with minor estimation error in density function.

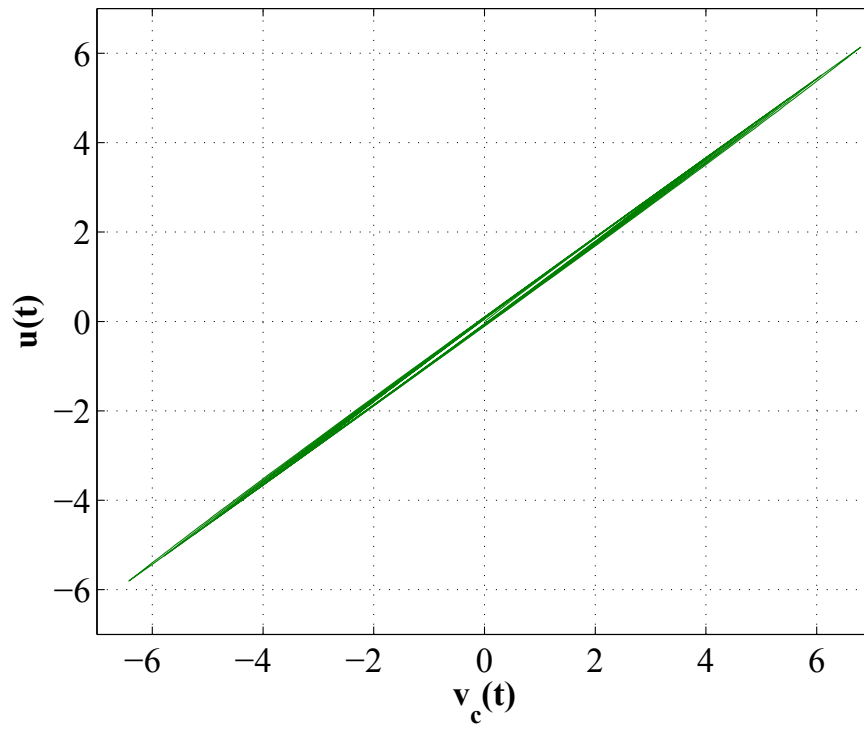


Figure 5.8: Input-output relationship of inverse compensation with minor estimation error in density function.

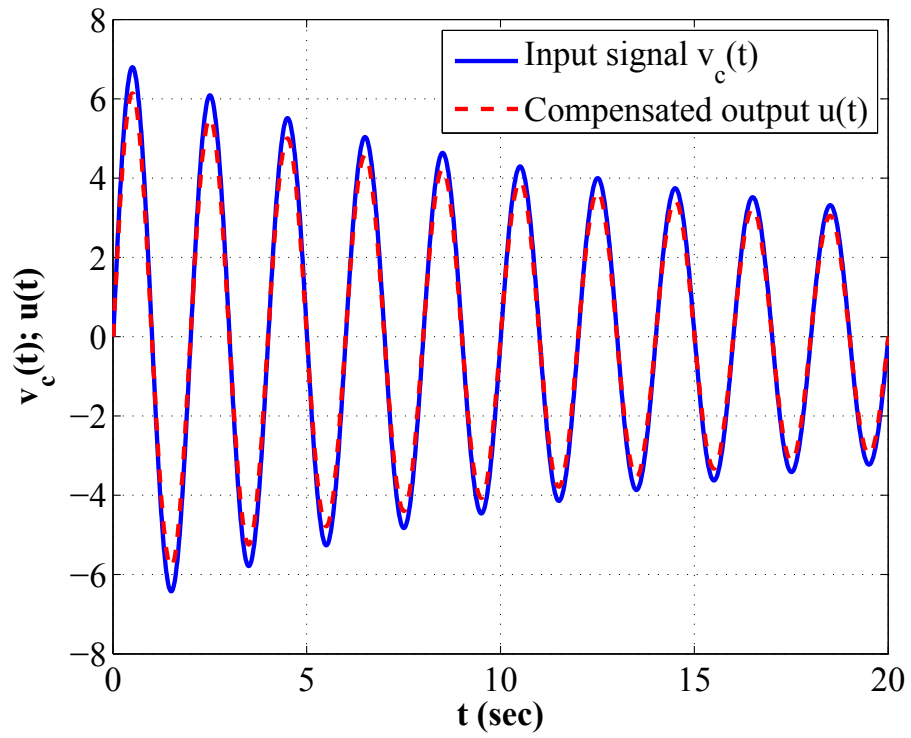


Figure 5.9: Compensated output tracks the reference input with minor estimation error in density function.

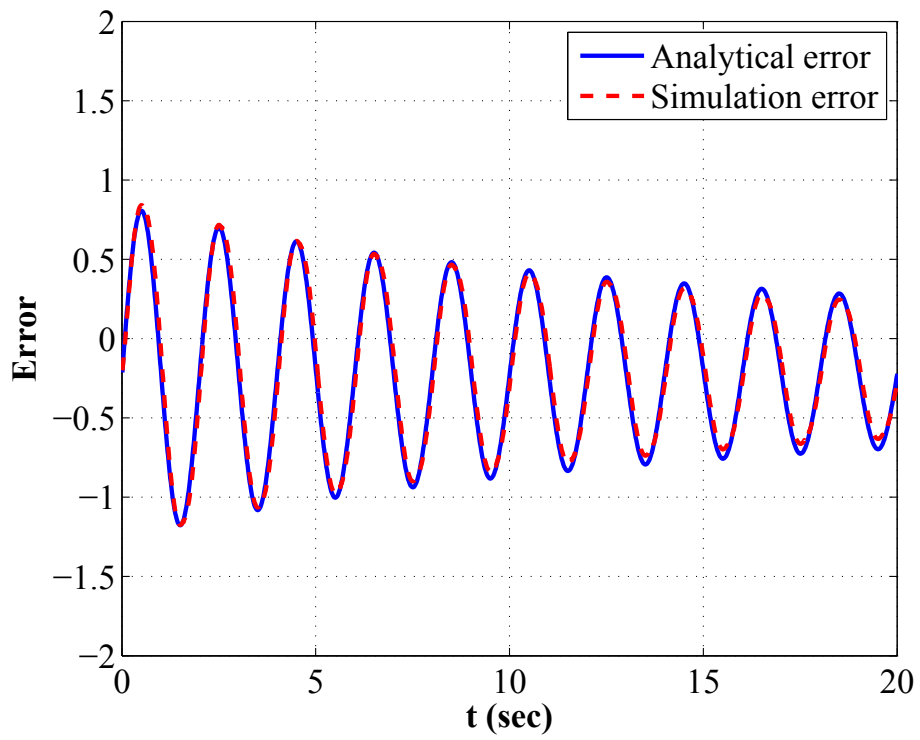


Figure 5.10: Inverse compensation error with major estimation error in density function.

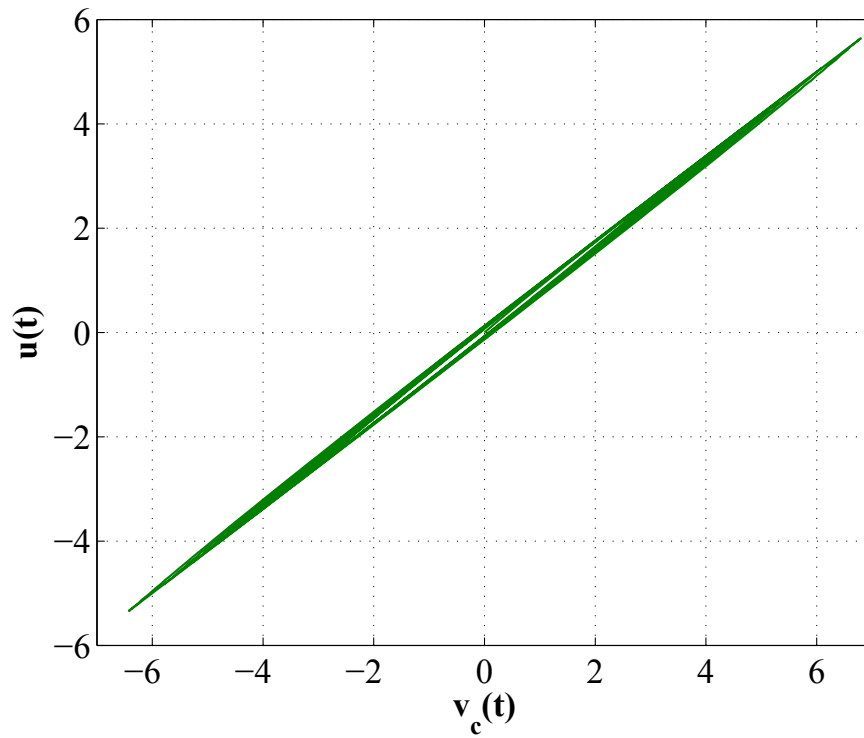


Figure 5.11: Input-output relationship of inverse compensation with major estimation error in density function.

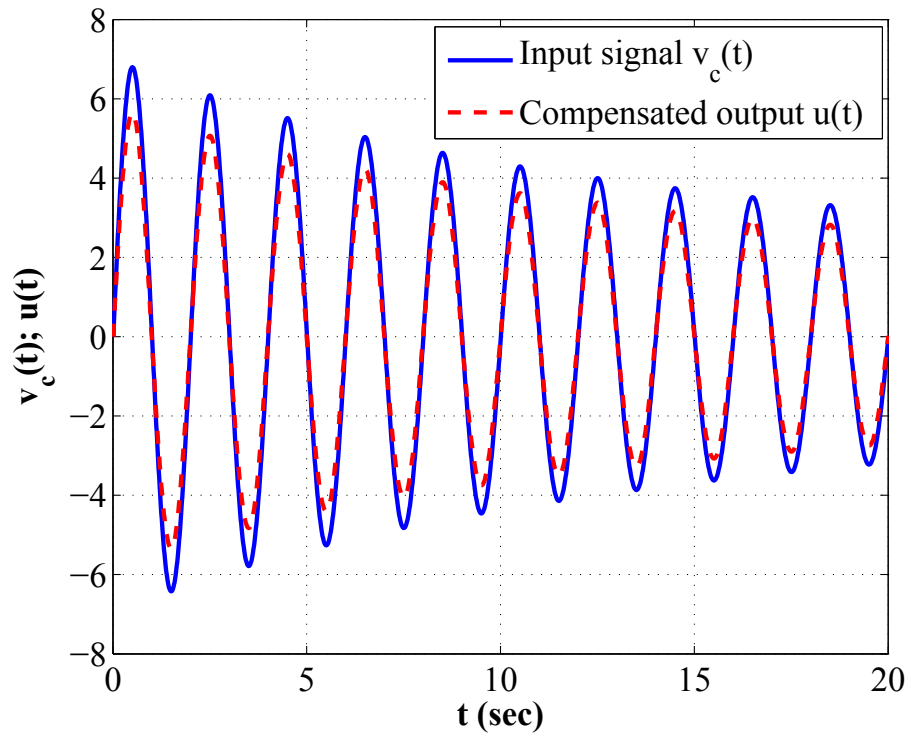


Figure 5.12: Compensated output tracks the reference input with major estimation error in density function.

# Chapter 6

## Controller Design I: State-Feedback

### Control

Recently, the control of nonlinear systems preceded by hysteresis nonlinearities has re-attracted much attention due to the rapid growth of applications of smart material based actuators. Many control approaches have been proposed in the literature (see, for example, [1, 3, 4, 15, 20, 22, 81, 91, 95, 97, 100–108]), which can generally be classified as two groups. The first is the use of inverse hysteresis as a feedforward compensator [3, 4, 15, 20, 22, 95, 97, 101, 105, 107, 108] and the second is without using the inverse construction [1, 81, 91, 102–104, 106]. For the first group, the strict stability proof is still a challenge task except [3] and [21] due to the fact that an error expression of the inverse compensation has not been established yet when the hysteresis is unknown. This explains the reason why the second group of controllers were developed, which usually satisfies the Lyapunov condition. In this chapter, it will be shown that a strict stability proof can be established for the inverse compensation scheme as well by taking consideration of error expression of the inverse compensation derived in Chapter 5 in the controller design, where a play operator-based model is used to describe the hysteresis nonlinearities. Comparing with a typical approach [1] in the second category, the benefit for such a design is that the proposed inverse based scheme can achieve the tracking

without necessarily adapting the uncertain parameters (the number could be large) in the hysteresis model, which is made possible by the introduction of the stop operator in the error formulation. Though the proposed approach incurs extra cost in implementing hysteresis inversion, it achieves gain in computational efficiency by not having to adapt the hysteresis parameters. Simulation example confirms the developed control approach.

## 6.1 Problem Statement

Consider a controlled system consisting of a nonlinear plant preceded by a hysteresis actuator, which is described as [1]

$$x^{(n)}(t) + \sum_{i=1}^k a_i Y_i(x(t), \dot{x}(t), \dots, x^{(n-1)}(t)) = bu(t) \quad (6.1)$$

$$u(t) = \Pi_m[v](t) \quad (6.2)$$

where  $Y_i$  are known continuous, linear or nonlinear functions. The parameters  $a_i$  and the control gain  $b$  are unknown constants. It is a common assumption that the sign of  $b$  is known. Without losing generality, it is assumed that  $b > 0$ .  $\Pi_m$  is the MGPI hysteresis operator, which was introduced in Chapter 3. The function  $u(t)$  is the output of hysteresis actuator (6.2), serving as the input signal of the nonlinear plant (6.1), and  $v(t)$  is the input signal to the actuator. In this chapter, it is assumed that the system states  $\mathbf{x} = [x, \dot{x}, \dots, x^{(n-1)}]^T$  are available to be measured.

The control objective is to design a control law for  $v(t)$  with unknown parameters of the system (6.1) and hysteresis (6.2), to drive the plant state  $x(t)$  to track a predefined desired trajectory,  $x_d(t)$ , i.e.,  $x(t) \rightarrow x_d(t)$  as  $t \rightarrow \infty$ .

Before proceeding, a basic assumption for  $x_d(t)$  is required, which is standard and generally satisfied.

*Assumption:* The desired trajectory  $\mathbf{x}_d = [x_d, \dot{x}_d, \dots, x_d^{(n-1)}]^T$  is continuous. Furthermore,  $[\mathbf{x}_d^T, x_d^{(n)}]^T / \Omega_d \rightarrow R^{n+1}$  with  $\Omega_d$  being a compact set.

As a matter of fact, focusing on the above control objective, a control scheme was developed in [1] without using inverse hysteresis cancelation. However, the following development will focus on an inverse compensation scheme, showing a strict stability proof with certain advantages over [1]. The control scheme attacked in the chapter is depicted in Fig. 6.1.

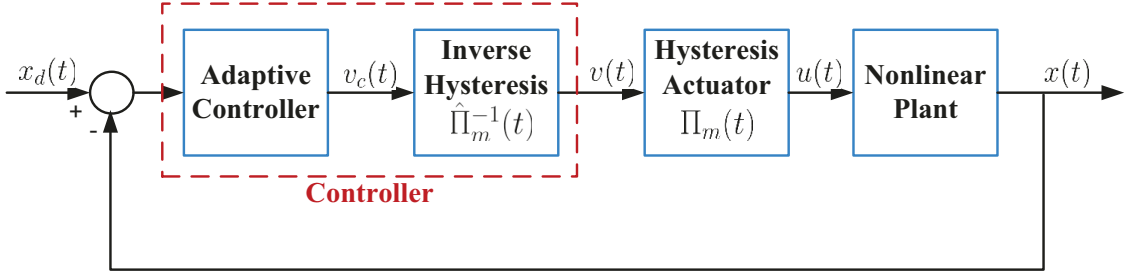


Figure 6.1: State-feedback control structure

It can be seen that the inverse hysteresis model  $\hat{\Pi}_m^{-1}(t)$  is the feedforward compensator and the feedback adaptive controller is expected to be designed in this chapter.

## 6.2 State-Feedback Controller Design

In [1], an adaptive variable structure controller has been designed to mitigate the hysteresis effect described by PI model without constructing the inverse model. In this chapter, with the inverse compensation error derived previously, an adaptive variable structure controller is developed to show the advantage of using inverse compensation. Meanwhile, since the inverse compensation error is derived in the form of (5.16), the boundness  $D$  will be adapted online. Note that in this section, the adaptive control law for  $v_c(t)$  as shown in Fig. 6.1 will be designed. Then, the control signal  $v(t)$  can be calculated by  $v(t) = \hat{\Pi}_m^{-1}[v_c](t)$ .

From (5.16), the output  $u(t)$  of the inverse compensation can be expressed by

$$u(t) = \chi_0 v_c(t) \quad d[v_c](t). \quad (6.3)$$

The close-loop control system (6.1) can then be re-written as

$$\begin{aligned}
\dot{x}_1 &= x_2 \\
\dot{x}_2 &= x_3 \\
&\vdots \\
\dot{x}_{n-1} &= x_n \\
\dot{x}_n &= \sum_{i=1}^k a_i Y_i(x_1, x_2, \dots, x_{n-1}) + \chi_b v_c(t) \quad d_b[v_c](t) \\
&= \mathbf{a}^T \mathbf{Y} + \chi_b v_c(t) \quad d_b[v_c](t)
\end{aligned} \tag{6.4}$$

where  $\mathbf{a} = [a_1, a_2, \dots, a_k]^T$ ,  $\mathbf{Y} = [Y_1, Y_2, \dots, Y_k]^T$ ,  $\chi_b = b\chi_0$  and  $d_b[v_c](t) = b \times d[v_c](t)$ . The boundness of  $d_b[v_c](t)$  is denoted by  $D_b = b \times D$ . The parameters  $\mathbf{a}$ ,  $\chi_b$  and  $D_b$  are unknown and have to be estimated. The estimated values are represented by  $\hat{\mathbf{a}}$ ,  $\hat{\chi}_b$  and  $\hat{D}_b$ , respectively. The errors between the real values and the estimated values are defined as follows.

$$\begin{aligned}
\tilde{\mathbf{a}}(t) &= \mathbf{a} - \hat{\mathbf{a}}(t) \\
\tilde{\beta}(t) &= \beta - \hat{\beta}(t) \\
\tilde{D}_b &= D_b - \hat{D}_b(t)
\end{aligned} \tag{6.5}$$

where  $\beta = \frac{1}{\chi_b}$ .

In order to facilitate the controller design, the introduction of the following new variables are necessary.

$$\begin{aligned}
z_1(t) &= x_1(t) - x_d(t) \\
z_i(t) &= x_i(t) - x_d^{(i-1)}(t) - \alpha_{i-1}(t), i = 2, 3, \dots, n \\
\alpha_1(t) &= -c_1 z_1(t) \\
\alpha_i(t) &= -c_i z_i(t) - z_{i-1}(t) + \dot{\alpha}_{i-1}(x_1, \dots, x_{i-1}, x_d, \dots, x_d^{(i-1)}), i = 2, 3, \dots, n-1
\end{aligned} \tag{6.6}$$

where  $c_i$ ,  $i = 1, 2, \dots, n-1$ , are positive design parameters.

According to (6.6), the time derivative of  $z_1$  is

$$\begin{aligned}\dot{z}_1(t) &= \dot{x}_1(t) - \dot{x}_d(t) = x_2(t) - \dot{x}_d(t) \\ &= z_2(t) + \alpha_1(t) = z_2(t) - c_1 z_1(t).\end{aligned}\tag{6.7}$$

Similarly, for  $z_i$ ,  $i = 2, 3, \dots, n-1$ , the time derivative  $\dot{z}_i$  can be obtained by

$$\begin{aligned}\dot{z}_i(t) &= \dot{x}_i(t) - \dot{x}_d^{(i)}(t) = \dot{\alpha}_{i-1} \\ &= z_{i+1}(t) - z_{i-1}(t) - c_i z_i(t)\end{aligned}\tag{6.8}$$

and the time derivative of  $z_n$  is

$$\begin{aligned}\dot{z}_n(t) &= \dot{x}_n(t) - \dot{x}_d^{(n)}(t) = \dot{\alpha}_{n-1} \\ &= \mathbf{a}^T \mathbf{Y} + \chi_b v_c(t) - d_b[v_c](t) - x_d^{(n)} - \dot{\alpha}_{n-1}.\end{aligned}\tag{6.9}$$

Based on the given plant and hysteresis model subject to the assumptions described above, the following control law is proposed.

$$v_c(t) = \frac{1}{\hat{\chi}_b} v_1(t) = \hat{\beta} v_1(t)\tag{6.10}$$

where

$$v_1(t) = -c_n z_n - z_{n-1} + \dot{\alpha}_{n-1} + x_d^{(n)} - \hat{\mathbf{a}}^T \mathbf{Y} + \text{sgn}(z_n) \hat{D}_b\tag{6.11}$$

and  $c_n$  is a positive design parameter.

The parameter  $\hat{\mathbf{a}}$ ,  $\hat{\beta}$  and function  $\hat{D}_b$  will be updated based on the following adaptation laws:

$$\dot{\hat{\mathbf{a}}} = \varepsilon_a \mathbf{Y} z_n\tag{6.12}$$

$$\dot{\hat{\beta}} = \varepsilon_b v_1 z_n\tag{6.13}$$

$$\dot{\hat{D}}_b = \varepsilon_D z_n\tag{6.14}$$

where  $\varepsilon_a$ ,  $\varepsilon_b$  and  $\varepsilon_D$  are adaptive parameters.

*Theorem:* For the plant given in (6.1) with the hysteresis  $\Pi_m(t)$  in (3.12), the inverse MGPI model  $\hat{\Pi}_m^{-1}(t)$  with the hysteresis loop compensator  $\hat{\Pi}_{com}(t)$  defined in (5.4) and the

inverse compensation error described as (5.16), the adaptive controller specified by (6.10) and (6.12)-(6.14) ensures that all the closed-loop signals are bounded and  $x(t) \infty x_d(t)$  as  $t \infty \in$ .

*Proof:* From (6.6), (6.9) and (6.10), one can obtain that

$$\begin{aligned} \dot{z}_n = & c_n z_n \quad z_{n-1} + \tilde{\mathbf{a}}^T \mathbf{Y} \quad \text{sgn}(z_n) \hat{D}_b \\ & d_b[v_c](t) \quad \chi_0 \tilde{\beta} v_1(t). \end{aligned} \quad (6.15)$$

To prove the stability of the closed-loop control system with the designed controller (6.10) and (6.11), the following Lyapunov function candidate is selected,

$$V(t) = \sum_{i=1}^n \frac{1}{2} z_i^2 + \frac{1}{2\varepsilon_a} \tilde{\mathbf{a}}^T \tilde{\mathbf{a}} + \frac{\chi_b}{2\varepsilon_b} \tilde{\beta}^2 + \frac{1}{2\varepsilon_D} \tilde{D}_b^2. \quad (6.16)$$

The derivative of  $V(t)$  is

$$\begin{aligned} \dot{V}(t) &= \sum_{i=1}^n z_i \dot{z}_i + \frac{1}{\varepsilon_a} \tilde{\mathbf{a}}^T \dot{\tilde{\mathbf{a}}} + \frac{\chi_b}{\varepsilon_b} \tilde{\beta} \dot{\tilde{\beta}} + \frac{1}{\varepsilon_D} \tilde{D}_b \dot{\tilde{D}}_b \\ &\geq \sum_{i=1}^n c_i z_i^2 + \frac{1}{\varepsilon_a} \tilde{\mathbf{a}}^T (\varepsilon_a \mathbf{Y} z_n + \dot{\tilde{\mathbf{a}}}) + \frac{\chi_b}{\varepsilon_b} \tilde{\beta} (\dot{\tilde{\beta}} - \varepsilon_b v_1(t) z_n) \\ &\quad + \frac{1}{\varepsilon_D} \tilde{D}_b \dot{\tilde{D}}_b - z_n \hat{D}_b + d_b[v_c](t) z_n \\ &\geq \sum_{i=1}^n c_i z_i^2 + \frac{1}{\varepsilon_a} \tilde{\mathbf{a}}^T (\varepsilon_a \mathbf{Y} z_n + \dot{\tilde{\mathbf{a}}}) + \frac{\chi_b}{\varepsilon_b} \tilde{\beta} (\dot{\tilde{\beta}} - \varepsilon_b v_1(t) z_n) \\ &\quad + \frac{1}{\varepsilon_D} \tilde{D}_b (\dot{\tilde{D}}_b + \varepsilon_D z_n) \\ &= \sum_{i=1}^n c_i z_i^2. \end{aligned} \quad (6.17)$$

Since  $V(t)$  is nonincreasing, it implies that  $z_i$ , for  $i = 1, 2, \dots, n$ ,  $\hat{\mathbf{a}}$ ,  $\hat{\beta}$  and  $\hat{D}_b$  are bounded. Furthermore, by applying the Lasalle-Yoshizawa theorem, it can be shown that  $z_i \infty 0$  ( $i = 1, 2, \dots, n$ ) as  $t \infty \in$ , which implies that  $x(t) \infty x_d(t)$  as  $t \infty \in$ . ■

**Remark:** Comparing with a typical approach [1] in the second category, the inverse hysteresis compensation is inserted into the control loop in an attempt to further improve

the control performance. The benefit for such a design is that the proposed inverse based scheme can achieve the tracking without necessarily adapting the uncertain parameters (the number could be large) in the hysteresis model, which is made possible by the introduction of the stop operator in the error formulation. Though the proposed approach incurs extra cost in implementing hysteresis inversion, it achieves gain in computational efficiency by not having to adapt the hysteresis parameters.

### 6.3 Simulation Studies

In this section, the adaptive variable structure controller developed above will be applied to an nonlinear system described by

$$\dot{x} = a \frac{1 - e^{-x(t)}}{1 + e^{-x(t)}} + bu(t) \quad (6.18)$$

where  $u(t)$  stands for the output of the inverse compensated hysteresis nonlinearity by (6.3). The actual parameter values of the nonlinear system are  $a = 1$  and  $b = 1$ . The desired trajectory is given as  $x_d(t) = 5\sin(2t) + \cos(3.2t)$ . The actual and estimated value of  $p_{m0}$  and  $\hat{p}_{m0}$  are 0.5 and 0.52. The actual and estimated density function of the MGPI model are  $p_m(r) = 0.5e^{-0.0014r^2}$  and  $\hat{p}_m(r) = 0.52e^{-0.002r^2}$ , for  $r \in [0, 100]$ , respectively, and the envelope function parameter is chosen as  $m_0 = 1.7$ . The control parameters are chosen as  $c_1 = 5.9468$ ,  $\varepsilon_a = 0.13$ ,  $\varepsilon_b = 0.05$  and  $\varepsilon_D = 0.02$ . The initial parameters of the controller are selected as  $\hat{a}(0) = 0.13$ ,  $\hat{b}(0) = 0.431$  and  $\hat{D}_b(0) = 16$ . The initial state of the system is  $x(0) = 2.05$  and the sample time is set to be 0.001.

Also, in the simulation the function  $sgn(z_n)$  in (6.11) is replaced by the saturation function  $sat(z_n/\tau)$ , where  $\tau = 0.01$ , to avoid the control chatter. The main penalty paid for the replacement is that it will introduce the tracking error. It should be noted that if the width of the linear region in the saturation function is chosen excessively thin, the controller runs the risk of exciting high frequency dynamics. This suggests that a tradeoff must be made between the width and the trajectory-following requirements.

To show the performance of using the control scheme with the inverse hysteresis compensation, the simulations were performed comparing with the approach developed in [1], where there is no inverse construction. Following the control approach in [1], the controller without inverse compensation can be obtained by

$$v_Q(t) = \hat{\phi}_Q(t)v_{Q1}(t) \quad (6.19)$$

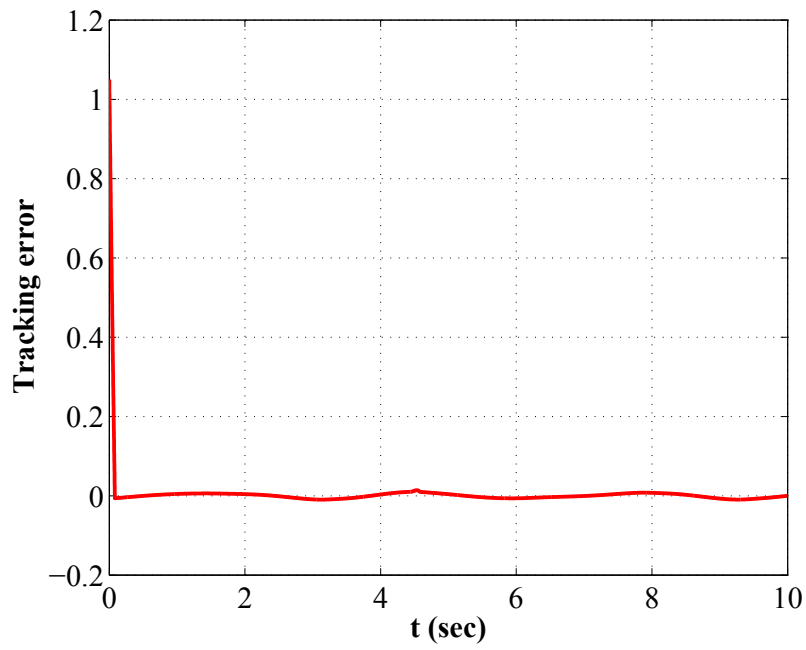
with

$$v_{Q1}(t) = c_1 z_1 \hat{a} \frac{1}{1 + e^{-x(t)}} + \dot{x}_d \operatorname{sgn}(z_1) \hat{B} \quad (6.20)$$

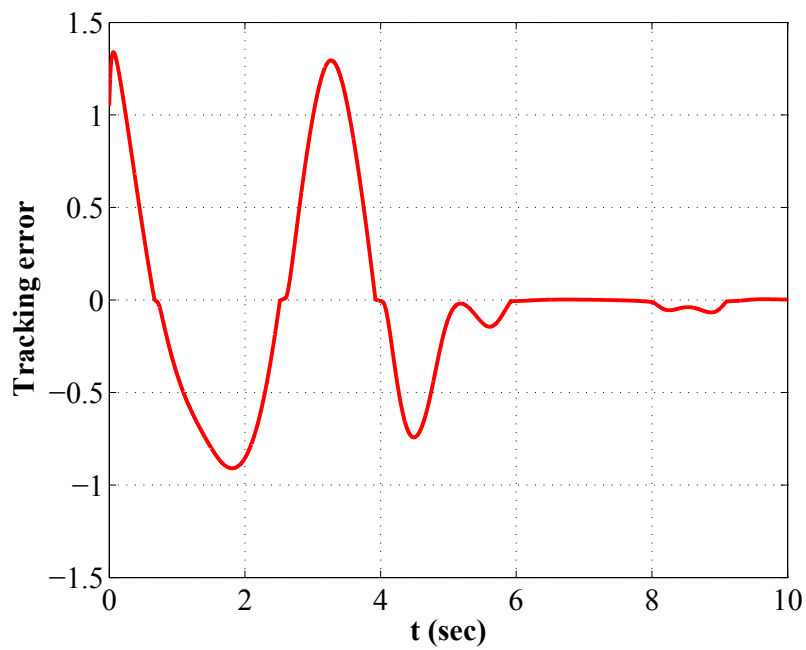
where  $\hat{\phi}_Q = \frac{1}{m_0 \hat{p}_{bm0}}$ ,  $\hat{B} = \int_0^\infty \hat{p}_{bm}(r) G_{mr}[v](t) dr$ ,  $p_{bm0} = bp_{m0}$  and  $p_{bm} = bp_m$ . Note that the parameters in both adaptive controllers are the same.

The simulations were conducted in Matlab. To show the superior performance of using the control scheme with the inverse hysteresis compensation, the simulations were performed comparing with the approach developed in [1], where there is no inverse construction. Note that the parameters in both adaptive controllers are selected the same. Fig. 6.2 shows the tracking errors of the proposed controller and the controller in [1], where Fig. 6.2(a) is the tracking error with an inverse MGPI model and Fig. 6.2(b) is the tracking error without the inverse compensation, respectively. The comparison of state trajectories of proposed controller and controller in [1] is provided in Fig. 6.3. Fig. 6.4 shows the control signals for both controllers.

It is clear that, with the similar control magnitudes, the control scheme with the inverse compensation has superior transient performance, for example, much shorter settling time. Furthermore, the control signal of the inverse control scheme is smoother than the control signal generated by the direct controller. Therefore, it can be concluded that the control scheme with the inverse hysteresis compensation has superior performance over the controller developed in [1].

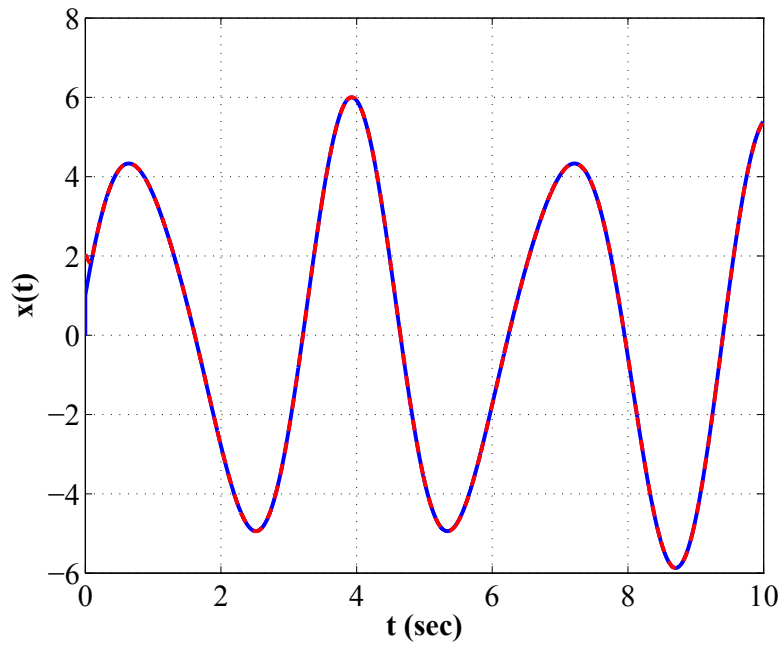


(a)

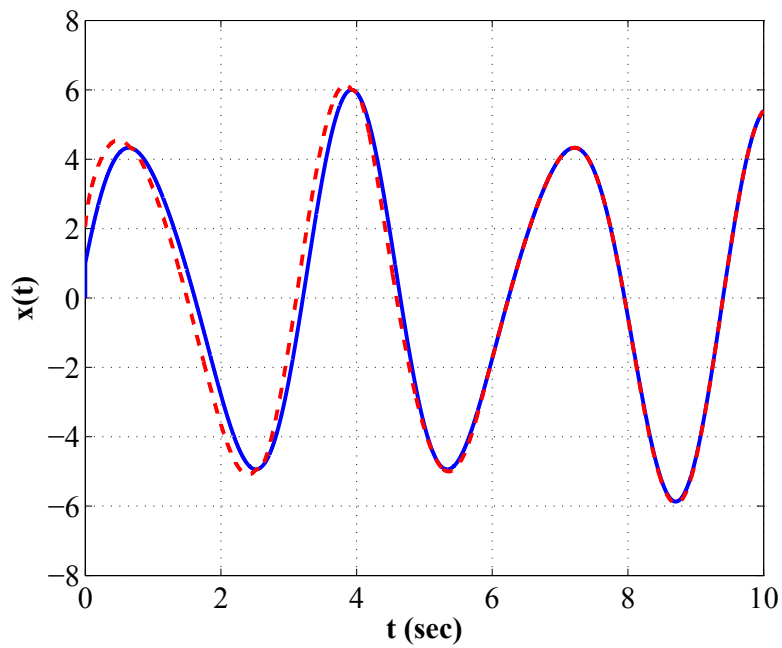


(b)

Figure 6.2: Tracking errors of state-feedback controller (a) with inverse compensation and (b) without inverse compensation.

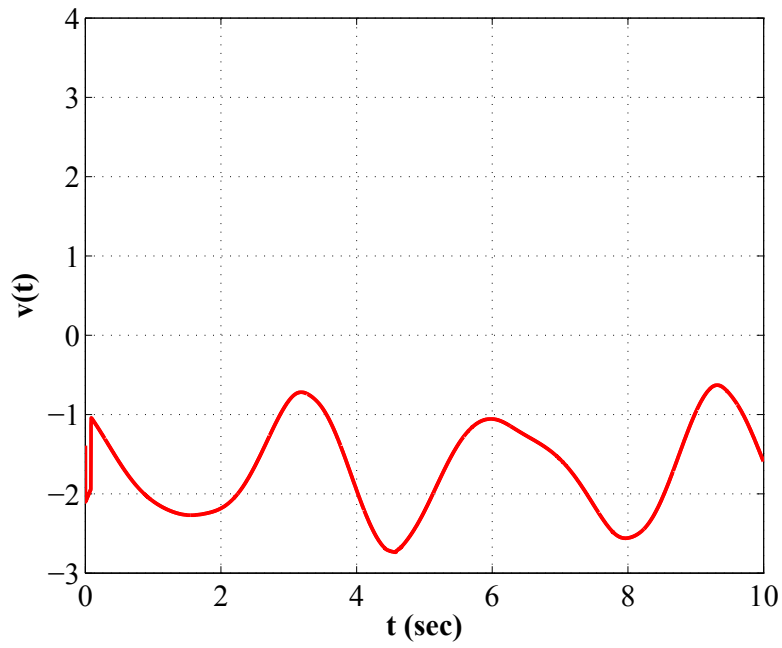


(a)

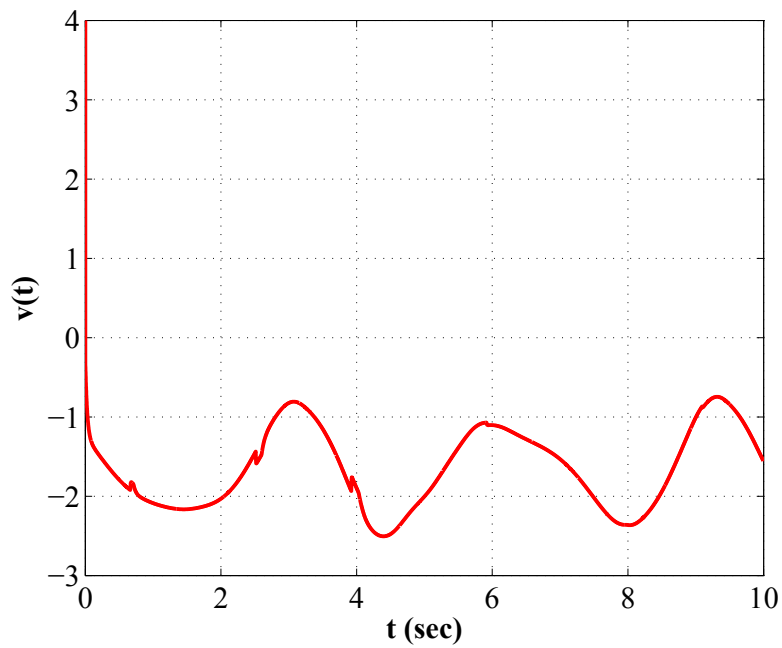


(b)

Figure 6.3: System states  $x(t)$  of state-feedback controller (a) with inverse compensation and (b) without inverse compensation.



(a)



(b)

Figure 6.4: Control signals  $v(t)$  of state-feedback controller (a) with inverse compensation and (b) without inverse compensation.

# Chapter 7

## Controller Design II: Output-Feedback Control

The development of control approaches for the systems preceded with the hysteresis effects has received great attentions in the recent decades. The most common way is to construct an inverse model as the compensator, which is pioneered by Tao and Kokotovic in [3]. The adaptive controller was then designed as a feedback compensator to stabilize the close-loop control systems. The representative works can be found in, see, for example, [28,34,82,101]. In particular, in [109] an adaptive variable structure controller has been developed along with the inverse construction for the MGPI model. The hysteresis nonlinearities and the tracking error of the dynamic system have been remedied successfully. However, most of the developed control methods in the literature are valid when the system states are measured. However, for a given particular dynamical system, in most of the case that the exactly knowledge of all the states is unavailable and the only accessible state is the output of the system. Therefore, it is significant to develop control schemes with observers to estimate the unavailable states from the measurements of a single output [22,23].

In this chapter, an output control scheme still using inverse compensation will be addressed. The MGPI model proposed in Chapter 3 is adopted for describing hysteresis non-

linearity and its corresponding inverse model obtained in Chapter 4 is used as the feedforward compensator. The analytical expression of the inverse compensation error derived in Chapter 5 is considered to facilitate the controller design. An observer-based robust adaptive output feedback controller is developed for a class of uncertain systems preceded by a smart material based actuators. the proposed output control scheme guarantees the global stability of the close-loop control system as well as achieves the tracking accuracy. The effectiveness of the developed controller is illustrated by the simulation studies.

## 7.1 Problem Statement

Consider a controlled system, consisting of a plant preceded by a hysteresis actuator, which is described as

$$x^{(n)}(t) + \sum_{i=1}^k a_i Y_i(x(t), \dot{x}(t), \dots, x^{(n-1)}(t)) = bu(t)$$

$$y = x \tag{7.1}$$

$$u(t) = \Pi_m[v](t) \tag{7.2}$$

where  $Y_i$  are known continuous, linear or nonlinear functions. The parameters  $a_i$  and the control gain  $b$  are unknown constants. It is a common assumption that the sign of  $b$  is known. Without losing generality, we assume that  $b > 0$ .  $\Pi_m(t)$  is the MGPI hysteresis model, which has be described in the Chapter 3. The function  $u(t)$  is the output of hysteresis actuator (7.2), serving as the input signal of the nonlinear plant (7.1), and  $v(t)$  is the input signal to the actuator.

When the states of the plant are unavailable except the system output  $y(t)$ , the control objective is to design a control law for  $v(t)$  with unknown parameters of the system (7.1) and hysteresis (7.2), to drive the system output  $y(t)$  to track a predefined desired trajectory,  $y_d(t)$ , i.e.,  $y(t) \infty y_d(t)$  as  $t \infty \in$ .

Before proceeding, a basic assumption for  $y_d(t)$  is required, which is standard and generally satisfied.

*Assumption:* The desired trajectory  $\mathbf{y}_d = [y_d, \dot{y}_d, \dots, y_d^{(n-1)}]^T$  is continuous. Furthermore,  $[\mathbf{y}_d^T, y_d^{(n)}]^T / \Omega_d \rightarrow R^{n+1}$  with  $\Omega_d$  being a compact set.

In this chapter, focusing on the above control objective, an output feedback control scheme using inverse hysteresis cancelation will be developed. The proposed control scheme can be depicted in Fig.7.1

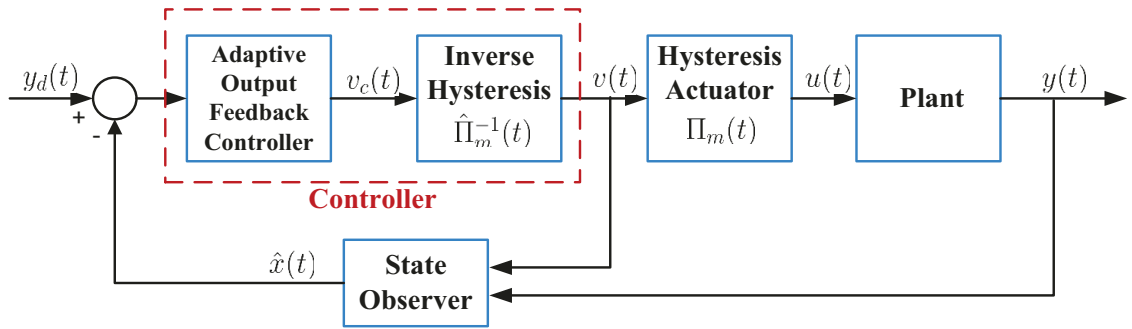


Figure 7.1: Output-feedback control structure

## 7.2 State Observer

For the purpose of the output feedback controller design, an state observer is required as the first step.

To construct such an observer, the plant (7.1) can be rewrite as

$$\begin{aligned} \dot{x} &= Ax + \mathbf{a}^T \mathbf{Y} e_n + bue_n \\ y &= cx \end{aligned} \tag{7.3}$$

where

$$\begin{aligned}
A &= \begin{bmatrix} 0 & & \\ \vdots & I_{n-1} & \\ 0 & \times\times\times 0 & \end{bmatrix}, \mathbf{a} = \begin{bmatrix} a_1 \\ \vdots \\ a_k \end{bmatrix}, \mathbf{Y} = \begin{bmatrix} Y_1 \\ \vdots \\ Y_k \end{bmatrix}, \\
c &= \begin{bmatrix} 1 \\ \vdots \\ 0 \end{bmatrix}^T, e_n = \begin{bmatrix} 0 \\ \vdots \\ 1 \end{bmatrix}.
\end{aligned} \tag{7.4}$$

From (5.16), the output of the hysteresis actuator  $u(t)$  with the inverse compensation when the hysteresis is unknown can be obtained by

$$u(t) = v_c(t) \quad e(t) = \chi_0 v_c(t) \quad d[v_c](t). \tag{7.5}$$

Thus, the plant (7.3) can be further written as

$$\begin{aligned}
\dot{x}(t) &= Ax(t) + \mathbf{a}^T \mathbf{Y} e_n + b \chi_0 v_c(t) e_n \quad b d[v_c](t) e_n \\
y &= cx.
\end{aligned} \tag{7.6}$$

To construct an observer for (7.6), we choose  $q = [q_1, \times\times\times, q_n]^T$  such that all eigenvalues of  $A_0 = A - qc$  are at some desired stable locations.

The estimate of  $x(t)$  can be obtained by

$$\hat{x}(t) = \xi_0 \sum_{i=1}^k a_i \xi_i + b \varrho \tag{7.7}$$

where

$$\begin{aligned}
\dot{\varrho} &= A_0 \varrho + e_n u \\
\dot{\xi}_0 &= A_0 \xi_0 + q y \\
\dot{\xi}_i &= A_0 \xi_i + Y_i e_n, i = 1, \times\times\times, k.
\end{aligned} \tag{7.8}$$

The state estimation error is denoted by  $\epsilon(t) = x(t) - \hat{x}(t)$  and it can be obtained that

$$\begin{aligned}
\dot{\epsilon} &= \dot{x} - \dot{\hat{x}} \\
&= Ax + \mathbf{a}^T \mathbf{Y} e_n + b\chi_0 v_c e_n - bd[v_c]e_n - A_0 \xi_0 - qc x - \mathbf{a}^T A_0 \xi_i - \mathbf{a}^T \mathbf{Y} e_n - bA_0 \varrho - be_n u \\
&= (A - qc)x - A_0(\xi_0 - \sum_{i=1}^k a_i \xi_i + b\varrho) \\
&= A_0(x - \hat{x}) \\
&= A_0 \epsilon.
\end{aligned} \tag{7.9}$$

Therefore, it can be proved that, with a proper choice of  $q$ , the states estimation error  $\epsilon$  will be vanished.

It worth mentioning that the signal  $u(t)$  is the output of the actuator, which usually can not be measured in the control systems in practice. Therefore, the signals  $\varrho$  in (7.8) is not available for controller design and need to be reparameterized. Let  $\delta$  denote  $(d)/(dt)$ . With  $\Lambda(\delta) \triangleq \det(\delta I - A_0)$ , we express  $\varrho(t)$  as

$$\begin{aligned}
\varrho &= [\varrho_1, \dots, \varrho_n]^T \\
&= [P_1(\delta), \dots, P_n(\delta)]^T \frac{1}{\Lambda(\delta)} u(t)
\end{aligned} \tag{7.10}$$

for some known polynomials  $P_i(\delta), i = 1, \dots, n$ . Note that  $u(t) = \chi_0 v_c(t) - d(t)$  from (7.5), we obtain that

$$\varrho_i = \chi_0 \omega_i - d_i \tag{7.11}$$

where

$$\omega_i = \frac{P_i(\delta)}{\Lambda(\delta)} v_c(t), d_i = \frac{P_i(\delta)}{\Lambda(\delta)} d(t) \tag{7.12}$$

for  $i = 1, 2, \dots, n$ .

In particular, we have

$$\hat{x}_2 = \xi_{02} - \sum_{i=1}^k a_i \xi_{i2} + b\chi_0 \omega_2 - bd_2 \tag{7.13}$$

$$\omega_2 = \frac{\delta + q_1}{\delta^n + q_1 \delta^{n-1} + \dots + q_n} v_c(t). \tag{7.14}$$

### 7.3 Adaptive Output Feedback Controller Design

In this chapter, with the inverse compensation error expressed in the form of (5.16) and the designed state observer (7.7), it is now ready to develop an adaptive output feedback controller to remedy the inverse compensation error as well as achieve the tracking accuracy. Note that in this section the adaptive control law will be designed for  $v_c(t)$  which is shown in Fig. 7.1. The control signal  $v(t)$  can then be calculated by  $v(t) = \hat{\Pi}_m^{-1}[v_c](t)$ .

The adaptive output feedback controller is achieved by using the recursive backstepping strategy. Before proceeding the controller design, some necessary definitions are given as follows,

$$\begin{aligned} \tilde{\mathbf{a}} &= \mathbf{a} & \hat{\mathbf{a}} & & \tilde{b} &= b & \hat{b} \\ \tilde{\phi} &= \phi & \hat{\phi} & & \tilde{D}_b &= D_b & \hat{D}_b \\ \tilde{\chi}_b &= \chi_b & \hat{\chi}_b & & \tilde{\chi}_0 &= \chi_0 & \hat{\chi}_0 \end{aligned} \quad (7.15)$$

where  $\phi = 1/b$ ,  $\chi_b = b\chi_0$  and  $D_b = bD$ .  $\hat{\mathbf{a}}$ ,  $\hat{b}$ ,  $\hat{\phi}$ ,  $\hat{\chi}_0$ ,  $\hat{\chi}_b$  and  $\hat{D}_b$  are the estimations of  $\mathbf{a}$ ,  $b$ ,  $\phi$ ,  $\chi_0$ ,  $\chi_b$  and  $D_b$ , respectively.

To construct the output feedback controller, the following alternative coordinates are introduced.

$$z_1 = y \quad y_d = x_1 \quad y_d \quad (7.16)$$

$$z_j = \hat{\chi}_0 \omega_2^{(j-2)} \quad \alpha_{j-1}, j = 2, 3, \dots, n. \quad (7.17)$$

where  $\alpha_{j-1}$  is the virtual control signal at the  $j$ th step and will be determined in the following development.

**Step 1:**

From (7.16),

$$\dot{z}_1 = \dot{x}_1 \quad \dot{y}_d = \xi_{02} + \mathbf{a}^T \xi_{i2} + b\chi_0 \omega_2 \quad b d_2 + \epsilon_2 \quad \dot{y}_d. \quad (7.18)$$

Noting that  $z_2 = \hat{\chi}_0 \omega_2 \quad \alpha_1$  as in (7.17) and  $\chi_0 \omega_2 = (\hat{\chi}_0 + \tilde{\chi}_0) \omega_2 = z_2 + \alpha_1 + \tilde{\chi}_0 \omega_2$ ,  $\dot{z}_1$  can be

expressed by

$$\dot{z}_1 = \dot{x}_1 \quad \dot{y}_d = \xi_{02} + \mathbf{a}^T \xi_{i2} + bz_2 + b\alpha_1 + b\tilde{\chi}_0\omega_2 \quad bd_2 + \epsilon_2 \quad \dot{y}_d. \quad (7.19)$$

The first virtual control law  $\alpha_1$  is then selected as

$$\alpha_1 = \hat{\phi}\psi \quad (7.20)$$

$$\psi = c_1 z_1 \quad l_1 z_1 \quad \xi_{02} \quad \hat{\mathbf{a}}^T \xi_{(2)} + \dot{y}_d \quad (7.21)$$

where  $c_1$  and  $l_1$  are positive constants and  $\xi_{(2)} \triangleq [\xi_{12}, \xi_{22}, \dots, \xi_{k2}]^T$ .  $\dot{z}_1$  in (7.19) can then be rewritten as

$$\dot{z}_1 = c_1 z_1 \quad l_1 z_1 + bz_2 + \tilde{\mathbf{a}}^T \xi_{(2)} + b\tilde{\chi}_0\omega_2 \quad b\tilde{\phi}\psi \quad bd_2 + \epsilon_2. \quad (7.22)$$

The Lyapunov function candidate for this step  $V_1$  is chosen as

$$V_1 = \frac{1}{2}z_1^2 + \frac{1}{2\kappa_a}\tilde{\mathbf{a}}^T\tilde{\mathbf{a}} + \frac{b}{2\kappa_\phi}\tilde{\phi}^2 + \frac{b}{2\kappa_{\chi_0}}\tilde{\chi}_0^2 + \frac{1}{2l_1}\epsilon^T P_0 \epsilon \quad (7.23)$$

where  $\kappa_a$ ,  $\kappa_\phi$  and  $\kappa_{\chi_0}$  are positive constants, and  $P_0 = P_0^T > 0$  satisfies the equation  $P_0 A_0 + a_0^T P_0 = -2I$ , where  $I$  represents the  $n \times n$  identity matrix.

The time derivative of  $V_1$  is obtained by

$$\begin{aligned} \dot{V}_1 &= z_1 \dot{z}_1 \quad \frac{1}{\kappa_a}\tilde{\mathbf{a}}^T \dot{\tilde{\mathbf{a}}} \quad \frac{b}{\kappa_\phi}\tilde{\phi} \dot{\tilde{\phi}} \quad \frac{b}{\kappa_{\chi_0}}\tilde{\chi}_0 \dot{\tilde{\chi}}_0 \quad \frac{1}{l_1}\epsilon^T \dot{\epsilon} \quad (7.24) \\ &= c_1 z_1^2 \quad l_1 z_1^2 + bz_1 z_2 + z_1 \tilde{\mathbf{a}}^T \xi_{(2)} + z_1 b\tilde{\chi}_0\omega_2 \quad z_1 b\tilde{\phi}\psi \quad z_1 bd_2 + z_1 \epsilon_2 \\ &\quad \frac{1}{\kappa_a}\tilde{\mathbf{a}}^T \dot{\tilde{\mathbf{a}}} \quad \frac{b}{\kappa_\phi}\tilde{\phi} \dot{\tilde{\phi}} \quad \frac{b}{\kappa_{\chi_0}}\tilde{\chi}_0 \dot{\tilde{\chi}}_0 \quad \frac{1}{l_1}\epsilon^T \dot{\epsilon} \\ &= c_1 z_1^2 + bz_1 z_2 + \frac{1}{\kappa_a}\tilde{\mathbf{a}}^T (\kappa_a z_1 \xi_{(2)}) \quad \dot{\tilde{\mathbf{a}}} + \frac{b}{\kappa_{\chi_0}}\tilde{\chi}_0 (\kappa_{\chi_0} z_1 \text{sgn}(b)\omega_2) \quad \dot{\tilde{\chi}}_0 \\ &\quad \frac{b}{\kappa_\phi}(\kappa_\phi z_1 \text{sgn}(b)\psi + \dot{\tilde{\phi}}) \quad z_1 d_{b2} \quad l_1 (z_1 \quad \frac{\epsilon}{2l_1})^2 + \frac{\epsilon^2}{4l_1} \quad \frac{1}{l_1}\epsilon^T \dot{\epsilon} \\ &\geq c_1 z_1^2 + bz_1 z_2 + \frac{1}{\kappa_a}\tilde{\mathbf{a}}^T (\kappa_a z_1 \xi_{(2)}) \quad \dot{\tilde{\mathbf{a}}} + \frac{b}{\kappa_{\chi_0}}\tilde{\chi}_0 (\kappa_{\chi_0} z_1 \text{sgn}(b)\omega_2) \quad \dot{\tilde{\chi}}_0 \\ &\quad \frac{b}{\kappa_\phi}(\kappa_\phi z_1 \text{sgn}(b)\psi + \dot{\tilde{\phi}}) \quad z_1 d_{b2} \quad \frac{3}{4l_1}\epsilon^T \dot{\epsilon} \end{aligned}$$

where  $d_{b2} \triangleq bd_2$  and  $\text{sgn}(\cdot)$  represents the sign function. The adaptive laws for  $\hat{\phi}$  and  $\hat{\chi}_0$  are selected as

$$\dot{\hat{\phi}} = \kappa_{\phi} z_1 \text{sgn}(b) \psi \quad (7.25)$$

$$\dot{\hat{\chi}}_0 = \kappa_{\chi_0} z_1 \text{sgn}(b) \omega_2, \quad (7.26)$$

respectively.

**Step 2:**

From (7.17), we can obtain that

$$\begin{aligned} \dot{z}_2 &= \dot{\hat{\chi}}_0 \omega_2 + \hat{\chi}_0 \dot{\omega}_2 - \dot{\alpha}_1 \\ &= z_3 + \alpha_2 + \hat{\chi}_0 \omega_2 - \dot{\alpha}_1 \\ &= z_3 + \alpha_2 + \hat{\chi}_0 \omega_2 - \frac{\partial \alpha_1}{\partial y} (\xi_{02} + \mathbf{a}^T \xi_{(2)} + b \chi_0 \omega_2 - d_{b2} + \epsilon_2) \\ &\quad - \frac{\partial \alpha_1}{\partial y_d} \dot{y}_d - \frac{\partial \alpha_1}{\partial \xi_0} \dot{\xi}_0 - \sum_{i=1}^k \frac{\partial \alpha_1}{\partial \xi_i} \dot{\xi}_i - \frac{\partial \alpha_1}{\partial \hat{\mathbf{a}}} \dot{\hat{\mathbf{a}}}. \end{aligned} \quad (7.27)$$

Let  $KT_2$  contain all the known terms in (7.27), then we have

$$\begin{aligned} \dot{z}_2 &= z_3 + \alpha_2 - \frac{\partial \alpha_1}{\partial y} \mathbf{a}^T \xi_{(2)} - \frac{\partial \alpha_1}{\partial y} \chi_b \omega_2 + \frac{\partial \alpha_1}{\partial y} d_{b2} \\ &\quad - \frac{\partial \alpha_1}{\partial y} \epsilon_2 - \frac{\partial \alpha_1}{\partial \hat{\mathbf{a}}} \dot{\hat{\mathbf{a}}} + KT_2. \end{aligned} \quad (7.28)$$

The virtual controller  $\alpha_2$  for step 2 is selected as

$$\begin{aligned} \alpha_2 &= -c_2 z_2 - l_2 \left( \frac{\partial \alpha_1}{\partial y} \right)^2 z_2 - KT_2 + \frac{\partial \alpha_1}{\partial y} \hat{\mathbf{a}}^T \xi_{(2)} + \frac{\partial \alpha_1}{\partial y} \hat{\chi}_b \omega_2 \\ &\quad - \hat{b} z_1 + \frac{\partial \alpha_1}{\partial \hat{\mathbf{a}}} \kappa_a (z_1 - \frac{\partial \alpha_1}{\partial y} z_2) \xi_{(2)} \end{aligned} \quad (7.29)$$

where  $c_2$  and  $l_2$  are positive constants.

Then  $\dot{z}_2$  can be rewritten as,

$$\begin{aligned} \dot{z}_2 &= z_3 - c_2 z_2 - \hat{b} z_1 - l_2 \left( \frac{\partial \alpha_1}{\partial y} \right)^2 z_2 - \frac{\partial \alpha_1}{\partial y} \tilde{\mathbf{a}}^T \xi_{(2)} - \frac{\partial \alpha_1}{\partial y} \tilde{\chi}_b \omega_2 \\ &\quad + \frac{\partial \alpha_1}{\partial y} d_{b2} - \frac{\partial \alpha_1}{\partial y} \epsilon_2 + \frac{\partial \alpha_1}{\partial \hat{\mathbf{a}}} (\kappa_a (z_1 - \frac{\partial \alpha_1}{\partial y} z_2) \xi_{(2)} - \dot{\hat{\mathbf{a}}}). \end{aligned} \quad (7.30)$$

The Lyapunov function candidate  $V_2$  in this step is selected as

$$V_2 = V_1 + \frac{1}{2}z_2^2 + \frac{1}{2\kappa_b}\tilde{b}^2 + \frac{1}{2\kappa_{\chi b}}\tilde{\chi}_b^2 + \frac{1}{2l_2}\epsilon^T P_0 \epsilon. \quad (7.31)$$

where  $\kappa_b$  and  $\kappa_{\chi b}$  are positive constants.

The time derivative of  $V_2$  can be obtained by

$$\begin{aligned} \dot{V}_2 &= \dot{V}_1 + z_2 \dot{z}_2 - \frac{1}{\kappa_b} \tilde{b} \dot{\tilde{b}} - \frac{1}{\kappa_{\chi b}} \tilde{\chi}_b \dot{\tilde{\chi}}_b - \frac{1}{l_2} \epsilon^T \dot{\epsilon} \\ &\geq c_1 z_1^2 + b z_1 z_2 + \frac{1}{\kappa_a} \tilde{\mathbf{a}}^T (\kappa_a z_1 \xi_{(2)} - \dot{\mathbf{a}}) - z_1 d_{b2} - \frac{3}{4l_1} \epsilon^T \epsilon \\ &\quad - \frac{1}{\kappa_b} \tilde{b} \dot{\tilde{b}} - \frac{1}{\kappa_{\chi b}} \tilde{\chi}_b \dot{\tilde{\chi}}_b + z_2 z_3 - c_2 z_2^2 - \hat{b} z_1 z_2 - l_2 \left( \frac{\partial \alpha_1}{\partial y} \right)^2 z_2^2 - z_2 \frac{\partial \alpha_1}{\partial y} \tilde{\mathbf{a}}^T \xi_{(2)} \\ &\quad - z_2 \frac{\partial \alpha_1}{\partial y} \tilde{\chi}_b \omega_2 + z_2 \frac{\partial \alpha_1}{\partial y} d_{b2} - z_2 \frac{\partial \alpha_1}{\partial y} \epsilon_2 + z_2 \frac{\partial \alpha_1}{\partial \hat{\mathbf{a}}} (\kappa_a (z_1 - \frac{\partial \alpha_1}{\partial y} z_2) \xi_{(2)} - \dot{\mathbf{a}}) - \frac{1}{l_2} \epsilon^T \epsilon \\ &= c_1 z_1^2 - c_2 z_2^2 + z_2 z_3 + \frac{1}{\kappa_b} \tilde{b} (\kappa_b z_1 z_2 - \dot{\tilde{b}}) + \frac{1}{\kappa_a} \tilde{\mathbf{a}}^T (\kappa_a (z_1 - \frac{\partial \alpha_1}{\partial y} z_2) \xi_{(2)} - \dot{\mathbf{a}}) \\ &\quad - \frac{1}{\kappa_{\chi b}} \tilde{\chi}_b (\kappa_{\chi b} \frac{\partial \alpha_1}{\partial y} z_2 \omega_2 + \dot{\tilde{\chi}}_b) + \frac{\partial \alpha_1}{\partial \hat{\mathbf{a}}} z_2 (\kappa_a (z_1 - \frac{\partial \alpha_1}{\partial y} z_2) \xi_{(2)} - \dot{\mathbf{a}}) - (z_1 - \frac{\partial \alpha_1}{\partial y} z_2) d_{b2} \\ &\quad - l_2 \left( z_2 - \frac{\epsilon}{2l_2} \right)^2 + \frac{\epsilon^2}{4l_2} - \frac{1}{l_2} \epsilon^T \epsilon - \frac{3}{4l_1} \epsilon^T \epsilon \\ &\geq c_1 z_1^2 - c_2 z_2^2 + z_2 z_3 + \frac{1}{\kappa_a} \tilde{\mathbf{a}}^T (\kappa_a (z_1 - \frac{\partial \alpha_1}{\partial y} z_2) \xi_{(2)} - \dot{\mathbf{a}}) - \frac{1}{\kappa_{\chi b}} \tilde{\chi}_b (\kappa_{\chi b} \frac{\partial \alpha_1}{\partial y} z_2 \omega_2 + \dot{\tilde{\chi}}_b) \\ &\quad + \frac{\partial \alpha_1}{\partial \hat{\mathbf{a}}} z_2 (\kappa_a (z_1 - \frac{\partial \alpha_1}{\partial y} z_2) \xi_{(2)} - \dot{\mathbf{a}}) - (z_1 - \frac{\partial \alpha_1}{\partial y} z_2) d_{b2} - \left( \frac{3}{4l_1} + \frac{3}{4l_2} \right) \epsilon^T \epsilon + \frac{1}{\kappa_b} \tilde{b} (\kappa_b z_1 z_2 - \dot{\tilde{b}}). \end{aligned} \quad (7.32)$$

The adaptive law for  $\hat{b}$  is selected as

$$\dot{\hat{b}} = \kappa_b z_1 z_2. \quad (7.33)$$

**Step  $j$ ,  $j = 3, 4, \dots, n - 1$ :**

Based on the definition in (7.17), we have

$$\begin{aligned} \dot{z}_j &= \hat{\chi}_0 \omega_2^{(j-1)} + \dot{\hat{\chi}}_0 \omega_2^{(j-2)} - \dot{\alpha}_{j-1} \\ &= z_{j+1} + \alpha_j + K T_j - \frac{\partial \alpha_{j-1}}{\partial y} \tilde{\mathbf{a}}^T \xi_{(2)} - \frac{\partial \alpha_{j-1}}{\partial y} \chi_b \omega_2 + \frac{\partial \alpha_{j-1}}{\partial y} d_{b2} - \frac{\partial \alpha_{j-1}}{\partial y} \epsilon_2 \\ &\quad - \frac{\partial \alpha_{j-1}}{\partial \hat{\mathbf{a}}} \dot{\hat{\mathbf{a}}} - \frac{\partial \alpha_{j-1}}{\partial \hat{\chi}_b} \dot{\hat{\chi}}_b \end{aligned} \quad (7.34)$$

where  $KT_j$  denotes the known terms in  $\dot{z}_j$ .

The virtual controller  $\alpha_j$  is chosen as

$$\begin{aligned} \alpha_j = & c_j z_j \quad z_{j-1} \quad KT_j \quad l_j \left( \frac{\partial \alpha_{j-1}}{\partial y} \right)^2 z_j + \frac{\partial \alpha_{j-1}}{\partial y} \hat{\mathbf{a}}^T \xi_{(2)} + \frac{\partial \alpha_{j-1}}{\partial y} \hat{\chi}_b \omega_2 \\ & + \frac{\partial \alpha_{j-1}}{\partial \hat{\mathbf{a}}} \kappa_a (z_1 \quad \sum_{i=1}^{j-1} \frac{\partial \alpha_i}{\partial y} z_{i+1}) \xi_{(2)} \quad \frac{\partial \alpha_{j-1}}{\partial \hat{\chi}_b} \kappa_{\chi b} \omega_2 \sum_{i=1}^{j-1} \frac{\partial \alpha_i}{\partial y} z_{i+1} \\ & \kappa_a \frac{\partial \alpha_{j-1}}{\partial y} \xi_{(2)} \sum_{i=1}^{j-2} \frac{\partial \alpha_i}{\partial \hat{\mathbf{a}}} z_{i+1} \quad \kappa_{\chi b} \frac{\partial \alpha_{j-1}}{\partial y} \omega_2 \sum_{i=2}^{j-2} \frac{\partial \alpha_i}{\partial \hat{\chi}_b} z_{i+1} \end{aligned} \quad (7.35)$$

where  $c_j$  and  $l_j$  are positive constants.

Then  $\dot{z}_j$  can be rewritten as

$$\begin{aligned} \dot{z}_j = & z_{j+1} \quad c_j z_j \quad z_{j-1} \quad l_j \left( \frac{\partial \alpha_{j-1}}{\partial y} \right)^2 z_j \quad \frac{\partial \alpha_{j-1}}{\partial y} \tilde{\mathbf{a}}^T \xi_{(2)} \quad \frac{\partial \alpha_{j-1}}{\partial y} \tilde{\chi}_b \omega_2 \\ & + \frac{\partial \alpha_{j-1}}{\partial y} d_{b2} \quad \frac{\partial \alpha_{j-1}}{\partial y} \epsilon_2 + \frac{\partial \alpha_{j-1}}{\partial \hat{\mathbf{a}}} (\kappa_a (z_1 \quad \sum_{i=1}^{j-1} \frac{\partial \alpha_i}{\partial y} z_{i+1}) \xi_{(2)} \quad \dot{\hat{\mathbf{a}}}) \\ & \frac{\partial \alpha_{j-1}}{\partial \hat{\chi}_b} (\kappa_{\chi b} (\sum_{i=1}^{j-1} \frac{\partial \alpha_i}{\partial y} z_{i+1}) \omega_2 + \dot{\hat{\chi}}_b) \quad \kappa_a \frac{\partial \alpha_{j-1}}{\partial y} \xi_{(2)} (\sum_{i=1}^{j-2} \frac{\partial \alpha_i}{\partial \hat{\mathbf{a}}} z_{i+1}) \\ & \kappa_{\chi b} \frac{\partial \alpha_{j-1}}{\partial y} \omega_2 (\sum_{i=2}^{j-2} \frac{\partial \alpha_i}{\partial \hat{\chi}_b} z_{i+1}). \end{aligned} \quad (7.36)$$

Select the  $j$ th Lyapunov function candidate  $V_j$  as

$$V_j = V_{j-1} + \frac{1}{2} z_j^2 + \frac{1}{2l_j} \epsilon^T P_0 \epsilon. \quad (7.37)$$

The time derivative of  $V_j$  can be obtained by

$$\begin{aligned} \dot{V}_j = & \dot{V}_{j-1} + z_j \dot{z}_j \quad \frac{1}{l_j} \epsilon^T \epsilon \\ \geq & \sum_{i=1}^j c_i z_i^2 + z_j z_{j+1} + \frac{1}{\kappa_a} \tilde{\mathbf{a}} (\kappa_a (z_1 \quad \sum_{i=1}^{j-2} \frac{\partial \alpha_i}{\partial y} z_{i+1}) \xi_{(2)} \quad \dot{\hat{\mathbf{a}}}) \\ & \frac{1}{\kappa_{\chi b}} \tilde{\chi}_b (\kappa_{\chi b} (\sum_{i=1}^{j-2} \frac{\partial \alpha_i}{\partial y} z_{i+1}) \omega_2 + \dot{\hat{\chi}}_b) + (\sum_{i=1}^{j-2} \frac{\partial \alpha_i}{\partial \hat{\mathbf{a}}} z_{i+1}) (\kappa_a (z_1 \quad \sum_{i=1}^{j-2} \frac{\partial \alpha_i}{\partial y} z_{i+1}) \xi_{(2)} \quad \dot{\hat{\mathbf{a}}}) \\ & (\sum_{i=2}^{j-2} \frac{\partial \alpha_i}{\partial \hat{\chi}_b} z_{i+1}) (\kappa_{\chi b} (\sum_{i=1}^{j-2} \frac{\partial \alpha_i}{\partial y} z_{i+1}) \omega_2 + \dot{\hat{\chi}}_b) \quad (\sum_{i=1}^{j-1} \frac{3}{4l_i}) \epsilon^T \epsilon \quad d_{b2} (z_1 \quad \sum_{i=1}^{j-2} \frac{\partial \alpha_i}{\partial y} z_{i+1}) \\ & l_j \left( \frac{\partial \alpha_{j-1}}{\partial y} \right)^2 z_j^2 \quad z_j \frac{\partial \alpha_{j-1}}{\partial y} \tilde{\mathbf{a}}^T \xi_{(2)} \quad z_j \frac{\partial \alpha_{j-1}}{\partial y} \tilde{\chi}_b \omega_2 + z_j \frac{\partial \alpha_{j-1}}{\partial y} d_{b2} \quad z_j \frac{\partial \alpha_{j-1}}{\partial y} \epsilon_2 \\ & + z_j \frac{\partial \alpha_{j-1}}{\partial \hat{\mathbf{a}}} (\kappa_a (z_1 \quad \sum_{i=1}^{j-1} \frac{\partial \alpha_i}{\partial y} z_{i+1}) \xi_{(2)} \quad \dot{\hat{\mathbf{a}}}) \end{aligned} \quad (7.38)$$

$$\begin{aligned}
& z_j \frac{\partial \alpha_{j-1}}{\partial \hat{\chi}_b} (\kappa_{\chi b} (\sum_{i=1}^{j-1} \frac{\partial \alpha_i}{\partial y} z_{i+1}) \omega_2 + \dot{\hat{\chi}}_b) \quad z_j \kappa_a \frac{\partial \alpha_{j-1}}{\partial y} \xi_{(2)} (\sum_{i=1}^{j-2} \frac{\partial \alpha_i}{\partial \hat{\mathbf{a}}} z_{i+1}) \\
& z_j \kappa_{\chi b} \frac{\partial \alpha_{j-1}}{\partial y} \omega_2 (\sum_{i=2}^{j-2} \frac{\partial \alpha_i}{\partial \hat{\chi}_b} z_{i+1}) \quad \frac{1}{l_j} \epsilon^T \epsilon \\
\geq & \sum_{i=1}^j c_i z_i^2 + z_j z_{j+1} \quad (\sum_{i=1}^j \frac{3}{4l_i}) \epsilon^T \epsilon \quad d_{b2}(z_1 \quad \sum_{i=1}^{j-1} \frac{\partial \alpha_i}{\partial y} z_{i+1}) \\
& + \frac{1}{\kappa_a} \tilde{\mathbf{a}} (\kappa_a (z_1 \quad \sum_{i=1}^{j-1} \frac{\partial \alpha_i}{\partial y} z_{i+1}) \xi_{(2)} \quad \dot{\mathbf{a}}) \quad \frac{1}{\kappa_{\chi b}} \tilde{\chi}_b (\kappa_{\chi b} (\sum_{i=1}^{j-1} \frac{\partial \alpha_i}{\partial y} z_{i+1}) \omega_2 + \dot{\hat{\chi}}_b) \\
& + (\sum_{i=1}^{j-2} \frac{\partial \alpha_i}{\partial \hat{\mathbf{a}}} z_{i+1}) (\kappa_a (z_1 \quad \sum_{i=1}^{j-1} \frac{\partial \alpha_i}{\partial y} z_{i+1}) \xi_{(2)} \quad \dot{\mathbf{a}}) \\
& \quad (\sum_{i=2}^{j-2} \frac{\partial \alpha_i}{\partial \hat{\chi}_b} z_{i+1}) (\kappa_{\chi b} (\sum_{i=1}^{j-1} \frac{\partial \alpha_i}{\partial y} z_{i+1}) \omega_2 + \dot{\hat{\chi}}_b) \\
& + z_j \frac{\partial \alpha_{j-1}}{\partial \hat{\mathbf{a}}} (\kappa_a (z_1 \quad \sum_{i=1}^{j-1} \frac{\partial \alpha_i}{\partial y} z_{i+1}) \xi_{(2)} \quad \dot{\mathbf{a}}) \quad z_j \frac{\partial \alpha_{j-1}}{\partial \hat{\chi}_b} (\kappa_{\chi b} (\sum_{i=1}^{j-1} \frac{\partial \alpha_i}{\partial y} z_{i+1}) \omega_2 + \dot{\hat{\chi}}_b) \\
= & \sum_{i=1}^j c_i z_i^2 + z_j z_{j+1} \quad (\sum_{i=1}^j \frac{3}{4l_i}) \epsilon^T \epsilon \quad d_{b2}(z_1 \quad \sum_{i=1}^{j-1} \frac{\partial \alpha_i}{\partial y} z_{i+1}) \\
& + \frac{1}{\kappa_a} \tilde{\mathbf{a}} (\kappa_a (z_1 \quad \sum_{i=1}^{j-1} \frac{\partial \alpha_i}{\partial y} z_{i+1}) \xi_{(2)} \quad \dot{\mathbf{a}}) \quad \frac{1}{\kappa_{\chi b}} \tilde{\chi}_b (\kappa_{\chi b} (\sum_{i=1}^{j-1} \frac{\partial \alpha_i}{\partial y} z_{i+1}) \omega_2 + \dot{\hat{\chi}}_b) \\
& + (\sum_{i=1}^{j-1} \frac{\partial \alpha_i}{\partial \hat{\mathbf{a}}} z_{i+1}) (\kappa_a (z_1 \quad \sum_{i=1}^{j-1} \frac{\partial \alpha_i}{\partial y} z_{i+1}) \xi_{(2)} \quad \dot{\mathbf{a}}) \\
& \quad (\sum_{i=2}^{j-1} \frac{\partial \alpha_i}{\partial \hat{\chi}_b} z_{i+1}) (\kappa_{\chi b} (\sum_{i=1}^{j-1} \frac{\partial \alpha_i}{\partial y} z_{i+1}) \omega_2 + \dot{\hat{\chi}}_b).
\end{aligned}$$

**Step n:**

In this step, the alternative coordinate  $z_n$  is expressed by

$$z_n = \hat{\chi}_0 \omega_2^{(n-2)} \quad \alpha_{n-1} \quad (7.39)$$

and the time derivative of  $z_n$  is obtained by

$$\dot{z}_n = \dot{\hat{\chi}}_0 \omega_2^{(n-2)} + \hat{\chi}_0 \omega_2^{(n-1)} \quad \dot{\alpha}_{n-1}. \quad (7.40)$$

Note that

$$\begin{aligned}
\hat{\chi}_0 \omega_2^{(n-1)} &= \hat{\chi}_0 \frac{\delta^n + q_1 \delta^{n-1}}{\Lambda(\delta)} v_c(t) \\
&= \hat{\chi}_0 v_c(t) + v_0(t)
\end{aligned} \quad (7.41)$$

where

$$v_0(t) = \frac{q_2 \delta^{n-2} + \dots + q_n}{\Lambda(\delta)} v_c(t). \quad (7.42)$$

Eq. (7.40) can be rewrite as

$$\begin{aligned}
\dot{z}_n &= \hat{\chi}_0 v_c(t) + v_0(t) + \dot{\hat{\chi}}_0 \omega_2^{(n-2)} \dot{\alpha}_{n-1} \\
&= \hat{\chi}_0 v_c(t) + KT_n \frac{\partial \alpha_{n-1}}{\partial y} \mathbf{a}^T \xi_{(2)} \frac{\partial \alpha_{n-1}}{\partial y} \chi_b \omega_2 + \frac{\partial \alpha_{n-1}}{\partial y} d_{b2} \frac{\partial \alpha_{n-1}}{\partial y} \epsilon_2 \\
&\quad \frac{\partial \alpha_{n-1}}{\partial \hat{\mathbf{a}}} \dot{\hat{\mathbf{a}}} \quad \frac{\partial \alpha_{n-1}}{\partial \hat{\chi}_b} \dot{\hat{\chi}}_b
\end{aligned} \tag{7.43}$$

where  $KT_n$  denotes the known terms in  $\dot{z}_n$ .

Therefore, the controller  $v_c(t)$  is designed as

$$v_c(t) = \frac{1}{\hat{\chi}_0} v_s(t) \tag{7.44}$$

where

$$\begin{aligned}
v_s(t) &= KT_n \quad c_n z_n \quad z_{n-1} \quad l_n \left( \frac{\partial \alpha_{n-1}}{\partial y} \right)^2 z_n + \frac{\partial \alpha_{n-1}}{\partial y} \mathbf{a}^T \xi_{(2)} + \frac{\partial \alpha_{n-1}}{\partial y} \hat{\chi}_b \omega_2 \\
&\quad + \frac{\partial \alpha_{n-1}}{\partial \hat{\mathbf{a}}} \kappa_a (z_1 \quad \sum_{i=1}^{n-1} \frac{\partial \alpha_i}{\partial y} z_{i+1}) \xi_{(2)} \quad \frac{\partial \alpha_{n-1}}{\partial \hat{\chi}_b} \kappa_{\chi b} (\sum_{i=1}^{n-1} \frac{\partial \alpha_i}{\partial y} z_{i+1}) \omega_2 \\
&\quad \kappa_a \frac{\partial \alpha_{n-1}}{\partial y} \xi_{(2)} (\sum_{i=1}^{n-2} \frac{\partial \alpha_i}{\partial \hat{\mathbf{a}}} z_{i+1}) \quad \kappa_{\chi b} \frac{\partial \alpha_{n-1}}{\partial y} \omega_2 (\sum_{i=2}^{n-2} \frac{\partial \alpha_i}{\partial \hat{\chi}_b} z_{i+1}) \quad z_{ss} \hat{D}_b
\end{aligned} \tag{7.45}$$

where  $c_n$  and  $l_n$  are positive constants,  $z_{ss} = z_s / z_n$  and  $z_s = z_1 \quad \sum_{i=1}^{n-1} \frac{\partial \alpha_i}{\partial y} z_{i+1}$ .

The adaptive laws for  $\hat{\mathbf{a}}$ ,  $\hat{\chi}_b$  and  $\hat{D}_b$  are given by

$$\dot{\hat{\mathbf{a}}} = \kappa_a (z_1 \quad \sum_{i=1}^{n-1} \frac{\partial \alpha_i}{\partial y} z_{i+1}) \xi_{(2)}, \tag{7.46}$$

$$\dot{\hat{\chi}}_b = \kappa_{\chi b} (\sum_{i=1}^{n-1} \frac{\partial \alpha_i}{\partial y} z_{i+1}) \omega_2, \tag{7.47}$$

$$\dot{\hat{D}}_b = \kappa_{D_b} z_s, \tag{7.48}$$

where  $\kappa_a$ ,  $\kappa_{\chi b}$  and  $\kappa_{D_b}$  are positive constants.

*Theorem:* For the plant given in (7.1) with the hysteresis  $\Pi_m(t)$  in (3.12), the inverse MGPI model  $\hat{\Pi}_m^{-1}(t)$  with the hysteresis loop compensator  $\hat{\Pi}_{com}(t)$  defined in (5.4) and the inverse compensation error described as (5.16), the designed state observer (7.7), the adaptive output feedback controller specified by (7.44) and the adaptive laws (7.25), (7.26), (7.33), (7.47), (7.48) and (7.48) ensures that all the closed-loop signals are bounded and  $y(t) \infty y_d(t)$  as  $t \infty \in$ .

*Proof:* From (7.43)-(7.45), it can be obtained that

$$\begin{aligned}
\dot{z}_n = & c_n z_n \quad z_{n-1} \quad l_n \left( \frac{\partial \alpha_{n-1}}{\partial y} \right)^2 z_n \quad \frac{\partial \alpha_{n-1}}{\partial y} \tilde{\mathbf{a}}^T \xi_{(2)} \quad \frac{\partial \alpha_{n-1}}{\partial y} \tilde{\chi}_b \omega_2 \\
& + \frac{\partial \alpha_{n-1}}{\partial y} d_{b2} \quad \frac{\partial \alpha_{n-1}}{\partial y} \epsilon_2 + \frac{\partial \alpha_{n-1}}{\partial \hat{\mathbf{a}}} (\kappa_a (z_1 \quad \Sigma_{i=1}^{n-1} \frac{\partial \alpha_i}{\partial y} z_{i+1}) \xi_{(2)} \quad \dot{\hat{\mathbf{a}}}) \\
& \frac{\partial \alpha_{n-1}}{\partial \hat{\chi}_b} (\kappa_{\chi b} (\Sigma_{i=1}^{n-1} \frac{\partial \alpha_i}{\partial y} z_{i+1}) \omega_2 + \dot{\chi}_b) \quad \kappa_a \frac{\partial \alpha_{n-1}}{\partial y} \xi_{(2)} (\Sigma_{i=1}^{n-2} \frac{\partial \alpha_i}{\partial \hat{\mathbf{a}}} z_{i+1}) \\
& \kappa_{\chi b} \frac{\partial \alpha_{n-1}}{\partial y} \omega_2 (\Sigma_{i=2}^{n-2} \frac{\partial \alpha_i}{\partial \hat{\chi}_b} z_{i+1}) \quad z_{ss} \hat{D}_b.
\end{aligned} \tag{7.49}$$

The Lyapunov function candidate  $V_n$  is selected as

$$V_n = V_{n-1} + \frac{1}{2} z_n^2 + \frac{1}{2\kappa_{D_b}} \tilde{D}_b^2 + \frac{1}{2l_n} \epsilon^T P_0 \epsilon \tag{7.50}$$

where  $\kappa_{D_b}$  is a positive constant.

$$\begin{aligned}
\dot{V}_n = & \dot{V}_{n-1} + z_n \dot{z}_n + \frac{1}{\kappa_{D_b}} \tilde{D}_b \dot{\tilde{D}}_b \quad \frac{1}{l_n} \epsilon^T \dot{\epsilon} \\
\geq & \Sigma_{i=1}^n c_i z_i^2 \quad (\Sigma_{i=1}^n \frac{3}{4l_i}) \epsilon^T \dot{\epsilon} + \frac{1}{\kappa_a} \tilde{\mathbf{a}} (\kappa_a (z_1 \quad \Sigma_{i=1}^{n-1} \frac{\partial \alpha_i}{\partial y} z_{i+1}) \xi_{(2)} \quad \dot{\hat{\mathbf{a}}}) \\
& \frac{1}{\kappa_{\chi b}} \tilde{\chi}_b (\kappa_{\chi b} (\Sigma_{i=1}^{n-1} \frac{\partial \alpha_i}{\partial y} z_{i+1}) \omega_2 + \dot{\chi}_b) + (\Sigma_{i=1}^{n-1} \frac{\partial \alpha_i}{\partial \hat{\mathbf{a}}} z_{i+1}) (\kappa_a (z_1 \quad \Sigma_{i=1}^{n-1} \frac{\partial \alpha_i}{\partial y} z_{i+1}) \xi_{(2)} \quad \dot{\hat{\mathbf{a}}}) \\
& (\Sigma_{i=2}^{n-1} \frac{\partial \alpha_i}{\partial \hat{\theta}_b} z_{i+1}) (\kappa_{\chi b} (\Sigma_{i=1}^{n-1} \frac{\partial \alpha_i}{\partial y} z_{i+1}) \omega_2 + \dot{\theta}_b) \quad z_s \hat{D}_b \quad z_s d_{b2} + \frac{1}{\kappa_{D_b}} \tilde{D}_b \dot{\tilde{D}}_b \\
\geq & \Sigma_{i=1}^n c_i z_i^2 \quad (\Sigma_{i=1}^n \frac{3}{4l_i}) \epsilon^T \dot{\epsilon} + \frac{1}{\kappa_a} \tilde{\mathbf{a}} (\kappa_a (z_1 \quad \Sigma_{i=1}^{n-1} \frac{\partial \alpha_i}{\partial y} z_{i+1}) \xi_{(2)} \quad \dot{\hat{\mathbf{a}}}) \\
& \frac{1}{\kappa_{\chi b}} \tilde{\chi}_b (\kappa_{\chi b} (\Sigma_{i=1}^{n-1} \frac{\partial \alpha_i}{\partial y} z_{i+1}) \omega_2 + \dot{\chi}_b) + (\Sigma_{i=1}^{n-1} \frac{\partial \alpha_i}{\partial \hat{\mathbf{a}}} z_{i+1}) (\kappa_a (z_1 \quad \Sigma_{i=1}^{n-1} \frac{\partial \alpha_i}{\partial y} z_{i+1}) \xi_{(2)} \quad \dot{\hat{\mathbf{a}}}) \\
& (\Sigma_{i=2}^{n-1} \frac{\partial \alpha_i}{\partial \hat{\chi}_b} z_{i+1}) (\kappa_{\chi b} (\Sigma_{i=1}^{n-1} \frac{\partial \alpha_i}{\partial y} z_{i+1}) \omega_2 + \dot{\chi}_b) \quad z_s \hat{D}_b + z_s d_{b2} + \frac{1}{\kappa_{D_b}} \tilde{D}_b \dot{\tilde{D}}_b \\
\geq & \Sigma_{i=1}^n c_i z_i^2 \quad (\Sigma_{i=1}^n \frac{3}{4l_i}) \epsilon^T \dot{\epsilon} + \frac{1}{\kappa_a} \tilde{\mathbf{a}} (\kappa_a (z_1 \quad \Sigma_{i=1}^{n-1} \frac{\partial \alpha_i}{\partial y} z_{i+1}) \xi_{(2)} \quad \dot{\hat{\mathbf{a}}}) \\
& \frac{1}{\kappa_{\chi b}} \tilde{\chi}_b (\kappa_{\chi b} (\Sigma_{i=1}^{n-1} \frac{\partial \alpha_i}{\partial y} z_{i+1}) \omega_2 + \dot{\chi}_b) + (\Sigma_{i=1}^{n-1} \frac{\partial \alpha_i}{\partial \hat{\mathbf{a}}} z_{i+1}) (\kappa_a (z_1 \quad \Sigma_{i=1}^{n-1} \frac{\partial \alpha_i}{\partial y} z_{i+1}) \xi_{(2)} \quad \dot{\hat{\mathbf{a}}}) \\
& (\Sigma_{i=2}^{n-1} \frac{\partial \alpha_i}{\partial \hat{\chi}_b} z_{i+1}) (\kappa_{\chi b} (\Sigma_{i=1}^{n-1} \frac{\partial \alpha_i}{\partial y} z_{i+1}) \omega_2 + \dot{\chi}_b) + z_s \tilde{D}_b + \frac{1}{\kappa_{D_b}} \tilde{D}_b \dot{\tilde{D}}_b \\
= & \Sigma_{i=1}^n c_i z_i^2 \quad (\Sigma_{i=1}^n \frac{3}{4l_i}) \epsilon^T \dot{\epsilon} + \frac{1}{\kappa_a} \tilde{\mathbf{a}} (\kappa_a (z_1 \quad \Sigma_{i=1}^{n-1} \frac{\partial \alpha_i}{\partial y} z_{i+1}) \xi_{(2)} \quad \dot{\hat{\mathbf{a}}}) \\
& \frac{1}{\kappa_{\chi b}} \tilde{\chi}_b (\kappa_{\chi b} (\Sigma_{i=1}^{n-1} \frac{\partial \alpha_i}{\partial y} z_{i+1}) \omega_2 + \dot{\chi}_b) + (\Sigma_{i=1}^{n-1} \frac{\partial \alpha_i}{\partial \hat{\mathbf{a}}} z_{i+1}) (\kappa_a (z_1 \quad \Sigma_{i=1}^{n-1} \frac{\partial \alpha_i}{\partial y} z_{i+1}) \xi_{(2)} \quad \dot{\hat{\mathbf{a}}})
\end{aligned} \tag{7.51}$$

$$\left(\sum_{i=2}^{n-1} \frac{\partial \alpha_i}{\partial \hat{\chi}_b} z_{i+1}\right) (\kappa_{\chi b} \left(\sum_{i=1}^{n-1} \frac{\partial \alpha_i}{\partial y} z_{i+1}\right) \omega_2 + \dot{\chi}_b) + \frac{1}{\kappa_{D_b}} \tilde{D}_b (\dot{\tilde{D}}_b + \kappa_{D_b} z_s).$$

$V_n$  is nonincreasing, it implies that  $z_i$ , for  $i = 1, 2, \dots, n$ ,  $\hat{\mathbf{a}}$ ,  $\hat{b}$ ,  $\hat{\phi}$ ,  $\hat{\chi}_0$ ,  $\hat{\chi}_b$  and  $\hat{D}_b$  are bounded. Furthermore, by applying the Lasalle-Yoshizawa theorem, it can be shown that  $z_i \rightarrow 0$  ( $i = 1, 2, \dots, n$ ) as  $t \rightarrow \infty$ , which implies that  $y(t) \rightarrow y_d(t)$  as  $t \rightarrow \infty$ . ■

Based on the output feedback control developed in (7.44), the control signal  $v(t)$  for the plant given in (7.1) with the hysteresis  $\Pi_m(t)$  in (3.12) is obtained by

$$v(t) = \hat{\Pi}_m^{-1}[v_c](t) \quad (7.52)$$

where  $\hat{\Pi}_m^{-1}$ , given in (5.3), is the inverse MGPI model constructed based on the estimated MGPI model.

## 7.4 Simulation Studies

In this section, the effectiveness of the proposed controller is verified by the simulation studies with two different plants.

### 7.4.1 Example 1:

In the first example, a second-order linear system with unknown parameters is considered, which can be described by

$$\begin{aligned} \ddot{x} &= ax + bu(t) \\ y &= x \end{aligned} \quad (7.53)$$

where  $u(t)$  stands for the output of the compensated hysteresis output (7.5). The parameter  $a$  and  $b$  are selected as  $a = 1$  and  $b = 1$  and assumed to be unknown in the simulation. The desired trajectory is given as  $y_d(t) = 5\sin(1.5t)$ . The initial state of the system is  $x(0) = 0$

and the sample time is 0.0001. The actual and estimated density function of the MGPI model  $\Pi_m(t)$  and  $\hat{\Pi}_m(t)$  are  $p_m(r) = 0.5e^{-0.0014r^2}$  and  $\hat{p}_m(r) = 0.52e^{-0.002r^2}$ , for  $r \in [0, 100]$ , respectively, and the envelope function parameter is chosen as  $m_0 = 1.7$ . For the state observer, the parameter  $q$  is selected as  $q = [q_1, q_2]^T = [1, 3]^T$ . The control parameters are summarized in Table 7.1.

Table 7.1: Output-feedback controller parameters in Example 1

$c_1$	125.598	$c_2$	189.475
$l_1$	0.0003	$l_2$	0.0003
$\hat{a}(0)$	0.6	$\kappa_a$	0.0008
$\hat{b}(0)$	0.75	$\kappa_b$	0.028
$\hat{\chi}_0(0)$	1.4	$\kappa_{\chi_0}$	0.0005
$\hat{\chi}_b(0)$	0.3	$\kappa_{\chi_b}$	0.001
$\hat{\phi}(0)$	1.3	$\kappa_\phi$	0.457
$\hat{D}_b(0)$	0.01	$\kappa_{D_b}$	0.0001

Fig. 7.2 and 7.3 show the tracking error and the control signal, respectively. The comparison between the desired trajectory  $y_d(t)$  and the actual system output  $y(t)$  can be found in Fig. 7.4. The simulation results demonstrate that the developed control algorithm can effectively compensate the effect of hysteresis as well as achieve admirable tracking accuracy.

### 7.4.2 Example 2:

A second order nonlinear plant preceded by a hysteresis actuator is considered in the second example. The nonlinear system is described as

$$\ddot{x} = a \frac{1 - e^{-x(t)}}{1 + e^{-x(t)}} + bu(t) \quad (7.54)$$

$$y = x$$

where  $u(t)$  stands for the output of the compensated hysteresis output (7.5). The parameter  $a$  and  $b$  are selected as  $a = 1$  and  $b = 1$  and assumed to be unknown in the simulation. The

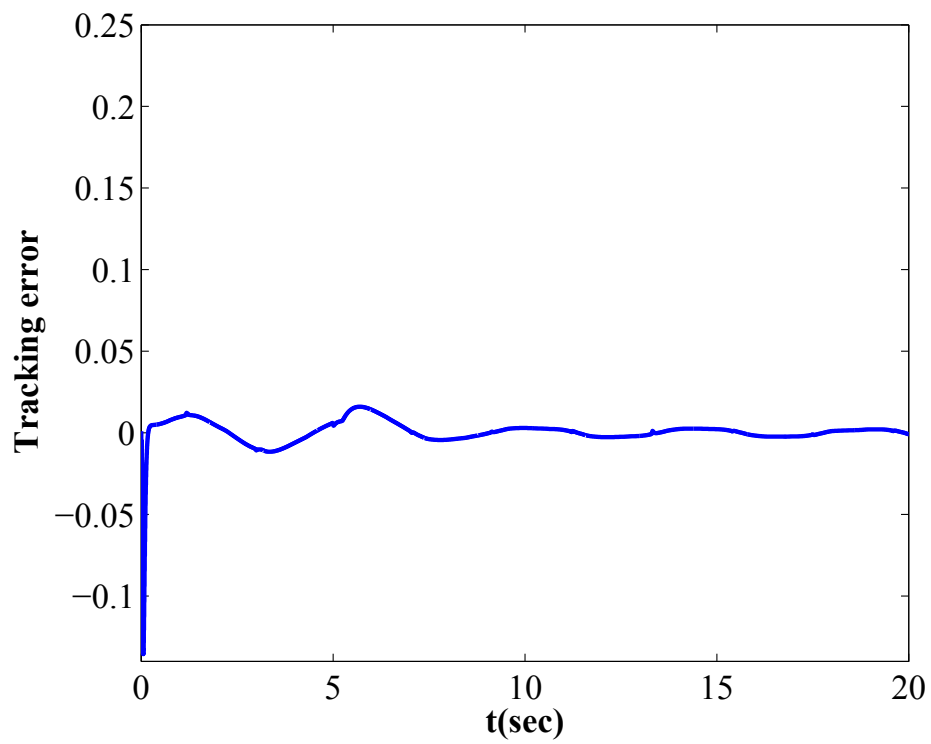


Figure 7.2: The tracking error of output-feedback controller in example 1.

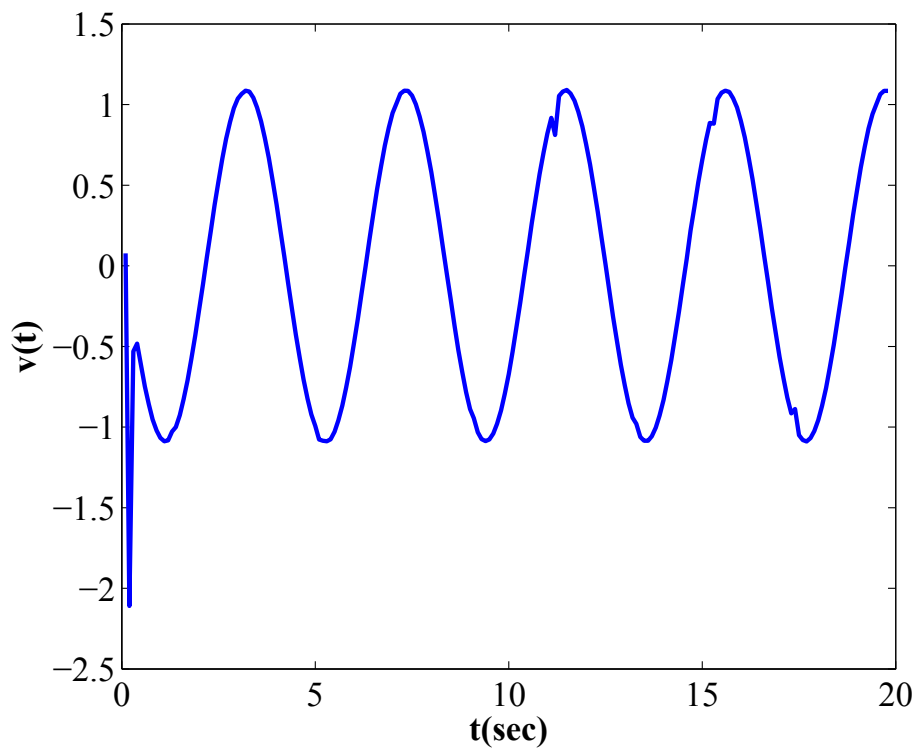


Figure 7.3: The controller signal  $v(t)$  of output-feedback controller in example 1.

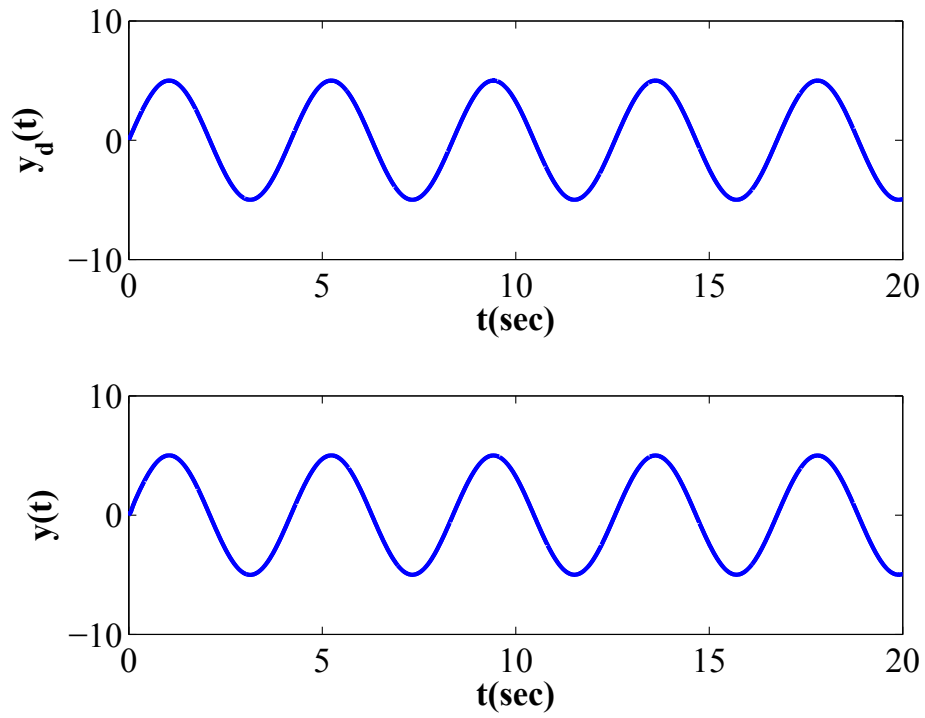


Figure 7.4: The desired output  $y_d(t)$  and the actual output  $y(t)$  of output-feedback controller in example 1.

desired trajectory is given as  $y_d(t) = 4\sin(t)$ . The initial state of the system is  $x(0) = 0$  and the sample time is 0.0005. The actual and estimated density function of the MGPI model  $\Pi_m(t)$  and  $\hat{\Pi}_m(t)$  are  $p_m(r) = 0.5e^{-0.0014r^2}$  and  $\hat{p}_m(r) = 0.52e^{-0.002r^2}$ , for  $r \in [0, 100]$ , respectively. The envelope function parameter is chosen as  $m_0 = 1.7$ . For the state observer, the parameter  $q$  is selected as  $q = [q_1, q_2]^T = [1, 3]^T$ . The control parameters are summarized in Table 7.2.

Table 7.2: Output-feedback controller parameters in Example 2

$c_1$	120.961	$c_2$	99.2
$l_1$	0.0003	$l_2$	0.0003
$\hat{a}(0)$	0.02	$\kappa_a$	0.0045
$\hat{b}(0)$	0.75	$\kappa_b$	0.032
$\hat{\chi}_0(0)$	1.4	$\kappa_{\chi 0}$	0.005
$\hat{\chi}_b(0)$	0.3	$\kappa_{\chi b}$	0.0125
$\hat{\phi}(0)$	1.3	$\kappa_{\phi}$	0.452
$\hat{D}_b(0)$	0.01	$\kappa_{D_b}$	0.004

The simulation results presented in Fig. 7.5, 7.6, and 7.7 are the tracking error, the control signal  $v(t)$  and the comparison of the desired output  $y_d(t)$  and the actual system output  $y(t)$ , respectively. It can be seen that the proposed inverse based output feedback controller by considering the inverse compensation error demonstrates excellent tracking performance for the nonlinear plant.

Based on the simulation results, it can be concluded that the developed observer for state estimation works efficiently and provides exponentially convergent estimates of the unmeasured states. In addition, the proposed adaptive output feedback control method not only guarantee the stability of the close-loop control system, but also ensure the desired tracking accuracy.

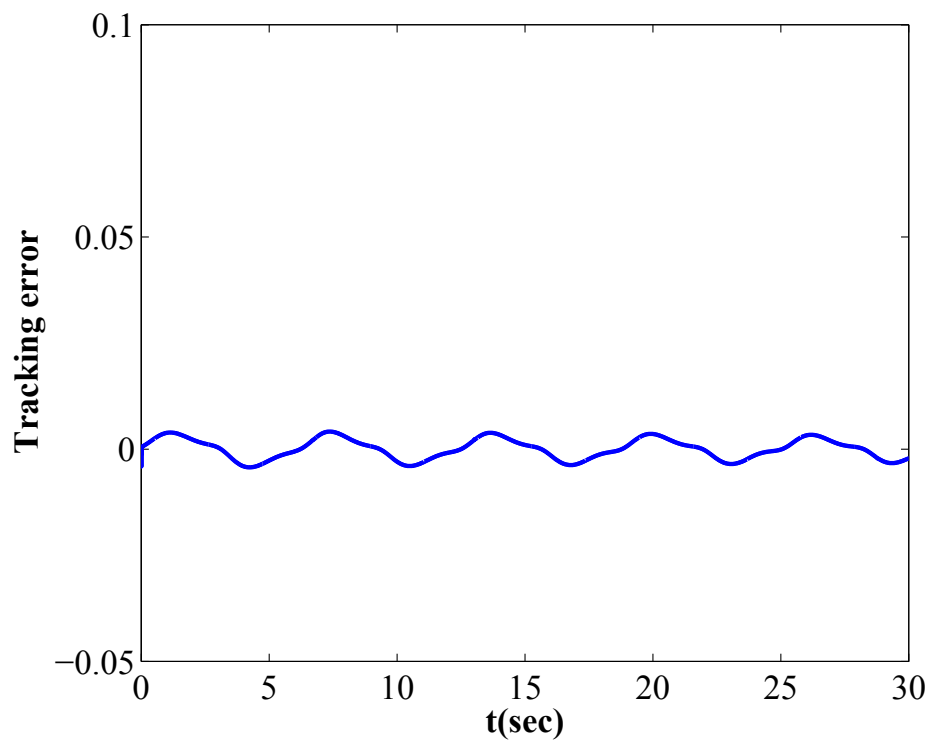


Figure 7.5: The tracking error of output-feedback controller in example 2.

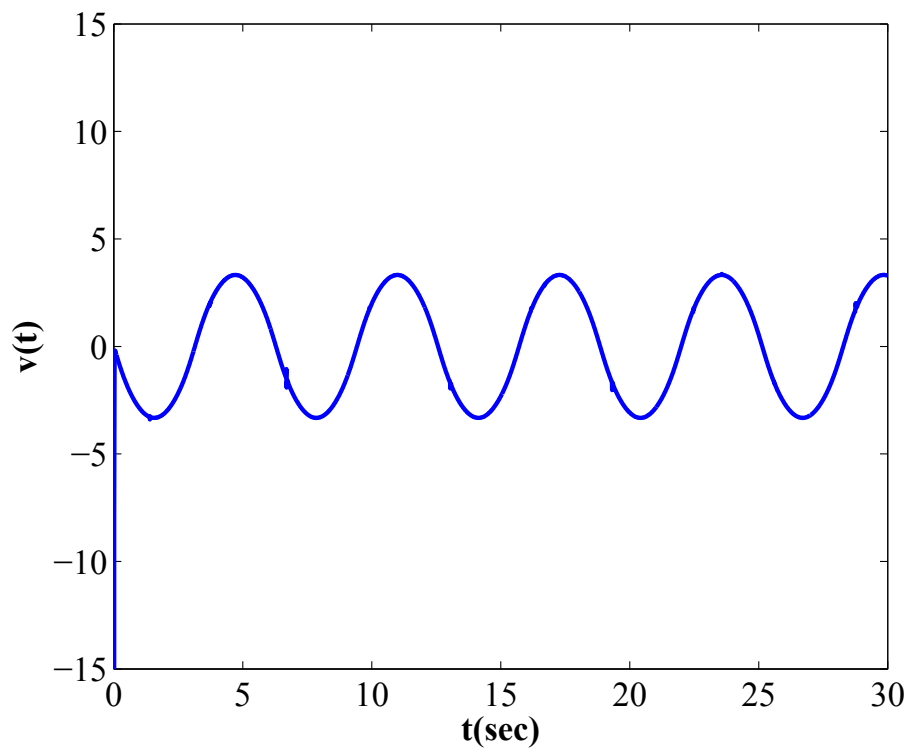


Figure 7.6: The controller signal  $v(t)$  of output-feedback controller in example 2.

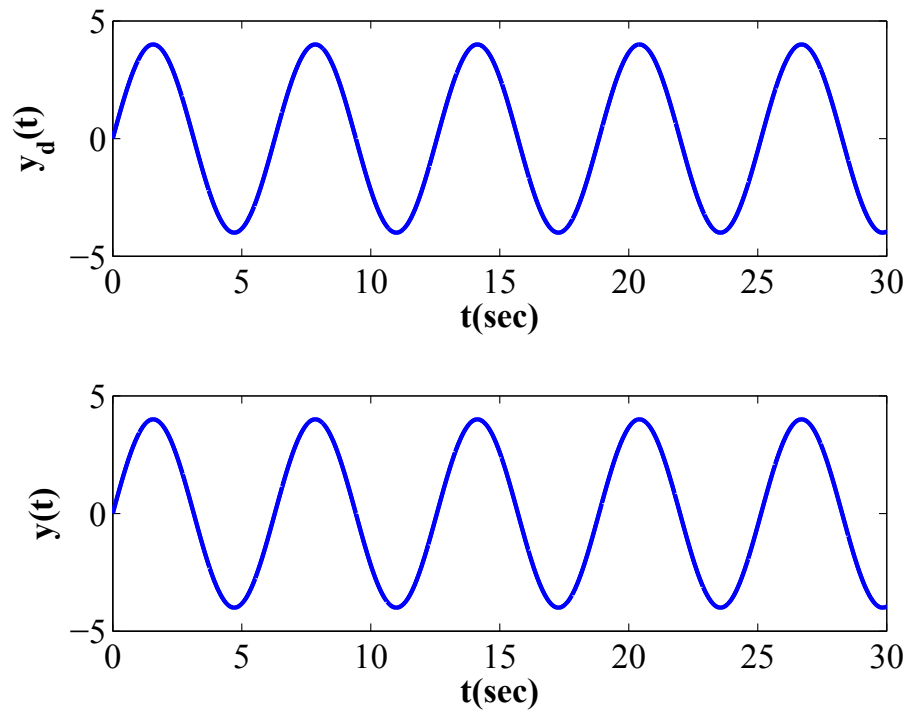


Figure 7.7: The desired output  $y_d(t)$  and the actual output  $y(t)$  of output-feedback controller in example 2.

# Chapter 8

## Experimental Implementation

In this chapter, the theoretical results obtained in previous chapters will be further substantiated in the laboratory. The experiment results achieved in this chapter will imply the possibility of implementing the proposed works in this dissertation into industries.

### 8.1 Experimental Setup

The piezoelectric actuators, which are well known by their light weight, high resolution, and rapid response speed, are widely used in micro/nanomanipulation systems [87,110–112]. The piezoelectric micropositioning stage (P-753.31 C) from Physik Instrumente Company is selected in the experiments. The architecture of experimental devices is shown in Fig. 8.1. The natural frequency of this piezoelectric actuator is 2.9 KHz and the maximum output displacement of the actuator is  $38\mu m$  from its static equilibrium point. A capacitive sensor (sensitivity =  $0.38\mu m/V$  ; resolution  $\geq 0.1nm$ ) is integrated with the actuator to measure the actuator displacement response. The excitation module is a voltage amplifier (LVPZT, E-505) with a fixed gain of ten in the range of 0 V to 100 V . The measured displacement is transferred to analogue voltage in the range of 0-10V by a position servo-control module (PSCM). The input voltage and output displacement signals will be obtained by using dSpace

ControlDesk data acquisition card at a sampling frequency of 10 kHz.

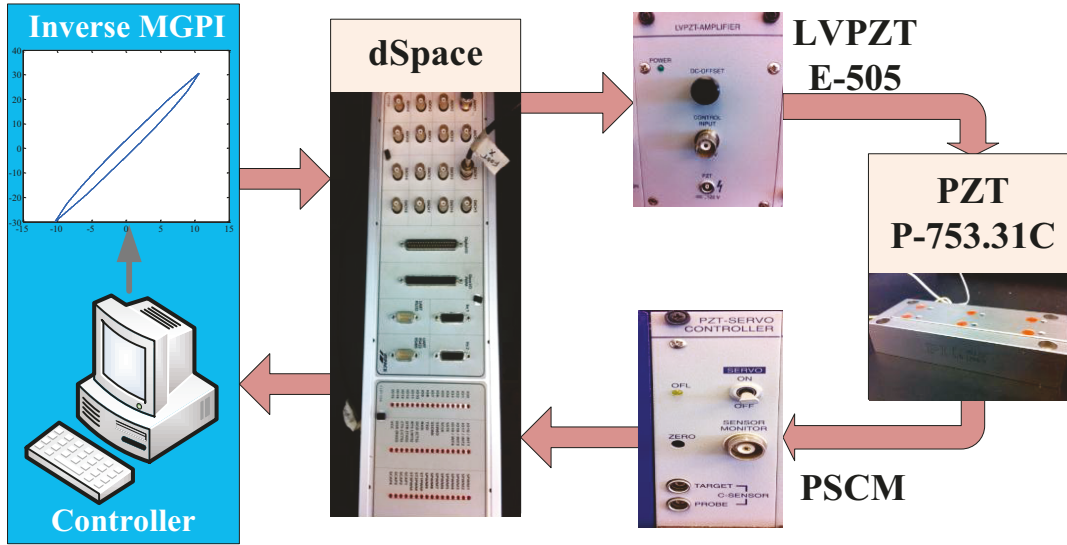


Figure 8.1: Experiment setup.

## 8.2 Hysteresis Parameters Identification and Model Validation

To model the hysteretic effect in PZT P-753.31C, the MGPI model is comprised by selecting  $N = 10$  modified generalized play operators with fixed threshold values  $r_k$ , which are determined by

$$r_k = c \times k \quad (8.1)$$

for  $k = 1, 2, \dots, 10$ .

The envelope function is selected as,

$$\gamma(v) = m_0 v + m_1 (m_0 > 0). \quad (8.2)$$

The model parameter  $c$ , density function weights  $p_{rk}$ , for  $k = 0, 1, \dots, 10$ ,  $m_0$  and  $m_1$ , with the initial state  $\{3, 0, 0, 0, 0, 0, 0, 0, 0, 0, 0, 1, 0\}$ , were identified through minimizing an

Table 8.1: Identified parameters of PZT P-753.31C

Parameters	PZT P-753.31C	Parameters	PZT P-753.31C
$c$	3.5000	$p_{r0}$	0.2422
$p_{r1}$	0.0681	$p_{r2}$	0.0272
$p_{r3}$	0.0179	$p_{r4}$	0.0199
$p_{r5}$	0.0057	$p_{r6}$	0.0202
$p_{r7}$	0.0410	$p_{r8}$	0.0001
$p_{r9}$	0.0001	$p_{r10}$	0.0001
$m_0$	0.9800	$m_1$	0.3933

error sum-squared function  $E_{ss}$ , given by

$$E_{ss} = \sum_{i=1}^Q (\Pi_\gamma(i) - \Pi_m(i))^2 \quad (8.3)$$

where  $\Pi_m$  is the displacement response of the MGPI model under a certain excitation.  $\Pi_\gamma$  is the measured displacement of PZT mode P-753.31C under the same input signal.  $Q$  is the number of data point considered.

The error minimization problem was solved by the function *fmincon* in MATLAB, subjected to the following constrains:

$$|c, p_{rk}, m_0| > 0.$$

The final model parameters are summarized in Table 8.1 and the fitness of the proposed MGPI model to the experimental data is illustrated by Fig. 8.2. The peak deviation between the MGPI model response and the experimental measured data is in the order of  $0.2 \mu m$ , as shown in Fig. 8.3. It should be mentioned that to avoid the error sum-squared function  $E_{ss}$  converge to a local minimum, the above procedures were used with different values of the initial states. All the results show the identified parameters are very similar.

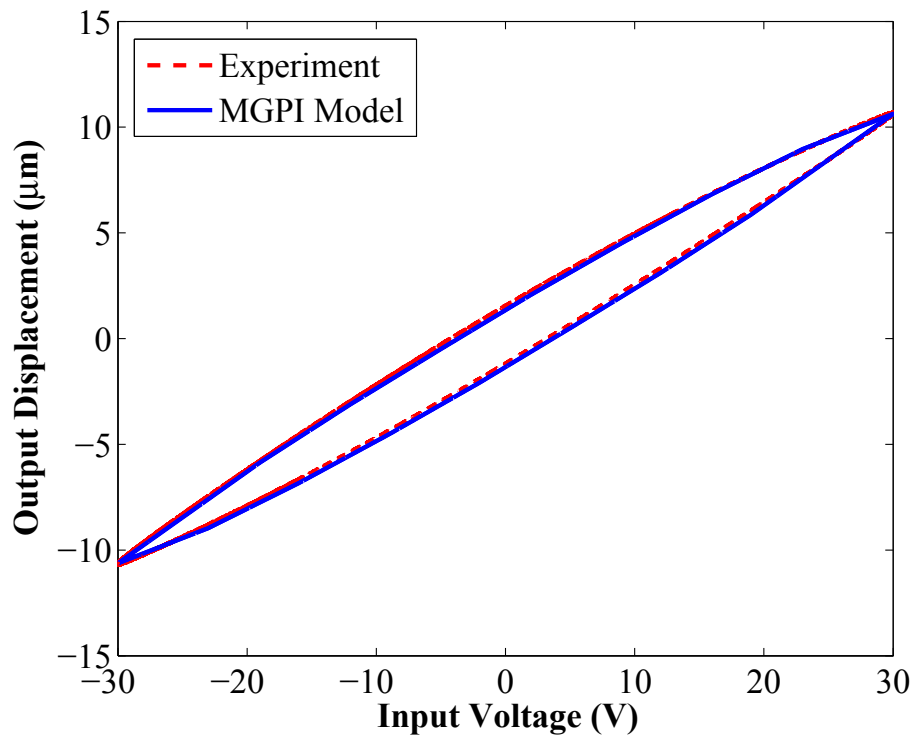


Figure 8.2: The identification result of MGPI model for PZT P-753.31C.

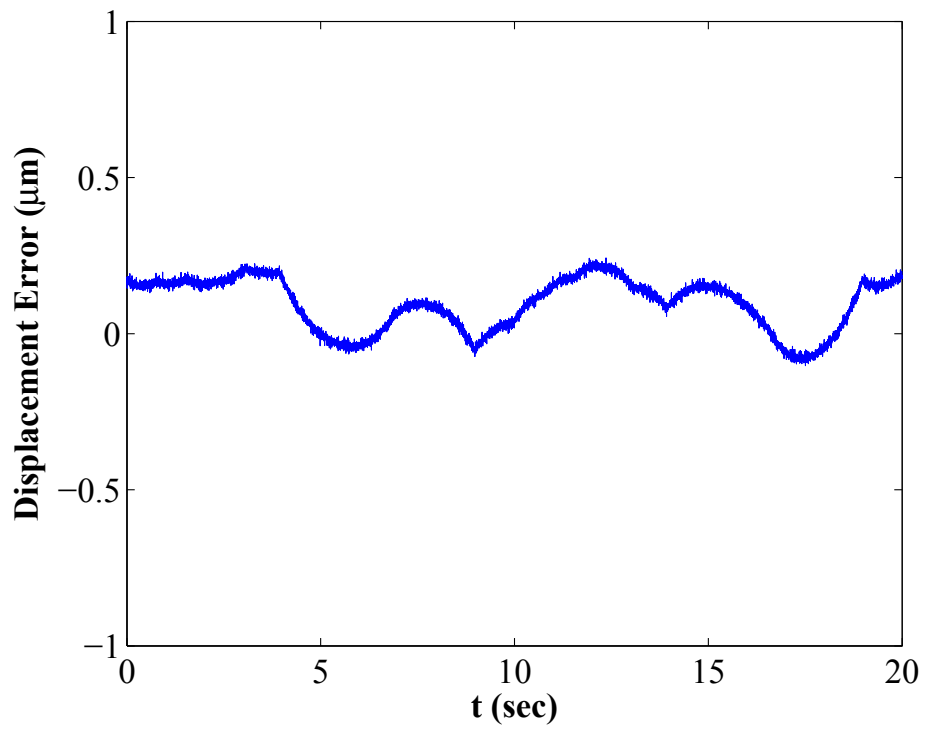


Figure 8.3: Displacement error between measured and model responses.

**Remark:** 1. It has been shown in the experiment that the MGPI model comprised of  $N = 10$  modified generalized play operators is accurate enough for describing the hysteresis effect in PZT P-753.31C. The increase of number  $N$  will lead to the unnecessary computational burden.

2. Under the input signals with higher frequencies (larger than 20Hz for example), the hysteresis nonlinearities in the PZT become rate-dependent. In this case, the rate-dependent hysteresis model is required. In this dissertation research, with the proposed rate-independent MGPI model, only the input excitations with lower frequencies are selected in the experiments.

### 8.3 Experimental Verification of Inverse Compensation

Based on the MGPI model determined in Table 8.1, the experimental verification of the proposed inverse compensation are provided in Fig. 8.4 and Fig. 8.5. The inverse MGPI model  $\Pi_m^{-1}$  is calculated based on (4.15), (4.25), and (4.26). The thresholds  $s_i$  and the density weights  $q_{s_i}$  for  $i = 1, \dots, N$  are shown in Table 8.2.

Table 8.2: Thresholds and weights obtained for the inverse MGPI model for PZT P-753.31C

$s_0$	$s_1$	$s_2$	$s_3$	$s_4$	$s_5$
0	0.8227	1.8852	3.0435	4.2638	5.5562
$s_6$	$s_7$	$s_8$	$s_9$	$s_{10}$	
6.8677	8.1795	9.6357	11.0923	12.5492	
$q_{s0}$	$q_{s1}$	$q_{s2}$	$q_{s3}$	$q_{s4}$	$q_{s5}$
4.2808	0.9663	0.2741	0.1569	0.1565	0.0417
$q_{s6}$	$q_{s7}$	$q_{s8}$	$q_{s9}$	$q_{s10}$	
0.0007	0.2662	0.0006	0.0006	0.0006	

Figure 8.4(a) shows the hysteresis nonlinearity of PZT P-753.31C described by the MGPI under the reference input signal  $v_c(t) = 15.2 + 11.4\sin(2\pi t)$ . The compensated result is

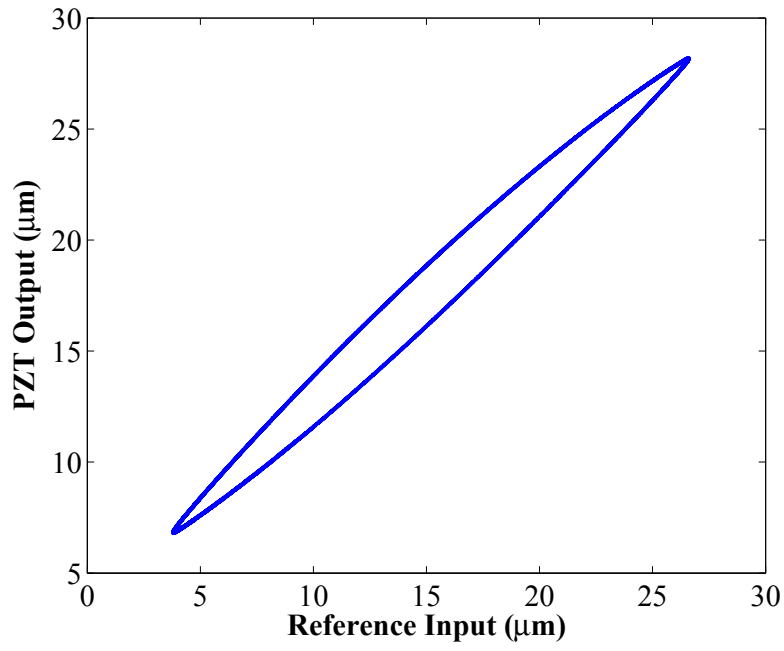
shown in Fig. 8.4(b). In Fig. 8.5, the proposed inverse scheme has been further confirmed by applying a more complex reference input signal  $v_c(t) = 19 + 2.28\sin(4.283t) + 3.8\sin(2\pi t)$ . The input-output relation before and after the inverse compensation are shown in Fig. 8.5(a) and Fig. 8.5(b), respectively. The experimental results show the effectiveness of the inverse compensation approach proposed in Chapter 4. However, since the validated MGPI model is only an estimation of the actual hysteresis nonlinearity in the PZT P-753.31C, the open-loop inverse compensation can not completely remedy the hysteresis effect and usually yield some degree of inverse hysteresis compensation error, which can be clearly observed from Fig. 8.4(b) and Fig. 8.5(b).

## 8.4 Experimental Verification of Adaptive Output Feedback Controller

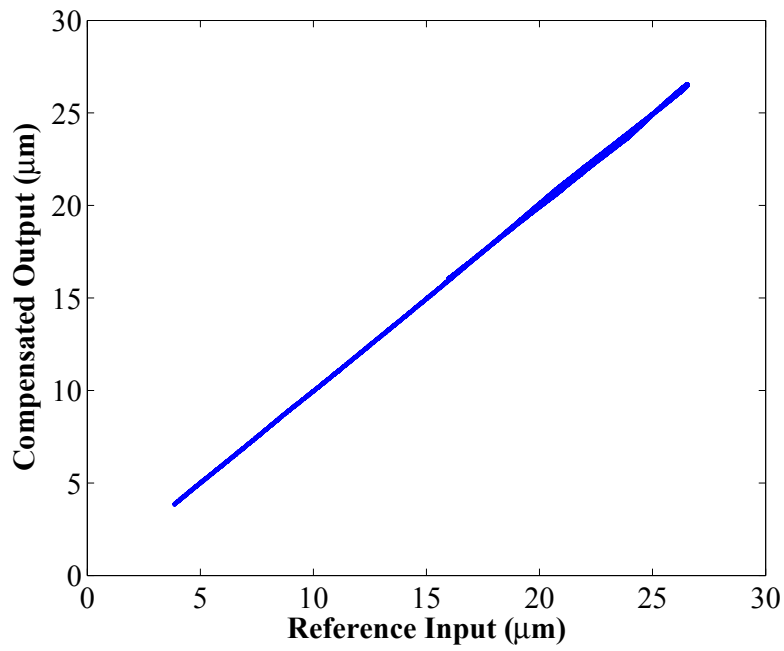
In this section, the adaptive output feedback controller developed in Chapter 7 is illustrated on the piezo micropositioning stage P-753.31C. The dynamic model of PZT P-753.31C is described by [87]

$$\begin{aligned} \dot{x} &= -4090x + 0.0116u \\ y &= x \\ u &= \Pi_m[v](t) \end{aligned} \tag{8.4}$$

where  $y(t)$  denotes the output displacement,  $u(t)$  is the output of the MGPI model  $\Pi_m[v](t)$ . The parameters of the MGPI model are identified in previous section as shown in Table 8.1.  $v(t)$  is the output of the inverse MGPI model  $\Pi_m^{-1}[v_c](t)$ . The objective is to design the control signal  $v_c(t)$  to control the system output  $y(t)$  to follow a desired trajectory  $y_d(t) = 10 + 5\sin(2\pi t)$ . First, the inverse MGPI model  $v(t) = \Pi_m^{-1}[v_c](t)$  is chosen as in (4.15), (4.25), and (4.26). Then the control design in (7.44) is applied to the plant. In the experiment, the controller parameters is selected as  $c = 278.3$ . The initial value and adaptive law for the unknown parameters are chosen as  $\hat{a}(0) = 4000$ ,  $\hat{\chi}_b(0) = 0.02$ ,  $\hat{D}_b(0) = 0.01$ ,

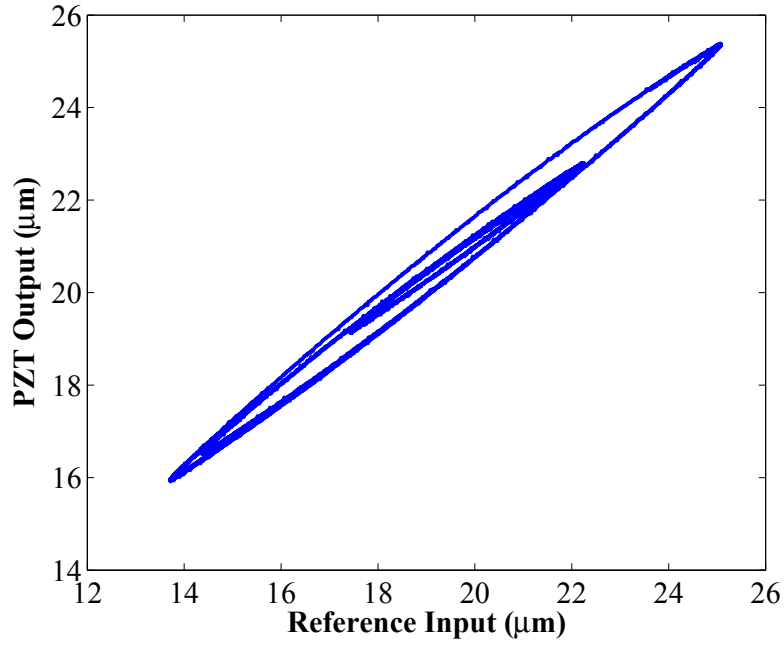


(a)

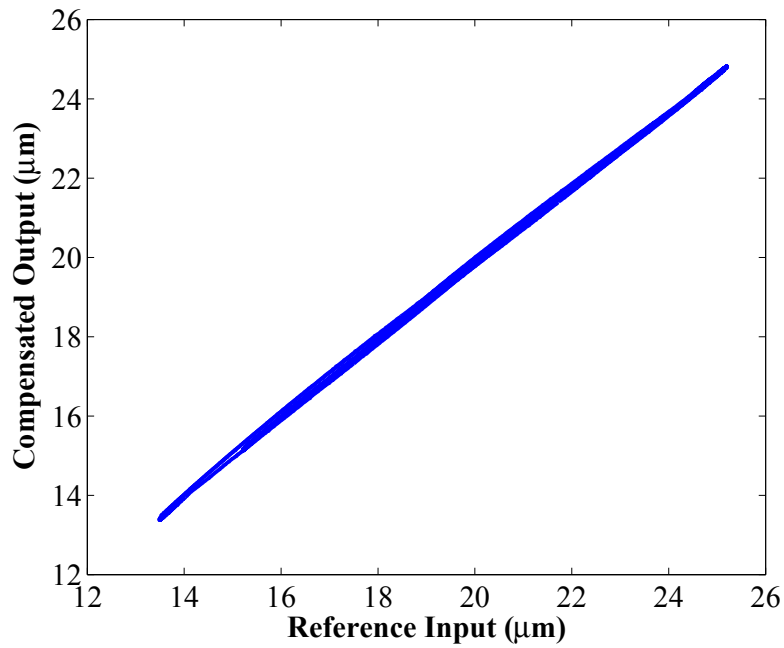


(b)

Figure 8.4: (a) The MGPI model of PZT P-753.31C with input signal  $v_c(t) = 15.2 + 11.4\sin(2\pi t)$ ; (b) The compensated output with applying the inverse MGPI model.



(a)



(b)

Figure 8.5: (a) The MGPI model of PZT P-753.31C with input signal  $v_c(t) = 19 + 2.28\sin(4.283t) + 3.8\sin(2\pi t)$ ; (b) The compensated output with applying the inverse MGPI model.

$\kappa_a = 0.8$ ,  $\kappa_{\chi b} = 0.0001$ , and  $\kappa_{D_b} = 0.004$ , respectively.

The experiment results represented in Fig. 8.6 is the tracking error. Fig. 8.7 shows that the system output  $y(t)$  perfectly tracks the reference desired trajectory  $y_d(t)$ . Fig. 8.8 shows the control signal  $v(t)$ . Clearly, the experimental results verify that the theoretical design of the adaptive output feedback controller proposed in Chapter 7 works efficiently for the piezoelectric actuator.

The experimental results in this chapter demonstrate effectiveness of the theoretical findings proposed in previous chapters.

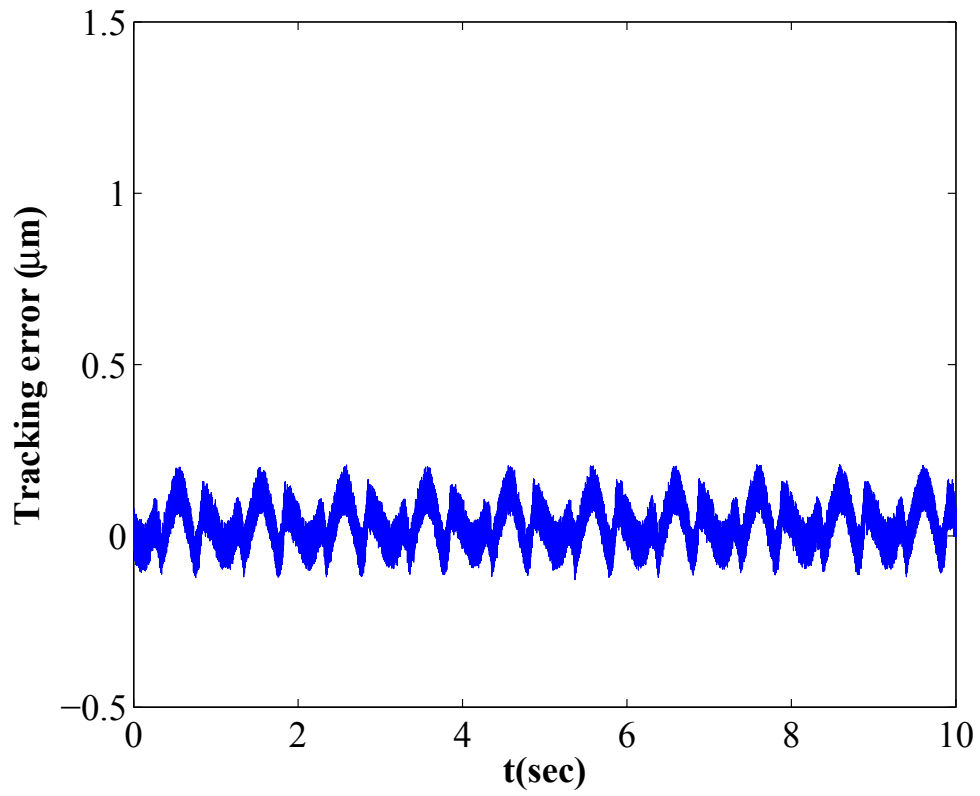


Figure 8.6: The tracking error in experiment.

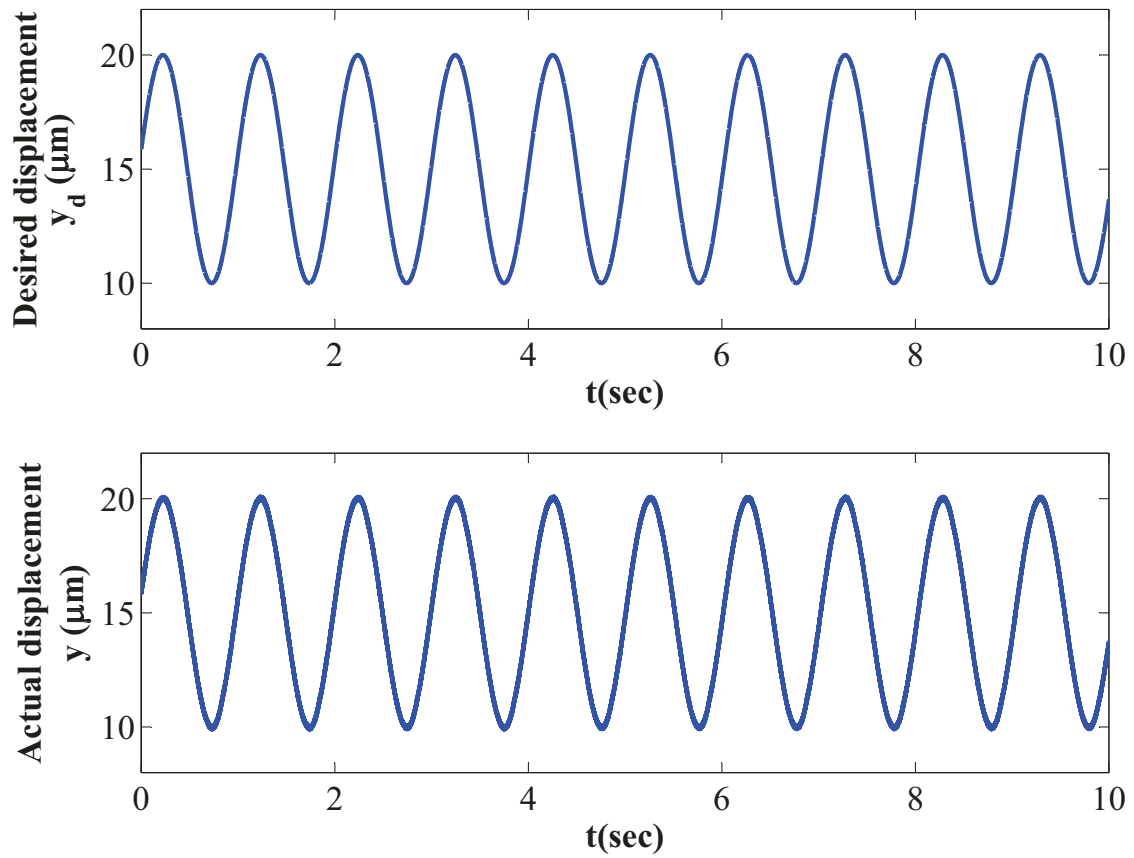


Figure 8.7: The desired output  $y_d(t)$  and the actual output  $y(t)$  in experiment.

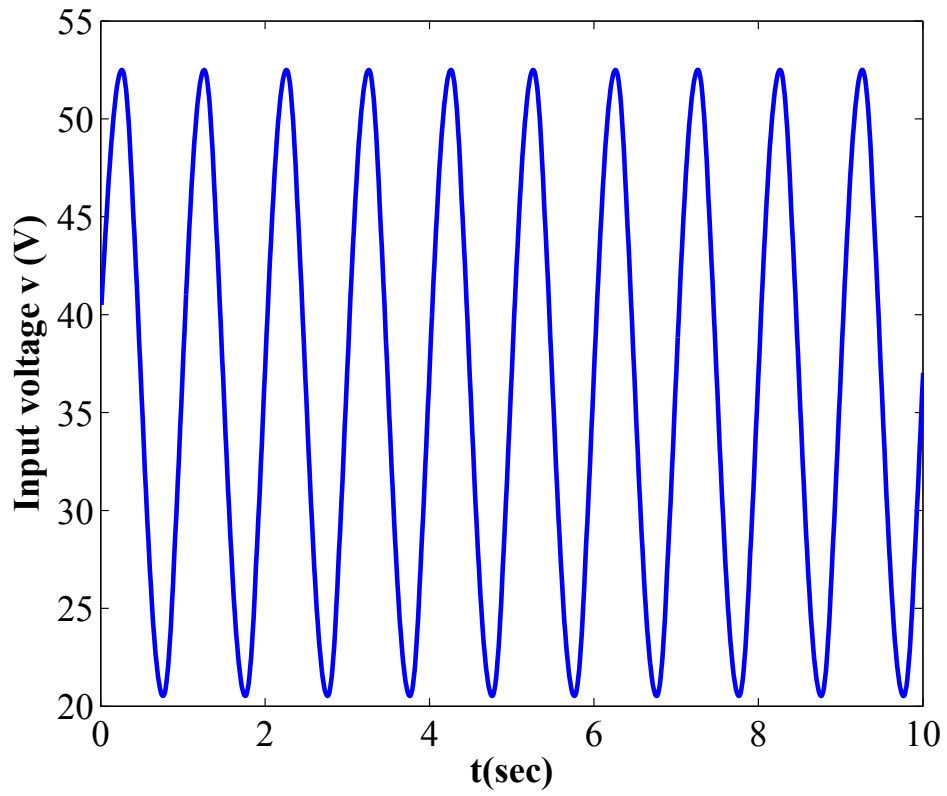


Figure 8.8: The control input voltage  $v(t)$  in experiment.

# Chapter 9

## Conclusions and Future Work

### 9.1 Concluding Remarks

The hysteresis effect, which is known as the non-smooth and non-differentiable nonlinearity, widely exhibits in smart material based actuators, such as piezoceramics actuators, magnetostrictive actuators, and shape memory alloy actuators. When a plant is preceded with such the undesired effect, the control systems usually suffer from the undesirable inaccuracies, detrimental oscillation, or even instability.

This dissertation research has extensively addressed controller designs for hysteresis compensation with the consideration of the proposed modified generalized Prandtl-Ishlinskii model and its inversion, while guaranteeing the fundamental requirement of control system stability and ensuring the tracking precision. The major contributions of the dissertation research are summarized as follows.

- ≤ As an extension of the Prandtl-Ishlinskii model, a modified generalized Prandtl-Ishlinskii model has been proposed to describe a more general class of hysteresis shapes. The proposed modified generalized Prandtl-Ishilinskii is capable of describing the symmetric or asymmetric major and minor hysteresis loops with output saturation.

≤ Two essential properties, the wiping out property and the congruency property, for the proposed modified generalized Prantl-Ishlinskii model have been inspected. It has been shown that the modified generalized Prantl-Ishlinskii model fulfills these two properties. This result provides the necessary and sufficient conditions for the hysteresis nonlinearity to be represented by the proposed modified generalized Prantl-Ishlinskii model on the set of piece-wise monotonic inputs.

≤ Compared to the generalized Prantl-Ishlinskii model, the benefit of the modified generalized Prantl-Ishlinskii model is that the concept of initial loading curve can be utilized and the inverse model can be therefore constructed based on the strict theoretical proof. In this dissertation research, the analytical inverse expression of the modified generalized Prantl-Ishlinskii model with a general form of the envelope function has been derived, which is applied as a feedforward compensator for the hysteresis compensation in the control systems. The numerical implementation has been subsequently provided. The effectiveness of the obtained inverse model has been verified under different inputs in the simulation studies. The simulation results show that the constructed inverse feedforward compensator can remarkably mitigate the hysteresis effects.

≤ In the practical control systems, the hysteresis is usually unknown. The application of the inverse models which are constructed based on the approximate hysteresis models will result in the inverse compensation error. The expression of such inverse compensation error is essential for the strict stability proof of the closed-loop control system. In this dissertation research, the analytical expression of the inverse compensation error for the modified generalized Prantl-Ishlinskii model has been derived. The nonlinear part of the obtained inverse compensation error formula is bounded so that it can be treated as a bounded disturbance. By considering the inverse error expression, the strict stability proof can be established based on the Lyapunov method for the closed-loop control system. It is also worth mentioning that the benefit of the proposed formula of the inverse compensation error is that the designed adaptive controllers can achieve the tracking without necessarily adapting the uncertain parameters(the num-

ber could be large) in the hysteresis model except for only one parameter related to the boundary, which is made possible by the introduction of the stop operator in the error formulation.

≤ An inverse based adaptive variable structure controller has been designed with the consideration of the inverse compensation error. The global stability of the system and tracking a desired trajectory to a certain precision are achieved. It has also been proved that by taking consideration of error expression of the inverse compensation in the controller design, the inverse based scheme generates a superior transient performance over the direct compensation methods without inverse constructions.

≤ An inverse based adaptive output-feedback controller has been developed for systems preceded by unknown hysteresis effect, which is described by the proposed modified generalized Prandtl-Ishlinskii model with unknown parameters, when not all the system states are available. An state observer has also been design for the system states estimations. The global stability of the system has been guaranteed and the tracking accuracy has been ensured by considering the above proposed inverse compensation error expression.

≤ The above theoretical findings have been verified in the experiments on a piezoelectric micropositioning stage (PZT P-753.31 C). Based on the experiment results, it can be shown that the theoretical results proposed in this dissertation research have great potential to be applied into the control systems in industries.

## 9.2 Recommendations for Future Works

As the continuation of the studies in this dissertation research, the following research topics in this area can be conducted in the future.

≤ In Chapter 4, the inversion of the MGPI model with identical envelope functions has

been investigated. However, for the case that  $\gamma_r(v) \neq \gamma_l(v)$ , the inverse construction is still an open problem.

≤ Rate-independent property is one of the characteristics of the proposed modified generalized Prandtl-Ishlinskii model. However, it has been observed in laboratory that some smart material based actuators exhibit rate-dependent hysteresis. Therefore, it is desirable to extend the current research to rate-dependent circumstances.

≤ Further efforts are also desirable for compensation of rate-dependent modified generalized Prandtl-Ishlinskii model using the inversion as a feedforward compensator.

### 9.3 Publications

Several papers reporting results of this dissertation research have been published/submitted in journals and well-known international conferences as listed below. These papers were written under the guidance of my supervisor, Dr. C.-Y. Su. Other co-authors of some of the papers contributed partially through extensive discussions with remarkable recommendations, initial simulations, or the combinations of the above.

≤ S. Liu, C.-Y. Su and Z. Li, “Robust adaptive inverse control of a class of nonlinear systems with modified generalized Prandtl-Ishlinskii hysteresis model,” *IEEE Transactions on Automatic Control*, 2013 (Accepted for Publication).

≤ S. Liu and C.-Y. Su, “Analytical hysteresis inverse compensation for a modified generalized Prandtl-Ishlinskii model,” *in the Proceedings of the 2013 American Control Conference (ACC)*, Washington, DC, pp. 4759-4764, 2013 .

≤ Z. Li, S. Liu and C.-Y. Su, “A novel analytical inverse compensation approach for Preisach model,” *in the Proceedings of the 6th International Conference on Intelligent Robotics and Applications (ICIRA)*, Busan, Korea, pp. 656-665, 2013.

- ≤ Z. Li, Y. Feng, S. Liu and C.-Y. Su, “Prescribed Adaptive Control of a Class of Non-linear System Preceded by Actuators with Hysteresis,” *in the Proceedings of the 2013 IFAC Conference on Manufacturing Modelling, Management, and Control*, Saint Petersburg, Russia, pp. 1849-1854, 2013.
- ≤ S. Liu and C.-Y. Su, “Analytical hysteresis inverse compensation for smart actuators with a modified generalized Prandtl-Ishlinskii model,” submitted to *IEEE Transactions on Nanotechnology*.
- ≤ S. Liu and C.-Y. Su, “Adaptive output feedback control of uncertain systems with modified generalized Prandtl-Ishlinskii hysteresis,” submitted to *The 19th World Congress of the International Federation of Automatic Control*, Cape Town, South Africa, 2014.
- ≤ S. Liu and C.-Y. Su, “Inverse Error Analysis and Adaptive Output Feedback Control of Uncertain Systems Preceded with Hysteresis Actuators”, submitted to *IET Control Theory & Applications*.
- ≤ S. Liu, X. Sheng, Z. Li and C.-Y. Su, “Inverse control of a class of nonlinear systems with modified generalized Prandtl-Ishlinskii hysteresis,” *in the Proceedings of the 38th Annual Conference on IEEE Industrial Electronics Society (IECON)*, Montreal, QC, Canada, pp. 2319-2324, 2012.
- ≤ S. Liu, Z. Li and C.-Y. Su, “Robust adaptive control of a class of nonlinear system with an asymmetric shifted Prandtl-Ishlinskii hysteresis model,” *in the Proceedings of the 2012 International Conference on Advanced Mechatronic Systems (ICAMechS)*, Tokyo, Japan, pp. 217-222, 2012.
- ≤ S. Liu and C.-Y. Su, “A note on the properties of a generalized Prandtl-Ishlinskii model,” *Smart Material and Structures*, vol. 20, no. 8, pp. 1-6, 2011.

# Bibliography

- [1] C. Y. Su, Q. Wang, X. Chen, and S. Rakheja, “Adaptive variable structure control of a class of nonlinear systems with unknown Prandtl-Ishlinskii hysteresis,” *IEEE Transactions on Automatic Control*, vol. 50, no. 12, pp. 2069–2074, 2005.
- [2] S. O. R. Moheimani and G. C. Goodwin, “Guest editorial introduction to the special issue on dynamics and control of smart structures,” *IEEE Transaction on Control System Technology*, vol. 9, pp. 3–4, 2001.
- [3] G. Tao and P. V. Kokotovic, “Adaptive control of plants with unknown hysteresis,” *IEEE Transaction on Automatic Control*, vol. 40, no. 2, pp. 200–212, 1995.
- [4] G. Tao and F. L. L. (Eds), *Adaptive control of nonsmooth Dynamics systems*. Spring, 2001.
- [5] J. W. Macki, P. Nistri, and P. Zecca, “Mathematical models for hysteresis,” *SIAM Review*, vol. 35, no. 1, pp. 94–123, 1993.
- [6] P. M. Sain, M. K. Sain, and B. F. Spencer, “Models for hysteresis and application to structural control,” in *Proceedings of American Control Conference*, vol. 1, pp. 16 –20, June 1997.
- [7] I. D. Mayergoyz, *Mathematical models of hysteresis*. Springer-Verlag, 1991.
- [8] I. D. Mayergoyz, “Hysteresis models from the mathematical and control theory point of view,” *Journal of Applied Physics*, vol. 57, no. 8, pp. 3803–3805, 1985.

- [9] M. Brokate, “Some mathematical properties of the Preisach model for hysteresis,” *IEEE Transactions on Magnetics*, vol. 25, no. 4, pp. 2922–2924, 1989.
- [10] G. V. Webb, D. C. Lagoudas, and A. J. Kurdila, “Hysteresis modeling of SMA actuators for control applications,” *Journal of Intelligent Material Systems and Structures*, vol. 9, pp. 432–448, 1998.
- [11] M. Krasnoselskii and A. Pokrovskii, *Systems with hysteresis*. Springer, 1989.
- [12] M. Brokate and J. Sprekels, *Hysteresis and phase transitions*. Springer-Verlag, 1996.
- [13] Q. Wang, C. Y. Su, and T. Tan, “On the control of plants with hysteresis: overview and a Prandtl-Ishlinskii hysteresis based control approach,” *ACTA Automatica Sinica*, vol. 31, no. 1, pp. 92–104, 2005.
- [14] G. Bertotti and I. D. Mayergoyz, *The science of hysteresis: Mathematical modeling and applications, Volume 1*. Elsevier, 2006.
- [15] P. Krejci and K. Kuhnen, “Inverse control of systems with hysteresis and creep,” *IEE Proceedings on Control Theory and Applications*, vol. 148, no. 3, pp. 185–192, 2001.
- [16] H. Jiang, H. Ji, J. Qiu, and Y. Chen, “A modified Prandtl-Ishlinskii model for modeling asymmetric hysteresis of piezoelectric actuators,” *IEEE Transactions on Ultrasonics, Ferroelectrics, and Frequency Control*, vol. 57, no. 5, pp. 1200–1210, 2010.
- [17] R. Dong and Y. Tan, “A modified Prandtl-Ishlinskii modeling method for hysteresis,” *Physica B: Condensed Matter*, vol. 404, no. 8-11, pp. 1336–1342, 2009.
- [18] J. Shen, W. Jywea, H. Chiang, and Y. Shub, “Precision tracking control of a piezoelectric-actuated system,” *Precision Engineering*, vol. 32, no. 2, pp. 71–78, 2008.
- [19] M. A. Janaidel, S. Rakheja, and C. Y. Su, “A generalized Prandtl-Ishlinskii model for characterizing the hysteresis and saturation nonlinearities of smart actuators,” *Smart Materials and Structures*, vol. 18, no. 045001, 2009.

- [20] M. A. Janaidel, S. Rakheja, and C. Y. Su, “An analytical generalized Prandtl-Ishlinskii model inversion for hysteresis compensation in micropositioning control,” *IEEE/ASME Transactions on Mechatronics*, vol. 16, no. 4, pp. 734–744, 2011.
- [21] A. Esbrook, X. Tan, and H. K. Khalil, “Control of systems with hysteresis via servo-compensation and its application to nanopositioning,” *IEEE Transaction on Control System Technology*, vol. 21, no. 3, pp. 725–738, 2013.
- [22] J. Zhou, C. Wen, and T. Li, “Adaptive output feedback control of uncertain nonlinear systems with hysteresis nonlinearity,” *IEEE Transactions on Automatic Control*, vol. 57, no. 10, pp. 2627–2633, 2012.
- [23] J. Zhou, C. Wen, and Y. Zhang, “Adaptive output control of nonlinear systems with unvertain dead-zone nonlinearity,” *IEEE Transactions on Automatic Control*, vol. 51, no. 3, pp. 504–511, 2006.
- [24] X. Tan and R. Iyer, “Modeling and control of hysteresis,” *IEEE Control Systems Magazine*, vol. 29, no. 1, pp. 26–29, 2009.
- [25] D. Hanssens and M. Ouyang, “Hysteresis in market response: when is marketing spending an investment?,” *Review of Maketing Science WP*, vol. 419, pp. 1–49, 2001.
- [26] C. Lin and S. Yang, “Precise positioning of piezo-actuated stages using hysteresis-observer based control,” *Mechatronics*, vol. 16, no. 7, pp. 417–426, 2006.
- [27] Y. Qin, Y. Tian, D. Zhang, B. Shirinzadeh, and S. Fatikow, “A novel direct inverse modeling approach for hysteresis compensation of piezoelectric actuator in feedforward applications,” *IEEE/ASME Transactions on Mechatronics*, vol. 18, no. 3, pp. 981–989, 2013.
- [28] X. Tan and J. S. Baras, “Modeling and control of hysteresis in magnetostrictive actuators,” *Automatica*, vol. 40, no. 9, pp. 1469–1480, 2004.

- [29] H. T. Banks and R. C. Smith, “Hysteresis modeling in smart material systems,” *Journal of Applied Mechanics and Engineering*, vol. 5, pp. 31–45, 2000.
- [30] J. A. Ewing, “Experimental research in magnetism,” *Philosophical Transactions of the Royal Society of London*, vol. 176, no. II, 1895.
- [31] D. Jiles and D. Atherton, “Theory of ferromagnetic hysteresis,” *Journal of Magnetism and Magnetic Materials*, vol. 61, no. 1-2, pp. 48–60, 1986.
- [32] V. Basso and G. Bertotti, “Hysteresis models for the description of domain wall motion,” *IEEE Transactions on Magnetics*, vol. 32, no. 5, pp. 4210–4212, 1996.
- [33] L. O. Chua and K. A. Stromsmoe, “Mathematical models for dynamic hysteresis loops,” *International Journal of Engineering Science*, vol. 9, no. 5, pp. 435–450, 1971.
- [34] P. Krejci and J. Sprekels, “On a class of multi-dimensional Prandtl-Ishlinskii operators,” *Physica B: Condensed Matter*, vol. 306, no. 1-4, pp. 185–190, 2001.
- [35] A. Visintin, *Models of hysteresis*. Springer, 1994.
- [36] Y. Wen, “Method for random vibration of hysteretic systems,” *Journal of the Engineering Mechanics Division*, vol. 102, no. 2, pp. 249–263, 1976.
- [37] D. C. Jiles and J. B. Thoelke, “Theory of ferromagnetic hysteresis: determination of model parameters from experimental hysteresis loops,” *IEEE Transactions on Magnetics*, vol. 25, pp. 3928–3930, 1989.
- [38] D. C. Jiles, “Modelling the effects of eddy current losses on frequency dependent hysteresis in electrically conducting media,” *IEEE Transactions on Magnetics*, vol. 30, pp. 4326–4328, 1994.
- [39] H. J. M. T. S. Adriaens, W. D. Koning, and R. Banning, “Modeling piezoelectric actuators,” *IEEE/ASME Transactions on Mechatronics*, vol. 5, no. 4, pp. 331–341, 2000.

- [40] F. Preisach, "Über die magnetische nachwirkung," *Zeitschrift für Physik*, vol. 94, pp. 277–302, 1935.
- [41] H. Hu and R. B. Mrad, "On the classical preisach model for hysteresis in piezoceramic actuators," *Mechatronics*, vol. 13, pp. 85–94, 2003.
- [42] Y. Yu, N. Naganathan, and R. Dukkipati, "Preisach modeling of hysteresis for piezoceramic actuator system," *Mechanism and Machine Theory*, vol. 37, pp. 49–59, 2002.
- [43] P. Ge and M. Jouaneh, "Modeling hysteresis in piezoceramic actuators," *Precision Engineering*, vol. 17, no. 3, pp. 211–221, 1995.
- [44] R. B. Gorbet, K. A. Morris, and D. W. L. Wang, "Passivity-based stability and control of hysteresis in smart actuators," *IEEE Transactions on Control Systems Technology*, vol. 9, no. 1, pp. 5–16, 2001.
- [45] R. B. Gorbet, D. W. L. Wang, and K. A. Morris, "Preisach model identification of a two-wire sma actuator," in *Proceedings of IEEE International Conference on Robotics and Automation*, pp. 2161–2167, May 1998.
- [46] H. Banks, A. Kurdile, and G. Webb, "Identification of hysteresis control influence operators representing smart actuators," *Mathematical Problems in Engineering*, vol. 3, no. 4, pp. 287–328, 1997.
- [47] W. Galinaities, *Two methods for modeling scalar hysteresis and their use in controlling actuators with hysteresis*. PhD thesis, Virginia Tech, Blacksburg, 1999.
- [48] L. Prandtl, "Ein gedankenmodell zur kinetischen theorie der festen korper," *ZAMM*, vol. 8, pp. 85–106, 1928.
- [49] A. Y. Ishlinskii, "Some applications of statistical methods to describing deformations of bodies," *Izv. AN SSSR, Techn. Ser.*, no. 9, pp. 580–590, 1944.
- [50] P. Krejci, *Hysteresis, convexity and dissipation in hyperbolic equations*. Gakuto Int. Series Math. Sci. and Appl., Vol. 8, 1996.

- [51] J. Peng and X. B. Chen, “A survey of modeling and control of piezoelectric actuators,” *Modern Mechanical Engineering*, vol. 3, no. 1, pp. 1–20, 2013.
- [52] M. A. Janaidel, C. Y. Su, and S. Rakheja, “Development of the rate-dependent prandtl-ishlinskii model for smart actuators,” *Smart Materials and Structures*, vol. 17, no. 035026, 2008.
- [53] K. Kuhnen and H. Janocha, “Complex hysteresis modeling of a broad class of hysteretic actuator nonlinearities,” in *Proceedings of the 8th International Conference on New Actuators*, pp. 688–691, 2002.
- [54] P. Duhem, “Die dauernden aenderungen und die thermodynamik,” *I, Z. Phys. Chem*, vol. 22, pp. 543–589, 1897.
- [55] M. L. Hodgdon, “Applications of a theory of ferromagnetic hysteresis,” *IEEE Transactions on Magnetics*, vol. 24, pp. 218–221, 1988.
- [56] M. L. Hodgdon, “Mathematical heory and calculations of magnetic hysteresis curves,” *IEEE Transactions on Magnetics*, vol. 24, pp. 3120–3122, 1988.
- [57] R. Bouc, “A mathematical model for hysteresis,” *Acustica*, vol. 24, pp. 16–25, 1971.
- [58] M. Rakotondrabe, “Bouc-wen modeling and inverse multiplicative structure to compensate hysteresis nonlinearity in piezoelectric actuators,” *IEEE Transactions on Automation Science and Engineering*, vol. 8, no. 2, pp. 428–231, 2011.
- [59] T. Low and W. Guo, “Modeling of a three-layer piezoelectric bimorph beam with hysteresis,” *Journal of Microelectromechanical Systems*, vol. 4, no. 4, pp. 230–237, 1995.
- [60] B. F. J. Spencer, S. J. Dyke, M. K. Sain, and J. D. Carlson, “Phenomenological model of a magnetorheological damper,” *ASCE Journal of Engineering Mechanics*, vol. 123, pp. 230–238, 1997.

- [61] G. Foliente, "Hysteresis modeling of wood joints and structural systems," *Journal of Structural Engineering*, vol. 121, no. 6, pp. 1013–1022, 1995.
- [62] P. Ge and M. Jouaneh, "Tracking control of a piezoceramic actuator," *IEEE Transactions on Control Systems Technology*, vol. 4, no. 3, pp. 209–216, 1996.
- [63] D. Croft, G. Shedd, and S. Devasia, "Creep, hysteresis, and vibration compensation for piezoactuators: atomic force microscopy application," in *Proceedings of American Control Conference*, vol. 3, pp. 2123–2128, June 2000.
- [64] N. Takahashi, S. H. Miyabara, and K. Fujiwara, "Problems in practical finite element analysis using Preisach hysteresis model," *IEEE Transactions on Magnetics*, vol. 35, no. 3, pp. 1243–1246, 1999.
- [65] C. Visone, "Hysteresis modelling and compensation for smart sensors and actuators," *Journal of Physics: Conference Series*, vol. 138, no. 1, p. 012028, 2008.
- [66] X. Tan and O. Bennani, "Fast inverse compensation of Preisach-type hysteresis operators using field-programmable gate arrays," in *Proceedings of American Control Conference*, vol. 3, pp. 2123–2128, June 2008.
- [67] S. Rosenbaum, M. Ruderman, T. Strohla, and T. Bertram, "Use of Jiles-Atherton and Preisach hysteresis models for inverse feed-forward control," *IEEE Transactions on Magnetics*, vol. 46, no. 12, pp. 3984–4989, 2010.
- [68] S. Xiao and Y. Li, "Modeling and high dynamic compensating the rate-dependent hysteresis of piezoelectric actuators via a novel modified inverse preisach model," *IEEE Transactions on Control Systems Technology*, 2012. doi:10.1109/TCST.2012.2206029.
- [69] Y. Guo, J. Mao, and K. Zhou, "Rate-dependent modeling and control of gma based on hammerstein model with preisach operator," in *Proceedings of International Conference on Mechatronics and Automation*, pp. 343–347, August 2012.

- [70] W. S. Galinaitis and R. C. Rogers, "Control of a hysteretic actuator using inverse hysteresis compensation," *Proceeding in SPIE Smart Structures and Materials*, vol. 3323, pp. 267–277, 1998.
- [71] Y. Wang, C. Y. Su, and H. Hong, "Model reference control including adaptive inverse hysteresis for systems with unknown input hysteresis," in *Proceedings of Networking, Sensing and Control*, pp. 70–75, April 2007.
- [72] Z. Li, Y. Hu, Y. Liu, T. Chen, and P. Yuan, "Adaptive inverse control of non-linear systems with unknown complex hysteretic non-linearities," *IET Control Theory & Applications*, vol. 6, no. 1, pp. 1–7, 2012.
- [73] L. N. Hao and Z. Li, "Modeling and adaptive inverse control of hysteresis and creep in ionic polymer-metal composite actuators," *Smart Materials and Structures*, vol. 19, no. 025014, 2010.
- [74] M. A. Janaideh and P. Krejci, "Inverse rate-dependent prandtl-ishlinskii model for feed-forward compensation of hysteresis in a piezomicropositioning actuator," *IEEE/ASME Transactions on Mechatronics*, vol. 18, no. 5, pp. 1498–1507, 2013.
- [75] K. Kuhnen, "Modeling, identification and compensation of complex hysteretic nonlinearities: a modified Prandtl-Ishlinskii approach," *European Journal of Control*, vol. 9, no. 4, pp. 407–417, 2003.
- [76] B. K. Nguyen and K. Ahn, "Feedforward control of shape memory alloy actuators using fuzzy-based inverse Preisach model," *IEEE Transactions on Control Systems Technology*, vol. 17, no. 2, pp. 434–441, 2009.
- [77] E. Asua, V. Etxebarria, and A. Garcíla-Arribas, "Neural network-based micropositioning control of smart shape memory alloy actuators," *Engineering Applications of Artificial Intelligence*, vol. 21, no. 5, pp. 796–804, 2008.

- [78] G. Song, V. Chaudhry, and C. Batur, “A neural network inverse model for a shape memory alloy wire actuator,” *Journal of Intelligent Material Systems and Structures*, vol. 14, no. 6, pp. 371–377, 2003.
- [79] J. Zhou, C. Zhang, and C. Wen, “Robust adaptive output control of uncertain nonlinear plants with unknown backlash nonlinearity,” *IEEE Transactions on Automatic Control*, vol. 52, no. 3, pp. 503–509, 2007.
- [80] Y. Cao, L. Cheng, X. B. Chen, and J. Y. Peng, “An inversion-based model predictive control with an integral-of-error state variable for piezoelectric actuators,” *IEEE/ASME Transactions on Mechatronics*, vol. 18, no. 3, pp. 895–904, 2013.
- [81] Q. Wang and C. Y. Su, “Robust adaptive control of a class of nonlinear systems including actuator hysteresis with prandtl-ishlinskii presentations,” *Automatica*, vol. 42, no. 5, pp. 859–867, 2006.
- [82] X. Chen, C. Y. Su, and T. Fukuda, “Adaptive control for the systems preceded by hysteresis,” *IEEE Transactions on Automatic Control*, vol. 53, no. 4, pp. 1019–1025, 2008.
- [83] Y. Feng, C. Y. Su, H. Hong, and S. S. Ge, “Robust adaptive control for a class of nonlinear systems with generalized Prandtl-Ishlinskii hysteresis,” in *Proceedings of Decision and Control*, pp. 4833–4838, December 2007.
- [84] X. Chen, T. Hisayama, and C. Y. Su, “Pseudo-inverse-based adaptive control for uncertain discrete time systems preceded by hysteresis,” *Automatica*, vol. 45, no. 2, pp. 469–476, 2009.
- [85] Y. Li and Q. Xu, “Adaptive sliding model control with perturbation estimation and pid sliding surface for motion tracking of a piezo-driven micromanipulator,” *IEEE Transactions on Control Systems Technology*, vol. 18, no. 4, pp. 798–810, 2010.

- [86] J. Y. Peng and X. B. Chen, “Integrated pid-based sliding model state estimation and control for piezoelectric actuators,” *IEEE/ASME Transactions on Mechatronics*, 2012. doi:10.1109/TMECH.2012.2222428.
- [87] G.-Y. Gu, L.-M. Zhu, C.-Y. Su, and H. Ding, “Motion control of piezoelectric positioning stages: modeling, controller design, and experimental evaluation,” *IEEE/ASME Transactions on Mechatronics*, vol. 18, no. 5, pp. 1459 – 1471, 2013.
- [88] Y. Feng, C. A. Rabbath, H. Hong, M. A. Janaideh, and C. Y. Su, “Robust control for shape memory alloy micro-actuators based flap positioning system,” in *Proceedings of American Control Conference*, pp. 4181–4186, June 2010.
- [89] M. A. Janaideh, Y. Feng, S. Rakheja, Y. Tan, and C. Y. Su, “Robust stability and performance analysis of systems with hysteresis nonlinearities,” in *Proceedings of 48th IEEE Conference on Decision and Control and 28th Chinese Control Conference*, pp. 7279–7284, December 2009.
- [90] T. E. Pare and J. P. How, “Robust stability and performance analysis of systems with hysteresis nonlinearities,” in *Proceedings of American Control Conference*, vol. 3, pp. 1904–1908, June 1998.
- [91] C. Y. Su, Y. Stepanenko, J. Svoboda, and T. P. Leung, “Robust adaptive control of a class of nonlinear systems with unknown backlash-like hysteresis,” *IEEE Transactions on Automatic Control*, vol. 45, no. 12, pp. 2427–2432, 2000.
- [92] F. Ikhouane and J. Rodellar, “A linear controller for hysteretic systems,” *IEEE Transactions on Automatic Control*, vol. 51, no. 2, pp. 340–344, 2006.
- [93] X. Chen and T. Hisayama, “Adaptive sliding-mode position control for piezo-actuated stage,” *IEEE Transactions on Industrial Electronics*, vol. 55, no. 11, pp. 3927–3934, 2008.

- [94] S. Majima, K. Kodama, and T. Hasegawa, "Modeling of shape memory alloy actuator and tracking control system with the model," *IEEE Transactions on Control Systems Technology*, vol. 9, no. 1, pp. 54–59, 2001.
- [95] X. Tan and J. S. Baras, "Adaptive identification and control of hysteresis in smart materials," *IEEE Transactions on Automatic Control*, vol. 50, no. 6, pp. 827–839, 2005.
- [96] S. Liu and C. Y. Su, "A note on the properties of a generalized Prandtl-Ishlinskii model," *Smart Materials and Structures*, vol. 20, p. 087003, 2011.
- [97] R. Iyer and X. Tan, "Control of hysteresis systems through inverse compensation," *IEEE Control Systems Magazine*, vol. 29, no. 1, pp. 83–99, 2009.
- [98] A. Bergqvist, *On Magnetic Hysteresis Modelling*. Royal Institute of Technology, Electric Power Engineering, 1994.
- [99] M. A. Janaideh, C. Y. Su, and S. Rakheja, "Inverse compensation error of the prandtl-ishlinskii models," in *Proceedings of 51th IEEE Conference on Decision and Control*, pp. 1597–1602, December 2012.
- [100] G.-Y. Gu and L.-M. Zhu, "Modeling of rate-depedent hysteresis in piezoeletric actuators using a family of ellipses," *Sensors & Actuators: A. Physical*, vol. 157, no. 2, pp. 303–309, 2011.
- [101] X. Chen, T. Hisayama, and C.-Y. Su, "Adaptive control for uncertain continuous-time systems using implicit inversion of prandtl-ishlinskii hysteresis representation," *IEEE Transactions on Automatic Control*, vol. 55, no. 10, pp. 2357–2363, 2010.
- [102] B. Ren, S. S. Ge, T. H. Lee, and C.-Y. Su, "Adaptive neural control for a class of nonlinear systems with uncertain hysteresis inputs and time-varying state delays," *IEEE Transaction on Systems, Man, and Cybernetics-Part B: Cybernetics*, vol. 39, no. 2, pp. 431–443, 2009.

- [103] B. Ren, S. S. Ge, C.-Y. Su, and T. H. Lee, "Adaptive neural control for a class of uncertain nonlinear systems in pure-feedback form with hysteresis input," *IEEE Transaction on Neural Networks*, vol. 20, no. 7, pp. 1148–1164, 2009.
- [104] C. Y. Su, Y. Feng, H. Hong, and X. Chen, "Adaptive control of system involving complex hysteretic nonlinearities: a generalised prandtl-ishlinskii modelling approach," *International Journal of Control*, vol. 82, no. 10, pp. 1786–1793, 2009.
- [105] P.-K. Wong, Q. Xu, C.-M. Vong, and H.-C. Wong, "Rate-dependent hysteresis modeling and control of a piezostage using online support vector machine and relevance vector machine," *IEEE Transactions on Industrial Electronics*, vol. 59, no. 4, pp. 1988–2001, 2012.
- [106] J. Zhou, C. Wen, and C. Zhang, "Adaptive backstepping control of a class of uncertain nonlinear systems with unknown backlash-like hysteresis," *IEEE Transactions on Automatic Control*, vol. 49, no. 10, pp. 1751–1757, 2004.
- [107] Y. Shan and K. K. Leang, "Accounting for hysteresis in repetitive control design: Nanopositioning example," *Automatica*, vol. 48, no. 8, pp. 1751–1758, 2012.
- [108] X. Chen and T. Ozaki, "Adaptive control for plants in the presence of actuator and sensor uncertain hysteresis," *IEEE Transactions on Automatic Control*, vol. 56, no. 1, pp. 171–177, 2011.
- [109] S. Liu, X. Sheng, Z. Li, and C. Y. Su, "Inverse control of a class of nonlinear systems with modified generalized prandtl-ishlinskii hysteresis," in *Proceedings of the 38th Annual Conference on IEEE Industrial Electronics Society (IECON)*, pp. 2319–2324, 2012.
- [110] Y. Li and Q. Xu, "Design and robust repetitive control of a new parallel-kinematic xy piezostage for micro/nanomanipulation," *IEEE/ASME Transactions on Mechatronics*, vol. 17, no. 6, pp. 1120–1132, 2012.

- [111] Y. Xie, Y. Tan, and R. Dong, “Nonlinear modeling and decoupling control of xy micropositioning stages with piezoelectric actuators,” *IEEE/ASME Transactions on Mechatronics*, vol. 18, no. 3, pp. 821–832, 2012.
- [112] Q. Xu and Y. Li, “Model predictive discrete-time sliding mode control of a nanopositioning piezostage without modeling hysteresis,” *IEEE Transactions on Control Systems Technology*, vol. 20, no. 4, pp. 983–994, 2012.